

SLRQA: A Sparse Low-Rank Quaternion Model for Color Image Processing with Convergence Analysis

Zhanwang Deng^{*}, Yuqiu Su[†] and Wen Huang[‡]

Abstract

In this paper, we propose a Sparse Low-rank Quaternion Approximation (SLRQA) model for color image processing problems with noisy observations. The proposed SLRQA is a quaternion model that combines low-rankness and sparsity priors. Furthermore, it does not need an initial rank estimate. To solve the SLRQA model, a nonconvex proximal linearized ADMM (PL-ADMM) algorithm is proposed. Furthermore, the global convergence analysis of the PL-ADMM under mild assumptions is presented. When the observation is noise-free, an SLRQA-NF model of the limiting case of the SLRQA is proposed. Subsequently, a nonconvex proximal linearized ADMM (PL-ADMM-NF) algorithm for the SLRQA-NF is given. In numerical experiments, we verify the effectiveness of quaternion representation. Furthermore, for color image denoising and color image inpainting problems, SLRQA and SLRQA-NF models demonstrate superior performance both quantitatively and visually when compared with some state-of-the-art methods.

Key words: Color image denoising, Quaternion matrix completion, Nonconvex linearized ADMM.

1 Introduction

Low-rankness plays an important role in image processing and has been used in image denoising [10], image inpainting [15], image deblurring [26], and image filtering [7]. A commonly encountered approach for exploiting the low-rankness is to find a matrix with the lowest rank such that certain matching errors are minimized. Due to the existence of the rank function, such problems are known as NP-hard [25]. To overcome this difficulty, Candès et al. [6] have proved that the nuclear norm is the tightest convex relaxation of the NP-hard rank minimization function. In addition to the nuclear norm, other surrogates have also been proposed, such as weighted nuclear norm (WNNM) [14], Schatten p -norm [24], weighted Schatten p -norm [32], and log-determinant penalty [19], which

^{*}Academy for Advanced Interdisciplinary Studies, Peking University, Beijing, China. (dzw_opt2022@stu.pku.edu.cn)

[†]School of Mathematical Sciences, Xiamen University, Xiamen, China. (yuqiusu@stu.xmu.edu.cn)

[‡]Corresponding author. School of Mathematical Sciences, Xiamen University, Xiamen, China. (wen.huang@xmu.edu.cn). This work was supported by the National Natural Science Foundation of China (No. 12371311), the National Natural Science Foundation of Fujian Province (No. 2023J06004), the Fundamental Research Funds for the Central Universities (No. 20720240151), and Xiaomi Young Talents Program.

have shown competitive effectiveness in various applications. In addition to low-rankness, sparsity is also a significant property of natural images that has been considered in image recovery [35, 5], video recovery [34], texture repairing [21], and face recognition [40]. The intuition behind sparsity is that images under certain transforms are usually sparse, such as wavelet or discrete cosine transform (DCT). Moreover, quaternion representation has shown great potential for color image processing problems. A color image can be encoded as a pure quaternion matrix. As claimed in [10], the main advantage of quaternion representation is that a color image is treated as a pure quaternion matrix naturally and holistically, meaning that the correlation information among the three RGB channels is used. It is empirically shown in [10] that methods using quaternion representation outperform methods with monochromatic techniques. Moreover, quaternion has been increasingly used for color image processing in the past two decades [10].

These three priors, i.e. low-rankness, sparsity, and quaternion representation, all play important roles in image processing. However, models based on all these three priors are still limited. In the following subsection, we propose a quaternion-based model that combines low-rankness and sparsity properties to address problems arising in image processing.

1.1 A novel quaternion based model

Let $\dot{\mathbf{Y}} \in \mathbb{H}^{m \times n}$ denote an observed color image satisfying $\dot{\mathbf{Y}} = \mathcal{A}(\dot{\mathbf{X}}) + \varepsilon$, where $\dot{\mathbf{X}} \in \mathbb{H}^{m \times n}$ is the desired noiseless color image, $\mathbb{H}^{m \times n}$ denotes the set of all $m \times n$ quaternion matrices, \mathcal{A} denotes a linear operator, and ε is a random noise¹. According to the principle of maximizing the posterior probability, an approach to recover the image $\dot{\mathbf{X}}$ is to maximize likelihood estimation function, i.e., $\dot{\mathbf{X}}_* = \arg \max_{\dot{\mathbf{X}}} p(\dot{\mathbf{X}}|\dot{\mathbf{Y}})$. It follows from the Bayes rule that $p(\dot{\mathbf{X}}|\dot{\mathbf{Y}}) = \frac{p(\dot{\mathbf{Y}}|\dot{\mathbf{X}})p(\dot{\mathbf{X}})}{p(\dot{\mathbf{Y}})} \propto p(\dot{\mathbf{Y}}|\dot{\mathbf{X}})p(\dot{\mathbf{X}})$. By taking the logarithm, an equivalent optimization problem is given as follows:

$$\dot{\mathbf{X}}_* = \arg \min_{\dot{\mathbf{X}}} -\log p(\dot{\mathbf{Y}}|\dot{\mathbf{X}}) - \log p(\dot{\mathbf{X}}) = \arg \min_{\dot{\mathbf{X}}} E(\dot{\mathbf{Y}}; \dot{\mathbf{X}}) + R(\dot{\mathbf{X}}), \quad (1)$$

where $E(\dot{\mathbf{Y}}; \dot{\mathbf{X}})$ is the negative log-likelihood function and is also called the data fitting term, and $R(\dot{\mathbf{X}})$ is the prior term. It is assumed throughout this paper that the entries of the noise ε are drawn from the Gaussian distribution with mean zero and variance τ^2 . It follows that $E(\dot{\mathbf{Y}}; \dot{\mathbf{X}}) = \frac{1}{2\tau^2} \|\mathcal{A}(\dot{\mathbf{X}}) - \dot{\mathbf{Y}}\|_{\mathbb{F}}^2$ if all the entries of $\dot{\mathbf{Y}}$ are observed, and $E(\dot{\mathbf{Y}}; \dot{\mathbf{X}}) = \frac{1}{2\tau^2} \|\mathcal{P}_{\Omega}(\mathcal{A}(\dot{\mathbf{X}})) - \mathcal{P}_{\Omega}(\dot{\mathbf{Y}})\|_{\mathbb{F}}^2$ if only partial entries of $\dot{\mathbf{Y}}$ are observed, where Ω denotes the indices of the observed entries, that is, $(\mathcal{P}_{\Omega}(\dot{\mathbf{Y}}))_{ij} = \dot{\mathbf{Y}}_{ij}$ if $(i, j) \in \Omega$ and $(\mathcal{P}_{\Omega}(\dot{\mathbf{Y}}))_{ij} = 0$ if $(i, j) \notin \Omega$.

By integrating the low-rankness and sparsity into the prior term, i.e., $R(\dot{\mathbf{X}}) = \sum_i \phi(\sigma_i(\dot{\mathbf{X}}), \gamma) + \lambda p(\mathcal{W}(\dot{\mathbf{X}}))$, and letting $\dot{\mathbf{W}} = \mathcal{W}(\dot{\mathbf{X}})$, we propose the following Sparse Low-rank Quaternion Approximation (SLRQA) model for color image processing:

$$\begin{aligned} \min_{\dot{\mathbf{X}}, \dot{\mathbf{W}} \in \mathbb{H}^{m \times n}} \quad & \sum_i \phi(\sigma_i(\dot{\mathbf{X}}), \gamma) + \lambda p(\dot{\mathbf{W}}) + \frac{1}{2\tau^2} \|\mathcal{P}_{\Omega}(\mathcal{A}(\dot{\mathbf{X}})) - \mathcal{P}_{\Omega}(\dot{\mathbf{Y}})\|_{\mathbb{F}}^2, \\ \text{s.t.} \quad & \mathcal{W}(\dot{\mathbf{X}}) = \dot{\mathbf{W}}, \end{aligned} \quad (2)$$

¹The definition of quaternion matrices is clarified in Section 2.

where $\dot{\mathbf{X}} \in \mathbb{H}^{m \times n}$ denotes a color image, $\dot{\mathbf{W}} \in \mathbb{H}^{m \times n}$ is the coefficient matrix under an orthogonal transform \mathcal{W} such as quaternion wavelet transform or quaternion discrete cosine transform (QDCT), \mathcal{A} is a known operator such as a total variation operator, a blurring operator or the Radon transform, $p(\dot{\mathbf{W}})$ is a function that has Lipschitz continuously differentiable and promotes the sparsity of $\dot{\mathbf{W}}$, ϕ is a nonconvex surrogate function that substitutes the rank function, $\sigma_i(\dot{\mathbf{X}})$ is the i -th singular value of $\dot{\mathbf{X}}$ defined in Section 2, $\sum_i \phi(\sigma_i(\dot{\mathbf{X}}), \gamma)$ promotes the low-rankness of $\dot{\mathbf{X}}$. Some nonconvex surrogate functions for ϕ have been given in [10, 23] and listed in Table 1.

Table 1: nonconvex surrogate functions $\phi(x, \gamma)$

Nonconvex function	Log-determinant	Schatten- γ	Logarithm	Laplace [9]	Weighted Schatten- γ [32]	ETP
$\phi(x, \gamma)$	$\log(1 + x^2)$	x^γ	$\log(\gamma + x)$	$1 - e^{-\frac{x}{\gamma}}$	wx^γ	$\frac{\lambda(1 - \exp(-\gamma x))}{1 - \exp(-\gamma)}$

The ℓ_1 norm has been widely used to promote sparsity. However, the Lipschitz continuous differentiability of $p(\dot{\mathbf{W}})$ is assumed in our convergence analysis². Therefore, a smoothing function such as the Huber function can be used as a substitution for $p(\dot{\mathbf{W}})$. It is empirically shown in Section 6 that such a substitution yields satisfactory performance. This strategy has been used in [38] to guarantee convergence theoretically.

When the observed color image is noise-free, or the variance τ^2 in the noise ε is zero, Model (2) is undefined due to the existence of a zero in the denominator of the data fitting term. In this case, one can reformulate the data fitting term as a constraint. It follows that a variant of SLRQA for the noise-free problem is given by

$$\begin{aligned} \min_{\dot{\mathbf{X}}, \dot{\mathbf{W}} \in \mathbb{H}^{m \times n}} \quad & \sum_i \phi(\sigma_i(\dot{\mathbf{X}}), \gamma) + \lambda p(\dot{\mathbf{W}}), \\ \text{s.t.} \quad & \mathcal{W}(\dot{\mathbf{X}}) = \dot{\mathbf{W}}, \quad \mathcal{P}_\Omega(\mathcal{A}(\dot{\mathbf{X}})) = \mathcal{P}_\Omega(\dot{\mathbf{Y}}). \end{aligned} \quad (3)$$

Since \mathcal{W} is an orthogonal transform such as quaternion wavelet transform or quaternion discrete cosine transform (QDCT) [12], we have $\sum_i \phi(\sigma_i(\dot{\mathbf{X}}), \gamma) = \sum_i \phi(\sigma_i(\dot{\mathbf{Q}}_1 \dot{\mathbf{W}} \dot{\mathbf{Q}}_2^*), \gamma) = \sum_i \phi(\sigma_i(\dot{\mathbf{W}}), \gamma)$, the superscript $*$ denotes the conjugate transpose operator. Let $\dot{\mathbf{Z}} = \mathcal{W}(\dot{\mathbf{X}})$. We propose a model named SLRQA-NF which is equivalent to (3) for noise-free problems:

$$\begin{aligned} \min_{\dot{\mathbf{Z}}, \dot{\mathbf{W}} \in \mathbb{H}^{m \times n}} \quad & \sum_i \phi(\sigma_i(\dot{\mathbf{Z}}), \gamma) + \lambda p(\dot{\mathbf{W}}), \\ \text{s.t.} \quad & \mathcal{P}_\Omega(\mathcal{A}\mathcal{W}^\#(\dot{\mathbf{W}})) = \mathcal{P}_\Omega(\dot{\mathbf{Y}}), \quad \dot{\mathbf{Z}} = \dot{\mathbf{W}}, \end{aligned} \quad (4)$$

where the superscript $\#$ denotes the adjoint operator which is defined in Section 2.

²We use a variant of the ADMM method to solve SLRQA. Note that such an assumption has been made for all the ADMM methods with global convergence guaranteed for nonconvex problems as far as we know, see, e.g., a review in [22]

1.2 Related work

The derivations of SLRQA and SLRQA-NF models are motivated by LADM [21] and LRQA [10] models. To be specific, LADM is a convex model that utilizes the sparsity and low-rankness properties while quaternion representation and nonconvex surrogate rank function have not been considered. LRQA is a quaternion-based model that makes use of the low-rankness property by replacing the nuclear norm with nonconvex surrogate functions, but it has not taken advantage of sparsity. SLRQA and SLRQA-NF models take advantage of LADM and LRQA by using quaternion representation, low-rankness, and sparsity. Next, we discuss some image processing models related to SLRQA and SLRQA-NF.

Image denoising (noisy observation and identity linear operator \mathcal{A}):

If the low-rankness prior is omitted, i.e. $\phi \equiv 0$, the Lipschitz continuous gradients assumption is dropped, and $p(\dot{\mathbf{W}}) = \|\dot{\mathbf{W}}\|_1$, then the classical analysis based approach [5] with an extension to quaternion representation is presented:

$$\min_{\dot{\mathbf{X}} \in \mathbb{H}^{m \times n}} \lambda \|\mathcal{W}(\dot{\mathbf{X}})\|_1 + \frac{1}{2\tau^2} \|\dot{\mathbf{X}} - \dot{\mathbf{Y}}\|_{\mathbb{F}}^2, \quad (5)$$

where the variable $\dot{\mathbf{W}}$ is eliminated by $\dot{\mathbf{W}} = \mathcal{W}(\dot{\mathbf{X}})$. If the sparse term $p(\dot{\mathbf{W}})$ is not used, then SLRQA becomes the LRQA denoising model in [10, Equation 20]

$$\min_{\dot{\mathbf{X}} \in \mathbb{H}^{m \times n}} \sum_i \phi(\sigma_i(\dot{\mathbf{X}}), \gamma) + \frac{1}{2\tau^2} \|\dot{\mathbf{X}} - \dot{\mathbf{Y}}\|_{\mathbb{F}}^2.$$

As noted in [10], LRQA is a generalization of other models such as the WNNM model.

Image deblurring (noisy observation and blurring kernel operator \mathcal{A}):

If the low-rankness prior is not used, i.e., $\phi \equiv 0$ and let $p(\dot{\mathbf{W}}) = \|\dot{\mathbf{W}}\|_1$, then the standard analysis based model for image deblurring in [5] with extensions to quaternion representation is presented

$$\min_{\dot{\mathbf{X}} \in \mathbb{H}^{m \times n}} \lambda \|\mathcal{W}(\dot{\mathbf{X}})\|_1 + \frac{1}{2\tau^2} \|\mathcal{A}(\dot{\mathbf{X}}) - \dot{\mathbf{Y}}\|_{\mathbb{F}}^2.$$

Image inpainting (partially observed images): If the observed image is noise-free, the linear operator \mathcal{A} is the identity, $p(\dot{\mathbf{W}}) = \|\dot{\mathbf{W}}\|_1$, and ϕ is the nuclear norm, then the SLRQA-NF model becomes the LADM model in [21] with an extension to quaternion representation:

$$\min_{\dot{\mathbf{W}} \in \mathbb{H}^{m \times n}} \|\dot{\mathbf{W}}\|_* + \lambda \|\dot{\mathbf{W}}\|_1, \quad \text{s.t. } \mathcal{P}_\Omega(\mathcal{W}^\#(\dot{\mathbf{W}})) = \mathcal{P}_\Omega(\dot{\mathbf{Y}}). \quad (6)$$

Furthermore, if the sparsity term ϕ is dropped and a nonconvex surrogate is used, then SLRQA-NF model becomes the LRQA [10, Equation 22] given by

$$\min_{\dot{\mathbf{X}} \in \mathbb{H}^{m \times n}} \sum_i \phi(\sigma_i(\dot{\mathbf{X}}), \gamma), \quad \text{s.t. } \mathcal{P}_\Omega(\dot{\mathbf{X}}) = \mathcal{P}_\Omega(\dot{\mathbf{Y}}). \quad (7)$$

The above-reviewed models do not simultaneously use the low-rankness, sparsity, and quaternion representation. Recently, a quaternion based model combined with low-rankness and sparsity

has been proposed in [17]. Specifically, the model is given by:

$$\begin{aligned} & \min_{\dot{\mathbf{L}} \in \mathbb{H}^{m \times r}, \dot{\mathbf{D}} \in \mathbb{H}^{r \times r}, \dot{\mathbf{R}} \in \mathbb{H}^{r \times n}, \dot{\mathbf{X}} \in \mathbb{H}^{m \times n}, \dot{\mathbf{W}} \in \mathbb{H}^{m \times n}} \|\dot{\mathbf{D}}\|_* + \lambda \|\dot{\mathbf{W}}\|_1, \\ \text{s.t. } & \dot{\mathbf{L}}^* \dot{\mathbf{L}} = \mathbf{I}_r, \dot{\mathbf{R}} \dot{\mathbf{R}}^* = \mathbf{I}_r, \mathcal{W}(\dot{\mathbf{X}}) = \dot{\mathbf{W}}, \dot{\mathbf{X}} = \dot{\mathbf{L}} \dot{\mathbf{D}} \dot{\mathbf{R}}, \mathcal{P}_\Omega(\dot{\mathbf{Y}} - \dot{\mathbf{L}} \dot{\mathbf{D}} \dot{\mathbf{R}}) = \mathbf{0}. \end{aligned} \quad (8)$$

where r is a prescribed number and the superscript $*$ denotes the conjugate transpose operator, see its definition in Section 2. Different from SLRQA models, Model (8) uses the nuclear norm to promote low-rank instead of nonconvex surrogate functions $\phi(\sigma_i(\dot{\mathbf{X}}), \gamma)$. Furthermore, it needs to estimate the rank r in the initialization phase while SLRQA does not. Another model that uses the three priors is proposed in [34, 35] for color image and video recovery.

The model is given by

$$\begin{aligned} & \min_{\dot{\mathbf{X}}} \|\dot{\mathbf{X}}\|_* - \sum_{i=r}^{\min(m,n)} \sigma_i(\dot{\mathbf{X}}) + \lambda \|\dot{\mathbf{W}}\|_1, \\ \text{s.t. } & \mathcal{P}_\Omega(\dot{\mathbf{X}} - \dot{\mathbf{Y}}) = 0, \mathcal{W}(\dot{\mathbf{X}}) = \dot{\mathbf{W}}. \end{aligned} \quad (9)$$

Note that Model (9) also needs to estimate the rank r and the low-rankness is promoted by penalizing a truncated nuclear norm, which is convex. Moreover, convergence analyses of the proposed algorithms for solving the existing models in [17, 34, 35] with three priors are not given.

In this paper, proximal linearized ADMM algorithms are proposed to solve Models (2) and (4). Note that the convergence of nonconvex ADMM and its variants has been studied widely. However, as far as we know, the existing ADMM and its variants either consider different optimization problems or use different optimization techniques. A nonexhaustive review is given as follows. Wang et al. [29] comprehensively study the convergence of ADMM for nonconvex and nonsmooth objective functions subject to coupled linear equality constraints. Their assumptions require that the solution of the subproblem is Lipschitz continuous with respect to the input, which is often overly stringent and hard to verify for practical applications. Hong et al. [18] study the convergence of ADMM for solving nonconvex consensus problems, but it is under the case where every constraint matrix has full column rank. Compared with the above analyses, our convergence analysis only needs one constraint matrix that has full column rank. In [36], Yashtini proposes a proximal linearized ADMM for solving linearly constrained nonconvex and possibly nonsmooth optimization problems. The proposed method employs a linearization strategy that targets both the quadratic penalty term and the objective function. Above all, all the nonconvex ADMM and their variant algorithms for nonconvex situations are different from PL-ADMM where only one variable is linearized in the situation. For the reviewed algorithms, the first two algorithms are traditional ADMM algorithms for nonconvex problems, while the ADMM of the last algorithm uses the technique of linearization for both two variables. For a detailed review of other non-convex ADMM algorithms, we refer the readers to [22].

1.3 Contribution

The main contributions of this paper are listed as follows:

- We propose a novel SLRQA model to address image processing problems with noise by maximizing the a posteriori probability estimate. The proposed SLRQA takes advantage of quaternion representation, low-rankness, and sparsity without requiring an estimation of the rank.
- We give a proximal linearized alternating direction method of multipliers (PL-ADMM) algorithm. Under mild conditions, we prove that the sequence generated by the algorithm converges to a stationary point. To the best of our knowledge, this is the first convergence analysis result of an algorithm for a quaternion-based image processing model.
- For noise-free observations, we propose a variant of SLRQA called SLRQA-NF. Inspired by PL-ADMM, an algorithm named PL-ADMM-NF is presented to solve the SLRQA-NF model.
- In the numerical experiments, we verify that the quaternion representation outperforms the RGB monochromatic representation. Moreover, compared with some representative state-of-the-art image processing models, the promising performance of SLRQA and SLRQA-NF demonstrates their superiority and robustness numerically and visually.

1.4 Organization

The rest of this paper is organized as follows. In Section 2, the preliminaries and notations are introduced. The PL-ADMM algorithm framework for solving SLRQA model is given in Section 3. The global convergence is established in Section 4. In Section 5, the PL-ADMM-NF algorithm for solving SLRQA-NF model is presented. In Section 6, extensive numerical experiments are conducted to demonstrate the performance of the models and algorithms by comparing them with other state-of-the-art methods. Finally, the conclusion is given in Section 7.

2 Preliminaries

Throughout this paper, scalars, real vectors, real matrices, and real tensor are respectively denoted by lowercase letters x , boldface lowercase letters \mathbf{x} , boldface capital letters \mathbf{X} , and boldface capital letters with a tilde $\tilde{\mathbf{X}}$ respectively. \mathbb{H} denotes the quaternion algebra proposed in [16]. A dot above a variable \dot{q} represents a quaternion number. A quaternion number consists of one real part and three imaginary parts:

$$\dot{q} = x_s + x_i \mathbf{i} + x_j \mathbf{j} + x_k \mathbf{k}.$$

where $x_s, x_i, x_j, x_k \in \mathbb{R}$, and $\mathbf{i}, \mathbf{j}, \mathbf{k}$ are three imaginary units. The quaternion \dot{q} is called a pure quaternion if and only if it has a zero real part, *i.e.* $x_s = 0$. The real part of \dot{q} is $\text{Re}(\dot{q}) = x_s$. The conjugate \bar{q} is defined as $\bar{q} = x_s - x_i \mathbf{i} - x_j \mathbf{j} - x_k \mathbf{k}$. The modulus $|\dot{q}|$ is defined as $|\dot{q}| = \sqrt{x_s^2 + x_i^2 + x_j^2 + x_k^2}$. The inverse of \dot{q} is given by $\dot{q}^{-1} = \frac{\bar{q}}{|\dot{q}|^2}$. For a quaternion matrix $\dot{\mathbf{X}}$, $\dot{\mathbf{X}}_{ij}$ denotes the i -th row, j -th column element of $\dot{\mathbf{X}}$ and $\dot{\mathbf{X}}_{ijk}$ to denote the i -th row, j -th and k -th imaginary units. The Frobenius norm of $\dot{\mathbf{X}}$ is defined as $\|\dot{\mathbf{X}}\|_F := \sqrt{\sum_{i=1}^n \sum_{j=1}^m |\dot{\mathbf{X}}_{ij}|^2}$. Accordingly,

the conjugate operator $\bar{\cdot}$, transpose operator $\dot{\mathbf{A}}^T$ and the conjugate transpose operator $\dot{\mathbf{A}}^*$ are defined as $\bar{\mathbf{A}} = (\bar{a})_{ij}$, $\dot{\mathbf{A}}^T = (\dot{a})_{ji}$ and $\dot{\mathbf{A}}^* = (\bar{a})_{ji}$, respectively. Furthermore, the multiplication rule of quaternion is given by: $\mathbf{i} \cdot 1 = \mathbf{i}$, $\mathbf{j} \cdot 1 = \mathbf{j}$, $\mathbf{k} \cdot 1 = \mathbf{k}$. $\mathbf{i}^2 = \mathbf{j}^2 = \mathbf{k}^2 = -1$, $\mathbf{ij} = -\mathbf{ji} = \mathbf{k}$, $\mathbf{jk} = -\mathbf{kj} = \mathbf{i}$, $\mathbf{ki} = -\mathbf{ik} = \mathbf{j}$. Note that the multiplication of two quaternions \dot{q}_1 and \dot{q}_2 is not commutative, i.e., $\dot{q}_1\dot{q}_2 \neq \dot{q}_2\dot{q}_1$ in general. $\dot{\mathbf{Q}}$ is called a unitary matrix if and only if $\dot{\mathbf{Q}}\dot{\mathbf{Q}}^* = \dot{\mathbf{Q}}^*\dot{\mathbf{Q}} = \mathbf{I}$, where \mathbf{I} denotes a real identity matrix. The inner product of two quaternion matrices $\dot{\mathbf{G}}_1, \dot{\mathbf{G}}_2 \in \mathbb{H}^{m \times n}$ is defined as $\langle \dot{\mathbf{G}}_1, \dot{\mathbf{G}}_2 \rangle := \text{tr}(\dot{\mathbf{G}}_1^* \dot{\mathbf{G}}_2)$. The image of a given matrix $\dot{\mathbf{G}}_1$ is denoted by $\text{range}(\dot{\mathbf{G}}_1)$. Given an operator $\mathcal{W} : \mathbb{H}^{m \times n} \rightarrow \mathbb{H}^{m \times n}$, the weighted norm is defined as $\|\dot{\mathbf{X}}\|_{\mathcal{W}} := \langle \mathcal{W}(\dot{\mathbf{X}}), \dot{\mathbf{X}} \rangle$. The operator norm is defined as $\|\mathcal{W}\| := \sup_{\dot{\mathbf{X}}} \frac{\|\mathcal{W}(\dot{\mathbf{X}})\|_{\mathbb{F}}}{\|\dot{\mathbf{X}}\|_{\mathbb{F}}}$. Let $\mathcal{W}^\#$ denote the adjoint operator of \mathcal{W} , i.e., $\langle \mathcal{W}(\dot{\mathbf{G}}_1), \dot{\mathbf{G}}_2 \rangle = \langle \dot{\mathbf{G}}_1, \mathcal{W}^\#(\dot{\mathbf{G}}_2) \rangle$ holds for any $\dot{\mathbf{G}}_1, \dot{\mathbf{G}}_2 \in \mathbb{H}^{m \times n}$. If \mathcal{W} is given by a quaternion matrix, then $\mathcal{W}^\#$ is the conjugate transpose of the matrix. For $\tilde{\dot{\mathbf{G}}} := (\dot{\mathbf{G}}_1, \dots, \dot{\mathbf{G}}_p) \in \mathbb{H}^{n_1 \times m_1} \times \dots \times \mathbb{H}^{n_p \times m_p}$, $\|\tilde{\dot{\mathbf{G}}}\|_{\mathbb{F}} := \sqrt{\sum_{i=1}^p \|\dot{\mathbf{G}}_i\|_{\mathbb{F}}^2}$. Hence we have $\sum_{i=1}^p \frac{1}{\sqrt{p}} \|\dot{\mathbf{G}}_i\|_{\mathbb{F}} \leq \|\tilde{\dot{\mathbf{G}}}\|_{\mathbb{F}} \leq \sum_{i=1}^p \|\dot{\mathbf{G}}_i\|_{\mathbb{F}}$, where the first equality follows from Cauchy-Schwarz inequality.

The quaternion singular value decomposition theorem will be used in the solving process of our algorithm. We state it as follows.

Theorem 2.1 (Quaternion singular value decomposition (QSVD)[37]). *For any given quaternion matrix $\dot{\mathbf{A}} \in \mathbb{H}^{m \times n}$, there exist two unitary quaternion matrices $\dot{\mathbf{U}} \in \mathbb{H}^{m \times m}$, $\dot{\mathbf{V}} \in \mathbb{H}^{n \times n}$ such that*

$$\dot{\mathbf{A}} = \dot{\mathbf{U}} \begin{pmatrix} \Sigma & \mathbf{0} \\ \mathbf{0} & \mathbf{0} \end{pmatrix} \dot{\mathbf{V}}^*,$$

where $\Sigma \in \mathbb{R}^{r \times r}$ is a diagonal matrix with $\Sigma_{1,1} \geq \Sigma_{2,2} \geq \dots \geq \Sigma_{r,r} > 0$ being the singular values of $\dot{\mathbf{A}}$. We denote $\sigma_i(\dot{\mathbf{A}})$ to be the i -th singular value of $\dot{\mathbf{A}}$ and $\sigma_{\dot{\mathbf{A}}} = (\Sigma_{1,1}, \dots, \Sigma_{r,r}, 0, \dots, 0) \in \mathbb{R}^l$ as the singular value vector of $\dot{\mathbf{A}}$, where $l = \min\{m, n\}$.

According to the QSVD, the rank of a quaternion matrix is defined as the number of nonzero singular values while the nuclear norm $\|\dot{\mathbf{A}}\|_*$ is defined as the sum of all nonzero singular values.

3 An Algorithm for SLRQA model

The proposed proximal linearized alternating direction method of multipliers (PL-ADMM) is stated in Algorithm 1.

Each iteration of PL-ADMM minimizes the augmented Lagrangian function by using the alternating direction method. Specifically, the augmented Lagrangian function of SLRQA in (2) is given by

$$\begin{aligned} \mathcal{L}_\beta(\dot{\mathbf{X}}, \dot{\mathbf{W}}, \dot{\mathbf{A}}) &= \sum_i \phi(\sigma_i(\dot{\mathbf{X}}), \gamma) + \lambda p(\dot{\mathbf{W}}) + \frac{1}{2\tau^2} \|\mathcal{P}_\Omega(\dot{\mathbf{Y}}) - \mathcal{P}_\Omega(\mathcal{A}(\dot{\mathbf{X}}))\|_{\mathbb{F}}^2 \\ &\quad + \langle \dot{\mathbf{A}}, \mathcal{W}(\dot{\mathbf{X}}) - \dot{\mathbf{W}} \rangle + \frac{\beta}{2} \|\mathcal{W}(\dot{\mathbf{X}}) - \dot{\mathbf{W}}\|_{\mathbb{F}}^2, \end{aligned}$$

Algorithm 1 Proximal linearized-ADMM(PL-ADMM) for SLRQA in (2)

Input: A noisy observed image $\dot{\mathbf{Y}}$; an initial iterate $\dot{\mathbf{X}}_0 := \dot{\mathbf{Y}}$; two parameters $\mu \in (0, 2)$ and $\beta > 0$; a tolerance $\eta > 0$; two sequences of regularization parameters $\{L_{1,k}\}$ and $\{L_{2,k}\}$ satisfying $\sup_{k \geq 0} L_{i,k} < \infty$ and $\inf_{k > 0} L_{i,k} > 0$ for $i = 1, 2$;

Output: A recovered image $\dot{\mathbf{X}}_*$;

- 1: Set $\dot{\mathbf{W}}_0 = \mathbf{0}$ and $\dot{\mathbf{\Lambda}}_0 = \mathbf{0}$;
- 2: **for** $k = 0, 1, 2, \dots$ **do**
- 3: $\dot{\mathbf{X}}$ -subproblem:

$$\begin{aligned} \dot{\mathbf{X}}_{k+1} \in \arg \min_{\dot{\mathbf{X}}} & \sum_i \phi(\sigma_i(\dot{\mathbf{X}}), \gamma) \\ & + \frac{1}{2\tau^2} \|\mathcal{P}_\Omega(\dot{\mathbf{Y}}) - \mathcal{P}_\Omega(\mathcal{A}(\dot{\mathbf{X}}))\|_{\mathbb{F}}^2 + \frac{\beta}{2} \|\mathcal{W}(\dot{\mathbf{X}}) - \dot{\mathbf{W}}_k + \frac{\dot{\mathbf{\Lambda}}_k}{\beta}\|_{\mathbb{F}}^2 + \frac{L_{1,k}}{2} \|\dot{\mathbf{X}} - \dot{\mathbf{X}}_k\|_{\mathbb{F}}^2; \end{aligned}$$

- 4: $\dot{\mathbf{W}}$ -subproblem:

$$\dot{\mathbf{W}}_{k+1} = \arg \min_{\dot{\mathbf{W}}} \lambda \left\langle \nabla p(\dot{\mathbf{W}}_k), \dot{\mathbf{W}} \right\rangle + \frac{\beta}{2} \|\dot{\mathbf{W}} - (\mathcal{W}(\dot{\mathbf{X}}_{k+1}) + \frac{\dot{\mathbf{\Lambda}}_k}{\beta})\|_{\mathbb{F}}^2 + \frac{L_{2,k}}{2} \|\dot{\mathbf{W}} - \dot{\mathbf{W}}_k\|_{\mathbb{F}}^2;$$

- 5: Update Lagrange multipliers: $\dot{\mathbf{\Lambda}}_{k+1} = \dot{\mathbf{\Lambda}}_k + \mu\beta(\mathcal{W}(\dot{\mathbf{X}}_{k+1}) - \dot{\mathbf{W}}_{k+1})$;
 - 6: **if** $\|\dot{\mathbf{X}}_{k+1} - \dot{\mathbf{X}}_k\|_{\mathbb{F}} + \|\dot{\mathbf{W}}_{k+1} - \dot{\mathbf{W}}_k\|_{\mathbb{F}} + \|\mathcal{W}(\dot{\mathbf{X}}_{k+1}) - \dot{\mathbf{W}}_{k+1}\|_{\mathbb{F}} < \eta$ **then**
 - 7: Return $\dot{\mathbf{X}}_* = \dot{\mathbf{X}}_{k+1}$;
 - 8: **end if**
 - 9: **end for**
-

where $\dot{\mathbf{\Lambda}} \in \mathbb{H}^{m \times n}$ denotes the Lagrange multipliers and $\beta > 0$.

In Step 3, $\dot{\mathbf{X}}_{k+1}$ is obtained by minimizing $\mathcal{L}_\beta(\dot{\mathbf{X}}, \dot{\mathbf{W}}, \dot{\mathbf{\Lambda}}) + \frac{L_{1,k}}{2} \|\dot{\mathbf{X}} - \dot{\mathbf{X}}_k\|_{\mathbb{F}}^2$ for a fixed $\dot{\mathbf{W}}_k$ and $\dot{\mathbf{\Lambda}}_k$. This subproblem does not yield a closed-form solution in general and therefore may be solved by nonsmooth algorithms such as a subgradient method or the linearized Bregman algorithm in [4]. If the linear operator \mathcal{A} in (2) is the identity and all pixels of the noisy image $\dot{\mathbf{Y}}$ are observed, i.e., Ω indicates the whole image, then the $\dot{\mathbf{X}}$ -subproblem can be solved efficiently. Specifically, the subproblem can be reformulated as

$$\begin{aligned} \dot{\mathbf{X}}_{k+1} = \arg \min_{\dot{\mathbf{X}}} & \sum_i \phi(\sigma_i(\dot{\mathbf{X}}), \gamma) + \\ & \frac{\tau^2(\beta + L_{1,k}) + 1}{2\tau^2} \left\| \dot{\mathbf{X}} - \frac{\tau^2}{\tau^2(\beta + L_{1,k}) + 1} \left(\frac{1}{\tau^2} \dot{\mathbf{Y}} + \beta \mathcal{W}^\#(\dot{\mathbf{W}}_k - \frac{\dot{\mathbf{\Lambda}}_k}{\beta}) + L_{1,k} \dot{\mathbf{X}}_k \right) \right\|_{\mathbb{F}}^2, \end{aligned} \tag{10}$$

If $\phi(\sigma_i(\dot{\mathbf{X}}), \gamma) = \sigma_i(\dot{\mathbf{X}})$, the $\dot{\mathbf{X}}$ -subproblem has a closed-form solution by using the soft thresholding method on the singular values [4]. When a nonconvex surrogate function $\phi(\sigma_i(\dot{\mathbf{X}}), \gamma)$ is used, the subproblem of $\dot{\mathbf{X}}$ can be solved via a convex-concave procedure(CCP) in [20]. For completeness, CCP is stated in Algorithm 2. Lemma 3.1 is crucial in CCP and it transforms the matrix

optimization problem of $\hat{\mathbf{X}}$ into an optimization problem of singular values.

Lemma 3.1 ([10]). *Let $\hat{\mathbf{X}} = \hat{\mathbf{U}}\hat{\Sigma}\hat{\mathbf{V}}^* \in \mathbb{H}^{m \times n}$ be a singular value decomposition of $\hat{\mathbf{X}}$. The solution of*

$$\arg \min_{\dot{\mathbf{X}} \in \mathbb{H}^{m \times n}} \sum_i \phi(\sigma_i(\dot{\mathbf{X}}), \gamma) + \frac{\mu}{2} \|\hat{\mathbf{X}} - \dot{\mathbf{X}}\|_{\mathbb{F}}^2 \quad (11)$$

can be represented by $\dot{\mathbf{X}}_* = \dot{\mathbf{U}}\dot{\Sigma}_*\dot{\mathbf{V}}^*$, where $(\dot{\Sigma}_*)_{i,i} = (\sigma_*)_i$, for $i = 1, \dots, \min\{m, n\}$ where σ_* is obtained by

$$\sigma_* = \arg \min_{\sigma \geq 0} \phi(\sigma, \gamma) + \frac{\mu}{2} \|\sigma - \sigma_{\hat{\mathbf{X}}}\|_2^2. \quad (12)$$

In the k -th iteration of Algorithm 2, the function $\phi(\sigma, \gamma)$ is approximated by a linearized function $\phi(\sigma_k, \gamma) + \nabla_{\sigma} \phi(\sigma_k, \gamma)^T \sigma$. It follows that the update of σ in Problem (12) at σ_k is given by

$$\sigma_{k+1} = \max \left\{ \sigma_{\hat{\mathbf{X}}} - \frac{\nabla_{\sigma} \phi(\sigma_k, \gamma)}{\mu}, \mathbf{0} \right\}. \quad (13)$$

It has been shown in [20, Theorem 4] that any limit points of $\{\sigma_k\}_{k=1}^{\infty}$ are stationary points of (12).

Algorithm 2 CCP to solve Problem (11)

Input: A quaternion matrix $\hat{\mathbf{X}} \in \mathbb{H}^{m \times n}$; a nonconvex function ϕ ; a constant $\mu > 0$; a tolerance η_C ; and an initial iterate $\sigma_0 = \mathbf{0}$;

Output: $\dot{\mathbf{X}}_*$;

- 1: Compute QSVD $\hat{\mathbf{X}} = \hat{\mathbf{U}}\hat{\Sigma}\hat{\mathbf{V}}^*$ and let $\sigma_{\hat{\mathbf{X}}}$ satisfy $\hat{\Sigma} = \text{diag}(\sigma_{\hat{\mathbf{X}}})$;
 - 2: **for** $k = 1, 2, \dots$ **do**
 - 3: Compute σ_k by (13);
 - 4: **if** $\|\sigma_{k-1} - \sigma_k\|_2 < \eta_C$ **then**
 - 5: Set $\sigma_* = \sigma_k$ and return $\dot{\mathbf{X}}_* = \dot{\mathbf{U}}\dot{\Sigma}_*\dot{\mathbf{V}}^*$, where $\dot{\Sigma}_* = \text{diag}(\sigma_*)$;
 - 6: **end if**
 - 7: **end for**
-

In Step 4, the $\dot{\mathbf{W}}$ -subproblem approximately minimizes $\mathcal{L}_{\beta}(\dot{\mathbf{X}}, \dot{\mathbf{W}}, \dot{\mathbf{A}}) + \frac{L_{2,k}}{2} \|\dot{\mathbf{W}} - \dot{\mathbf{W}}_k\|_{\mathbb{F}}^2$ for a fixed $\dot{\mathbf{X}}_{k+1}$ and $\dot{\mathbf{A}}_k$. Specifically, the objective function of the $\dot{\mathbf{W}}$ -subproblem is obtained by using a linearized strategy for $p(\dot{\mathbf{W}})$ in $\mathcal{L}_{\beta}(\dot{\mathbf{X}}, \dot{\mathbf{W}}, \dot{\mathbf{A}}) + \frac{L_{2,k}}{2} \|\dot{\mathbf{W}} - \dot{\mathbf{W}}_k\|_{\mathbb{F}}^2$. It follows that $\dot{\mathbf{W}}_{k+1}$ has a closed form solution

$$\dot{\mathbf{W}}_{k+1} = \frac{1}{\beta + L_{2,k}} \left(\beta \mathcal{W}(\dot{\mathbf{X}}_{k+1}) + \dot{\mathbf{A}}_k + L_{2,k} \dot{\mathbf{W}}_k \right) - \frac{\lambda}{\beta + L_{2,k}} \nabla p(\dot{\mathbf{W}}_k). \quad (14)$$

Step 5 is used to update the Lagrange multipliers. The difference between the classic ADMM for convex function and PL-ADMM is that $\mu \in (0, 2)$ in PL-ADMM rather than $\mu \in (0, \frac{\sqrt{5}+1}{2})$ [8].

4 Convergence analysis

The global convergence is established for a generalization of SLRQA in (2):

$$\begin{aligned} \min_{\dot{\mathbf{X}}, \dot{\mathbf{W}}} \quad & f(\dot{\mathbf{X}}) + g(\dot{\mathbf{W}}) + \frac{1}{2\tau^2} \|\mathcal{P}_\Omega(\mathcal{A}(\dot{\mathbf{X}})) - \mathcal{P}_\Omega(\dot{\mathbf{Y}})\|_{\mathbb{F}}^2, \\ \text{s.t.} \quad & \mathcal{C}(\dot{\mathbf{X}}) + \mathcal{B}(\dot{\mathbf{W}}) = \dot{\mathbf{B}}, \end{aligned} \quad (15)$$

where f is continuous and g is continuously differentiable, $\mathcal{C}, \mathcal{B} : \mathbb{H}^{m \times n} \rightarrow \mathbb{H}^{m \times n}$ are given linear maps and $\dot{\mathbf{B}} \in \mathbb{H}^{m \times n}$. Specifically, if $f(\dot{\mathbf{X}}) = \sum_i \phi(\sigma_i(\dot{\mathbf{X}}), \gamma)$, $g(\dot{\mathbf{W}}) = p(\dot{\mathbf{W}})$, $\mathcal{B} = -\mathbf{I}$, $\mathcal{C} = \mathcal{W}$, and $\dot{\mathbf{B}} = \mathbf{0}$, then Problem (15) becomes the SLRQA in (2).

The augmented Lagrangian function of (15) is

$$\begin{aligned} \mathcal{L}_\beta(\dot{\mathbf{X}}, \dot{\mathbf{W}}, \dot{\mathbf{A}}) &= f(\dot{\mathbf{X}}) + g(\dot{\mathbf{W}}) + \frac{1}{2\tau^2} \|\mathcal{P}_\Omega(\mathcal{A}(\dot{\mathbf{X}})) - \mathcal{P}_\Omega(\dot{\mathbf{Y}})\|_{\mathbb{F}}^2 + \left\langle \dot{\mathbf{A}}, \mathcal{C}(\dot{\mathbf{X}}) + \mathcal{B}(\dot{\mathbf{W}}) - \dot{\mathbf{B}} \right\rangle \\ &+ \frac{\beta}{2} \|\mathcal{C}(\dot{\mathbf{X}}) + \mathcal{B}(\dot{\mathbf{W}}) - \dot{\mathbf{B}}\|_{\mathbb{F}}^2 \\ &= f(\dot{\mathbf{X}}) + g(\dot{\mathbf{W}}) + \frac{1}{2\tau^2} \|\mathcal{P}_\Omega(\mathcal{A}(\dot{\mathbf{X}})) - \mathcal{P}_\Omega(\dot{\mathbf{Y}})\|_{\mathbb{F}}^2 + \frac{\beta}{2} \left\| \mathcal{C}(\dot{\mathbf{X}}) + \mathcal{B}(\dot{\mathbf{W}}) - \dot{\mathbf{B}} + \frac{\dot{\mathbf{A}}}{\beta} \right\|_{\mathbb{F}}^2 - \frac{1}{2\beta} \|\dot{\mathbf{A}}\|_{\mathbb{F}}^2. \end{aligned} \quad (16)$$

The proposed PL-ADMM for (15) is

$$\begin{aligned} \dot{\mathbf{X}}_{k+1} &\in \arg \min_{\dot{\mathbf{X}}} f(\dot{\mathbf{X}}) + \frac{1}{2\tau^2} \|\mathcal{P}_\Omega(\mathcal{A}(\dot{\mathbf{X}})) - \mathcal{P}_\Omega(\dot{\mathbf{Y}})\|_{\mathbb{F}}^2 \\ &+ \frac{\beta}{2} \left\| \mathcal{C}(\dot{\mathbf{X}}) + \mathcal{B}(\dot{\mathbf{W}}_k) - \dot{\mathbf{B}} + \frac{\dot{\mathbf{A}}_k}{\beta} \right\|_{\mathbb{F}}^2 + \frac{L_{1,k}}{2} \|\dot{\mathbf{X}} - \dot{\mathbf{X}}_k\|_{\mathbb{F}}^2, \\ \dot{\mathbf{W}}_{k+1} &\in \arg \min_{\dot{\mathbf{W}}} \left\langle \nabla g(\dot{\mathbf{W}}_k), \dot{\mathbf{W}} \right\rangle + \frac{\beta}{2} \left\| \mathcal{C}(\dot{\mathbf{X}}_{k+1}) + \mathcal{B}(\dot{\mathbf{W}}) - \dot{\mathbf{B}} + \frac{\dot{\mathbf{A}}_k}{\beta} \right\|_{\mathbb{F}}^2 + \frac{L_{2,k}}{2} \|\dot{\mathbf{W}} - \dot{\mathbf{W}}_k\|_{\mathbb{F}}^2, \\ \dot{\mathbf{A}}_{k+1} &= \dot{\mathbf{A}}_k + \mu\beta \cdot (\mathcal{C}(\dot{\mathbf{X}}_{k+1}) + \mathcal{B}(\dot{\mathbf{W}}_{k+1}) - \dot{\mathbf{B}}), \end{aligned} \quad (17)$$

which is a generalization of Algorithm 1.

The choices of β , $L_{1,k}$ and $L_{2,k}$ are crucial for the convergence of (17). Generally speaking, β should be chosen large enough, and $L_{1,k}$, $L_{2,k}$ should be chosen in a suitable range. In order to give the conditions of β and $L_{1,k}$, $L_{2,k}$, we introduce the following notations. Let $q_i := \sup_{k \geq 0} L_{i,k} < \infty$ and $q_i^- := \inf_{k > 0} L_{i,k} > 0$ for $i = 1, 2$. Define $\lambda_+^{\mathcal{B}^\# \mathcal{B}}$ as the smallest positive eigenvalue of $\mathcal{B}^\# \mathcal{B}$, and $\rho(\mu) := 1 - |\mu|$. For any sequence $\{\dot{\mathbf{U}}_k\}_{k \geq 0}$, define Δ operator by $\Delta \dot{\mathbf{U}}_k := \dot{\mathbf{U}}_k - \dot{\mathbf{U}}_{k-1}$.

The assumptions for the convergence analysis are given in Assumption 4.1, including the conditions of β , $L_{1,k}$, and $L_{2,k}$.

Assumption 4.1.

A1 The continuous function $f(\dot{\mathbf{X}})$ is coercive, i.e. $f(\dot{\mathbf{X}}) \rightarrow \infty$ if $\|\dot{\mathbf{X}}\|_{\mathbb{F}} \rightarrow \infty$, and $g(\dot{\mathbf{W}})$ is bounded from below.

A2 $g(\dot{\mathbf{W}})$ has L_g Lipschitz continuous gradient, i.e., for every $\dot{\mathbf{W}}_1, \dot{\mathbf{W}}_2$, it holds that

$$\|\nabla g(\dot{\mathbf{W}}_1) - \nabla g(\dot{\mathbf{W}}_2)\|_{\mathbb{F}} \leq L_g \|\dot{\mathbf{W}}_1 - \dot{\mathbf{W}}_2\|_{\mathbb{F}}. \quad (18)$$

It has been shown in [2, Lemma 5.7] that (18) implies that for every $\dot{\mathbf{W}}_1$ and $\dot{\mathbf{W}}_2$, it holds that

$$g(\dot{\mathbf{W}}_1) \leq g(\dot{\mathbf{W}}_2) + \langle \nabla g(\dot{\mathbf{W}}_2), \dot{\mathbf{W}}_1 - \dot{\mathbf{W}}_2 \rangle + \frac{L_g}{2} \|\dot{\mathbf{W}}_1 - \dot{\mathbf{W}}_2\|_{\mathbb{F}}^2. \quad (19)$$

A3 The matrix $\mathcal{B}^\# \mathcal{B}$ is full rank, $\text{range}(\mathcal{C}) \subseteq \text{range}(\mathcal{B})$, and $\dot{\mathbf{B}} \in \text{range}(\mathcal{B})$.

A4 The parameters $\beta > 0$, $\mu \in (0, 2)$, and there exist three constants $a_1 > 0$, $a_2 > 0$, and $r > 1$ such that

$$q_1^- \mathbf{I} \succeq a_1 \mathbf{I} \quad \text{and} \quad q_2^- \mathbf{I} + \beta \mathcal{B}^\# \mathcal{B} - (r\theta_0 + r\theta_1 + L_g) \mathbf{I} \succeq a_2 \mathbf{I}, \quad (20)$$

where \mathbf{I} is the identity matrix with correct size,

$$\theta_0 := \frac{2\mu(q_2 + L_g)^2}{\beta \lambda_{+}^{\mathcal{B}^\# \mathcal{B}} (\rho(\mu))^2}, \quad \text{and} \quad \theta_1 := \frac{2\mu q_2^2}{\beta \lambda_{+}^{\mathcal{B}^\# \mathcal{B}} (\rho(\mu))^2}. \quad (21)$$

A5 The parameter β satisfies $\beta > \frac{2L_g}{\lambda_{+}^{\mathcal{B}^\# \mathcal{B}} \rho(\mu)}$.

One can verify that A1, A2, and A3 in Assumption 4.1 are satisfied for SLRQA in (2). If β is chosen sufficiently large and the sequences $\{L_{1,k}\}$ and $\{L_{2,k}\}$ are chosen such that q_i^-, q_i , $i = 1, 2$ in suitable range, then A4 and A5 in Assumption 4.1 are also satisfied. For example, if set $L_{1,k} = L_{2,k} = 1$ for all k and let

$$\beta > \max \left\{ \frac{2L_g}{\lambda_{+}^{\mathcal{B}^\# \mathcal{B}} \rho(\mu)}, \frac{r(2\mu(1 + L_g)^2 + 2\mu)}{(\lambda_{+}^{\mathcal{B}^\# \mathcal{B}})^2 (\rho(\mu))^2} + \frac{L_g}{\lambda_{+}^{\mathcal{B}^\# \mathcal{B}}}, 1 \right\},$$

then A4 and A5 in Assumption 4.1 hold. Therefore, Assumption 4.1 is reasonable.

Lemmas 4.1 and 4.2 show that the augmented Lagrangian function \mathcal{L}_β is sufficiently descent when updating $\dot{\mathbf{W}}$ and $\dot{\mathbf{X}}$. They are used in Lemma 4.3 for bounding $\mathcal{L}_\beta(\dot{\mathbf{X}}_{k+1}, \dot{\mathbf{W}}_{k+1}, \dot{\mathbf{\Lambda}}_{k+1}) - \mathcal{L}_\beta(\dot{\mathbf{X}}_k, \dot{\mathbf{W}}_k, \dot{\mathbf{\Lambda}}_k)$.

Lemma 4.1 (Sufficient descent of \mathcal{L}_β for $\dot{\mathbf{X}}$ update). *The sequence $\{(\dot{\mathbf{X}}_k, \dot{\mathbf{W}}_k, \dot{\mathbf{\Lambda}}_k)\}_{k \geq 0}$ generated by (17) satisfies:*

$$\mathcal{L}_\beta(\dot{\mathbf{X}}_k, \dot{\mathbf{W}}_k, \dot{\mathbf{\Lambda}}_k) - \mathcal{L}_\beta(\dot{\mathbf{X}}_{k+1}, \dot{\mathbf{W}}_k, \dot{\mathbf{\Lambda}}_k) \geq \frac{L_{1,k}}{2} \|\Delta \dot{\mathbf{X}}_{k+1}\|_{\mathbb{F}}^2.$$

Proof. According to the $\dot{\mathbf{X}}_{k+1}$ update in (17), the following inequality holds:

$$\begin{aligned} & f(\dot{\mathbf{X}}_{k+1}) - f(\dot{\mathbf{X}}_k) + \frac{\beta}{2} \|\mathcal{C}(\dot{\mathbf{X}}_{k+1}) + \mathcal{B}(\dot{\mathbf{W}}_k) - \dot{\mathbf{B}} + \dot{\mathbf{\Lambda}}_k / \beta\|_{\mathbb{F}}^2 + \frac{L_{1,k}}{2} \|\Delta \dot{\mathbf{X}}_{k+1}\|_{\mathbb{F}}^2 \\ & + \frac{1}{2\tau^2} \|\mathcal{P}_\Omega((\mathcal{A}(\dot{\mathbf{X}}_{k+1}) - \dot{\mathbf{Y}}))\|_{\mathbb{F}}^2 \leq \frac{\beta}{2} \|\mathcal{C}(\dot{\mathbf{X}}_k) + \mathcal{B}(\dot{\mathbf{W}}_k) - \dot{\mathbf{B}} + \dot{\mathbf{\Lambda}}_k / \beta\|_{\mathbb{F}}^2 + \frac{1}{2\tau^2} \|\mathcal{P}_\Omega((\mathcal{A}(\dot{\mathbf{X}}_k) - \dot{\mathbf{Y}}))\|_{\mathbb{F}}^2. \end{aligned} \quad (22)$$

It follows that

$$\begin{aligned}
& \mathcal{L}_\beta(\dot{\mathbf{X}}_k, \dot{\mathbf{W}}_k, \dot{\mathbf{\Lambda}}_k) - \mathcal{L}_\beta(\dot{\mathbf{X}}_{k+1}, \dot{\mathbf{W}}_k, \dot{\mathbf{\Lambda}}_k) \\
&= f(\dot{\mathbf{X}}_k) - f(\dot{\mathbf{X}}_{k+1}) + \frac{1}{2\tau^2} \|\mathcal{P}_\Omega((\mathcal{A}(\dot{\mathbf{X}}_k) - \dot{\mathbf{Y}}))\|_{\mathbb{F}}^2 - \frac{1}{2\tau^2} \|\mathcal{P}_\Omega((\mathcal{A}(\dot{\mathbf{X}}_{k+1}) - \dot{\mathbf{Y}}))\|_{\mathbb{F}}^2 \\
&- \frac{\beta}{2} \|\mathcal{C}(\dot{\mathbf{X}}_{k+1}) + \mathcal{B}(\dot{\mathbf{W}}_k) - \dot{\mathbf{B}} + \dot{\mathbf{\Lambda}}_k/\beta\|_{\mathbb{F}}^2 + \frac{\beta}{2} \|\mathcal{C}(\dot{\mathbf{X}}_k) + \mathcal{B}(\dot{\mathbf{W}}_k) - \dot{\mathbf{B}} + \dot{\mathbf{\Lambda}}_k/\beta\|_{\mathbb{F}}^2 \geq \frac{L_{1,k}}{2} \|\Delta \dot{\mathbf{X}}_{k+1}\|^2,
\end{aligned}$$

which completes the proof. \square

Lemma 4.2 (Sufficient descent of \mathcal{L}_β for $\dot{\mathbf{W}}$ update). *Suppose A2 in Assumption 4.1 holds. The sequence $\{(\dot{\mathbf{X}}_k, \dot{\mathbf{W}}_k, \dot{\mathbf{\Lambda}}_k)\}_{k \geq 0}$ generated by (17) satisfies:*

$$\mathcal{L}_\beta(\dot{\mathbf{X}}_{k+1}, \dot{\mathbf{W}}_k, \dot{\mathbf{\Lambda}}_k) - \mathcal{L}_\beta(\dot{\mathbf{X}}_{k+1}, \dot{\mathbf{W}}_{k+1}, \dot{\mathbf{\Lambda}}_k) \geq \|\Delta \dot{\mathbf{W}}_{k+1}\|_{B_k}^2,$$

where $B_k := L_{2,k} \mathbf{I} - L_g \mathbf{I} + \frac{\beta}{2} \mathcal{B} \mathcal{B}^\#$.

Proof. According to the optimality condition of $\dot{\mathbf{W}}_{k+1}$, the following equality holds:

$$\nabla g(\dot{\mathbf{W}}_k) + \beta \mathcal{B}^\#(\mathcal{C}(\dot{\mathbf{X}}_{k+1}) + \mathcal{B}(\dot{\mathbf{W}}_{k+1}) - \dot{\mathbf{B}} + \dot{\mathbf{\Lambda}}_k/\beta) + L_{2,k} \Delta \dot{\mathbf{W}}_{k+1} = 0. \quad (23)$$

It follows that

$$\begin{aligned}
& \mathcal{L}_\beta(\dot{\mathbf{X}}_{k+1}, \dot{\mathbf{W}}_k, \dot{\mathbf{\Lambda}}_k) - \mathcal{L}_\beta(\dot{\mathbf{X}}_{k+1}, \dot{\mathbf{W}}_{k+1}, \dot{\mathbf{\Lambda}}_k) \\
&= g(\dot{\mathbf{W}}_k) - g(\dot{\mathbf{W}}_{k+1}) + \frac{\beta}{2} \|\mathcal{C}(\dot{\mathbf{X}}_{k+1}) + \mathcal{B}(\dot{\mathbf{W}}_k) - \dot{\mathbf{B}} + \frac{\dot{\mathbf{\Lambda}}_k}{\beta}\|_{\mathbb{F}}^2 - \frac{\beta}{2} \|\mathcal{C}(\dot{\mathbf{X}}_{k+1}) + \mathcal{B}(\dot{\mathbf{W}}_{k+1}) - \dot{\mathbf{B}} + \frac{\dot{\mathbf{\Lambda}}_k}{\beta}\|_{\mathbb{F}}^2 \\
&= g(\dot{\mathbf{W}}_k) - g(\dot{\mathbf{W}}_{k+1}) + \frac{\beta}{2} \|\mathcal{B}(\Delta \dot{\mathbf{W}}_{k+1})\|_{\mathbb{F}}^2 - \beta \left\langle \mathcal{B}^\#(\mathcal{C}(\dot{\mathbf{X}}_{k+1}) + \mathcal{B}(\dot{\mathbf{W}}_{k+1}) - \dot{\mathbf{B}} + \frac{\dot{\mathbf{\Lambda}}_k}{\beta}), \Delta \dot{\mathbf{W}}_{k+1} \right\rangle \\
&= g(\dot{\mathbf{W}}_k) - g(\dot{\mathbf{W}}_{k+1}) + \left\langle \nabla g(\dot{\mathbf{W}}_k), \Delta \dot{\mathbf{W}}_{k+1} \right\rangle + L_{2,k} \|\Delta \dot{\mathbf{W}}_{k+1}\|_{\mathbb{F}}^2 + \frac{\beta}{2} \|\mathcal{B} \Delta \dot{\mathbf{W}}_{k+1}\|_{\mathbb{F}}^2 \quad (\text{by (23)}) \\
&\geq \|\Delta \dot{\mathbf{W}}_{k+1}\|_{B_k}^2, \quad (\text{by Assumption A2})
\end{aligned}$$

which completes the proof. \square

Lemma 4.3 is used in Lemma 4.4, which is crucial for constructing a merit function.

Lemma 4.3. *Suppose A2 in Assumption 4.1 holds. The sequence $\{(\dot{\mathbf{X}}_k, \dot{\mathbf{W}}_k, \dot{\mathbf{\Lambda}}_k)\}_{k \geq 0}$ generated by (17) satisfies:*

$$\mathcal{L}_\beta(\dot{\mathbf{X}}_{k+1}, \dot{\mathbf{W}}_{k+1}, \dot{\mathbf{\Lambda}}_{k+1}) \leq \mathcal{L}_\beta(\dot{\mathbf{X}}_k, \dot{\mathbf{W}}_k, \dot{\mathbf{\Lambda}}_k) - \|\Delta \dot{\mathbf{W}}_{k+1}\|_{B_k}^2 - \frac{L_{1,k}}{2} \|\Delta \dot{\mathbf{X}}_{k+1}\|_{\mathbb{F}}^2 + \frac{1}{\beta \mu} \|\Delta \dot{\mathbf{\Lambda}}_{k+1}\|_{\mathbb{F}}^2.$$

Proof. According to the update of $\dot{\mathbf{\Lambda}}$ in (17), Lemma 4.1, and Lemma 4.2, we have

$$\begin{aligned}
\mathcal{L}_\beta(\dot{\mathbf{X}}_{k+1}, \dot{\mathbf{W}}_{k+1}, \dot{\mathbf{\Lambda}}_{k+1}) &= \mathcal{L}_\beta(\dot{\mathbf{X}}_{k+1}, \dot{\mathbf{W}}_{k+1}, \dot{\mathbf{\Lambda}}_k) + \frac{1}{\beta \mu} \|\Delta \dot{\mathbf{\Lambda}}_{k+1}\|_{\mathbb{F}}^2 \\
&\leq \mathcal{L}_\beta(\dot{\mathbf{X}}_k, \dot{\mathbf{W}}_k, \dot{\mathbf{\Lambda}}_k) - \|\Delta \dot{\mathbf{W}}_{k+1}\|_{B_k}^2 - \frac{L_{1,k}}{2} \|\Delta \dot{\mathbf{X}}_{k+1}\|_{\mathbb{F}}^2 + \frac{1}{\beta \mu} \|\Delta \dot{\mathbf{\Lambda}}_{k+1}\|_{\mathbb{F}}^2.
\end{aligned}$$

\square

Lemma 4.4. *Suppose A2, A3 in Assumption 4.1 hold, the sequence $\{(\dot{\mathbf{X}}_{k+1}, \dot{\mathbf{W}}_{k+1}, \dot{\mathbf{\Lambda}}_{k+1})\}_{k \geq 0}$ generated by (17) satisfies:*

$$\frac{1}{\beta\mu} \|\dot{\mathbf{\Lambda}}_{k+1}\|_{\mathbb{F}}^2 \leq \theta_0 \|\Delta \dot{\mathbf{W}}_k\|_{\mathbb{F}}^2 + \theta_1 \|\Delta \dot{\mathbf{W}}_{k+1}\|_{\mathbb{F}}^2 + \theta_2 \|\mathcal{B}^\#(\Delta \dot{\mathbf{\Lambda}}_k)\|_{\mathbb{F}}^2 - \theta_2 \|\mathcal{B}^\#(\Delta \dot{\mathbf{\Lambda}}_{k+1})\|_{\mathbb{F}}^2, \quad (24)$$

$$\begin{aligned} \mathcal{L}_\beta(\dot{\mathbf{X}}_{k+1}, \dot{\mathbf{W}}_{k+1}, \dot{\mathbf{\Lambda}}_{k+1}) + \|\Delta \dot{\mathbf{W}}_{k+1}\|_{B_{k-r\theta_1 \mathbf{I}}}^2 + \frac{L_{1,k}}{2} \|\Delta \dot{\mathbf{X}}_{k+1}\|_{\mathbb{F}}^2 + \frac{r-1}{\beta\mu} \|\Delta \dot{\mathbf{\Lambda}}_{k+1}\|_{\mathbb{F}}^2 \\ + r\theta_2 \|\mathcal{B}^\# \Delta \dot{\mathbf{\Lambda}}_{k+1}\|_{\mathbb{F}}^2 \leq \mathcal{L}_\beta(\dot{\mathbf{X}}_k, \dot{\mathbf{W}}_k, \dot{\mathbf{\Lambda}}_k) + r\theta_0 \|\Delta \dot{\mathbf{W}}_k\|_{\mathbb{F}}^2 + r\theta_2 \|\mathcal{B}^\#(\Delta \dot{\mathbf{\Lambda}}_k)\|_{\mathbb{F}}^2, \end{aligned} \quad (25)$$

where $r > 1, \theta_0, \theta_1$ are defined in (21), and $\theta_2 := \frac{|1-\mu|}{\beta\mu\lambda_+^{\mathcal{B}^\# \mathcal{B}} \rho(\mu)}$.

Proof. Let $k \geq 1$ be fixed and define the matrix

$$\dot{\mathbf{G}}_{k+1} := -L_{2,k} \Delta \dot{\mathbf{W}}_{k+1} - \nabla g(\dot{\mathbf{W}}_k). \quad (26)$$

It follows that $\Delta \dot{\mathbf{G}}_{k+1} = L_{2,k-1} \Delta \dot{\mathbf{W}}_k - L_{2,k} \Delta \dot{\mathbf{W}}_{k+1} + \nabla g(\dot{\mathbf{W}}_{k-1}) - \nabla g(\dot{\mathbf{W}}_k)$. By the triangle inequality, the following inequality holds:

$$\|\Delta \dot{\mathbf{G}}_{k+1}\|_{\mathbb{F}} \leq \|\nabla g(\dot{\mathbf{W}}_{k-1}) - \nabla g(\dot{\mathbf{W}}_k)\|_{\mathbb{F}} + L_{2,k} \|\Delta \dot{\mathbf{W}}_{k+1}\|_{\mathbb{F}} + L_{2,k-1} \|\Delta \dot{\mathbf{W}}_k\|_{\mathbb{F}}.$$

By A2 in Assumption 4.1, $\nabla g(\dot{\mathbf{W}})$ is L_g Lipschitz continuous and $q_2 = \sup_{k \geq 0} L_{2,k} < \infty$, we have $\|\Delta \dot{\mathbf{G}}_{k+1}\|_{\mathbb{F}} \leq (L_g + q_2) \|\Delta \dot{\mathbf{W}}_k\|_{\mathbb{F}} + q_2 \|\Delta \dot{\mathbf{W}}_{k+1}\|_{\mathbb{F}}$. Hence it follows that:

$$\|\Delta \dot{\mathbf{G}}_{k+1}\|_{\mathbb{F}}^2 \leq 2(L_g + q_2)^2 \|\Delta \dot{\mathbf{W}}_k\|_{\mathbb{F}}^2 + 2q_2^2 \|\Delta \dot{\mathbf{W}}_{k+1}\|_{\mathbb{F}}^2. \quad (27)$$

Expressing the optimality condition of $\dot{\mathbf{W}}$ subproblem using $\dot{\mathbf{G}}_{k+1}$, we have $\dot{\mathbf{G}}_{k+1} = \beta \mathcal{B}^\#(\mathcal{C}(\dot{\mathbf{X}}_{k+1}) + \mathcal{B}(\dot{\mathbf{W}}_{k+1}) - \dot{\mathbf{B}} + \dot{\mathbf{\Lambda}}_k/\beta)$. Combining this with the $\dot{\mathbf{\Lambda}}$ update, we obtain

$$\mathcal{B}^\# \dot{\mathbf{\Lambda}}_{k+1} = \mu \dot{\mathbf{G}}_{k+1} + (1 - \mu) \mathcal{B}^\# \dot{\mathbf{\Lambda}}_k. \quad (28)$$

It follows that $\mathcal{B}^\# \Delta \dot{\mathbf{\Lambda}}_{k+1} = \mu \Delta \dot{\mathbf{G}}_{k+1} + (1 - \mu) \mathcal{B}^\# \Delta \dot{\mathbf{\Lambda}}_k$. Since $\mu \in (0, 2)$, we have

$$\mathcal{B}^\# \Delta \dot{\mathbf{\Lambda}}_{k+1} = \rho(\mu) \cdot \frac{\mu \Delta \dot{\mathbf{G}}_{k+1}}{\rho(\mu)} + |1 - \mu| \cdot (\text{sign}(1 - \mu) \mathcal{B}^\# \Delta \dot{\mathbf{\Lambda}}_k),$$

By the convexity of $\|\cdot\|_{\mathbb{F}}^2$, the update of $\dot{\mathbf{\Lambda}}$ in (17) and A3 in Assumption 4.1, it follows that $\Delta \dot{\mathbf{\Lambda}}_{k+1} \in \text{range}(\mathcal{B})$. Hence, the following inequalities hold

$$\begin{aligned} \lambda_+^{\mathcal{B}^\# \mathcal{B}} \rho(\mu) \|\Delta \dot{\mathbf{\Lambda}}_{k+1}\|_{\mathbb{F}}^2 &\leq \rho(\mu) \|\mathcal{B}^\# \Delta \dot{\mathbf{\Lambda}}_{k+1}\|_{\mathbb{F}}^2 = \|\mathcal{B}^\# \Delta \dot{\mathbf{\Lambda}}_{k+1}\|_{\mathbb{F}}^2 - |1 - \mu| \|\mathcal{B}^\# \Delta \dot{\mathbf{\Lambda}}_{k+1}\|_{\mathbb{F}}^2 \\ &\leq \frac{\mu^2}{\rho(\mu)} \|\Delta \dot{\mathbf{G}}_{k+1}\|_{\mathbb{F}}^2 + |1 - \mu| \|\mathcal{B}^\# \Delta \dot{\mathbf{\Lambda}}_k\|_{\mathbb{F}}^2 - |1 - \mu| \|\mathcal{B}^\# \Delta \dot{\mathbf{\Lambda}}_{k+1}\|_{\mathbb{F}}^2, \end{aligned} \quad (29)$$

where the first inequality follows from A3 in Assumption 4.1 and the definition of $\lambda_+^{\mathcal{B}^\# \mathcal{B}}$. Dividing both sides of (29) by $\beta\mu\lambda_+^{\mathcal{B}^\# \mathcal{B}} \rho(\mu)$ and using (27) yield (24). Finally, Inequality (25) follows by multiplying the inequality (24) by $r > 1$ and combining it with Lemma 4.3. \square

Let $\mathcal{R}(\dot{\mathbf{X}}, \dot{\mathbf{W}}, \dot{\mathbf{\Lambda}}, \dot{\mathbf{W}}', \dot{\mathbf{\Lambda}}') := \mathcal{L}_\beta(\dot{\mathbf{X}}, \dot{\mathbf{W}}, \dot{\mathbf{\Lambda}}) + r\theta_0 \|\dot{\mathbf{W}} - \dot{\mathbf{W}}'\|_{\mathbb{F}}^2 + r\theta_2 \|\mathcal{B}^\#(\dot{\mathbf{\Lambda}} - \dot{\mathbf{\Lambda}}')\|_{\mathbb{F}}^2$. The merit function \mathcal{R}_k is defined by

$$\mathcal{R}_k := \mathcal{R}(\dot{\mathbf{X}}_k, \dot{\mathbf{W}}_k, \dot{\mathbf{\Lambda}}_k, \dot{\mathbf{W}}_{k-1}, \dot{\mathbf{\Lambda}}_{k-1}) = \mathcal{L}_\beta(\dot{\mathbf{X}}_k, \dot{\mathbf{W}}_k, \dot{\mathbf{\Lambda}}_k) + r\theta_0 \|\Delta \dot{\mathbf{W}}_k\|_{\mathbb{F}}^2 + r\theta_2 \|\mathcal{B}^\# \Delta \dot{\mathbf{\Lambda}}_k\|_{\mathbb{F}}^2. \quad (30)$$

If Assumption 4.1 holds, then it can be shown that the merit function is descent. Specifically, we have

$$\begin{aligned} & \mathcal{R}_{k+1} + a \left(\|\Delta \dot{\mathbf{X}}_{k+1}\|_{\mathbb{F}}^2 + \|\Delta \dot{\mathbf{W}}_{k+1}\|_{\mathbb{F}}^2 + \|\Delta \dot{\mathbf{\Lambda}}_{k+1}\|_{\mathbb{F}}^2 \right) \\ & \leq \mathcal{R}_{k+1} + \|\Delta \dot{\mathbf{W}}_{k+1}\|_{\mathcal{B}_{k-r(\theta_1+\theta_0)\mathbf{I}}}^2 + \frac{L_{1,k}}{2} \|\Delta \dot{\mathbf{X}}_{k+1}\|_{\mathbb{F}}^2 + \frac{r-1}{\beta\mu} \|\Delta \dot{\mathbf{\Lambda}}_{k+1}\|_{\mathbb{F}}^2 \leq \mathcal{R}_k \leq \mathcal{R}_{k_0}, \end{aligned} \quad (31)$$

where $a = \min\{a_1, a_2, \frac{r-1}{\beta\mu}\}$ and a_1, a_2 are defined in Assumption 4.1, the first inequality follows from A4, A5 in Assumption 4.1, the second inequality follows from Lemma 4.4, and the third inequality is due to induction of $\mathcal{R}_k \leq \mathcal{R}_{k+1}$ for any $k \geq k_0$.

Theorem 4.1 (Bounded sequence of $\{\dot{\mathbf{X}}_k, \dot{\mathbf{W}}_k, \dot{\mathbf{\Lambda}}_k\}_{k \geq 0}$). *Assume Assumption 4.1 holds. The sequence $\{\dot{\mathbf{X}}_k, \dot{\mathbf{W}}_k, \dot{\mathbf{\Lambda}}_k\}_{k \geq 0}$ generated by (17) is bounded.*

Proof. According to (31), there exists $k_0 \geq 1$ such that $\mathcal{R}_{k+1} \leq \mathcal{R}_{k_0}$ for all $k \geq k_0$. Hence the following inequality holds:

$$\begin{aligned} & f(\dot{\mathbf{X}}_{k+1}) + g(\dot{\mathbf{W}}_{k+1}) + \frac{1}{2\tau^2} \|\mathcal{P}_\Omega(\mathcal{A}(\dot{\mathbf{X}}_k)) - \mathcal{P}_\Omega(\dot{\mathbf{Y}})\|_{\mathbb{F}}^2 + \frac{\beta}{2} \left\| \mathcal{C}(\dot{\mathbf{X}}_{k+1}) + \mathcal{B}(\dot{\mathbf{W}}_{k+1}) - \dot{\mathbf{B}} + \frac{\dot{\mathbf{\Lambda}}_{k+1}}{\beta} \right\|_{\mathbb{F}}^2 \\ & - \frac{1}{2\beta} \|\dot{\mathbf{\Lambda}}_{k+1}\|_{\mathbb{F}}^2 + (r\theta_0 + a) \|\Delta \dot{\mathbf{W}}_{k+1}\|_{\mathbb{F}}^2 + a(\|\Delta \dot{\mathbf{X}}_{k+1}\|_{\mathbb{F}}^2 + \|\Delta \dot{\mathbf{\Lambda}}_{k+1}\|_{\mathbb{F}}^2) + r\theta_2 \|\mathcal{B}^\# \Delta \dot{\mathbf{\Lambda}}_{k+1}\|_{\mathbb{F}}^2 \leq \mathcal{R}_{k_0}. \end{aligned} \quad (32)$$

According to (28), we have

$$\mu \mathcal{B}^\# \dot{\mathbf{\Lambda}}_{k+1} = \mu \dot{\mathbf{G}}_{k+1} + (1 - \mu) \mathcal{B}^\# (\dot{\mathbf{\Lambda}}_k - \dot{\mathbf{\Lambda}}_{k+1}). \quad (33)$$

Since $\mu \in (0, 2)$, Equation (33) can be rewritten as:

$$\mu \mathcal{B}^\# \dot{\mathbf{\Lambda}}_{k+1} = \rho(\mu) \frac{\mu \dot{\mathbf{G}}_{k+1}}{\rho(\mu)} + |1 - \mu| \left(\text{sign}(1 - \mu) \mathcal{B}^\# (\dot{\mathbf{\Lambda}}_k - \dot{\mathbf{\Lambda}}_{k+1}) \right).$$

By the convexity of $\|\cdot\|^2$, we have $\lambda_{\mathcal{B}^\# \mathcal{B}} \mu^2 \|\dot{\mathbf{\Lambda}}_{k+1}\|_{\mathbb{F}}^2 \leq \frac{\mu^2}{\rho(\mu)} \|\dot{\mathbf{G}}_{k+1}\|_{\mathbb{F}}^2 + |1 - \mu| \|\mathcal{B}^\# \Delta \dot{\mathbf{\Lambda}}_{k+1}\|_{\mathbb{F}}^2$. According to definition (26), we have $\|\dot{\mathbf{G}}_{k+1}\|_{\mathbb{F}}^2 \leq 2q_2^2 \|\Delta \dot{\mathbf{W}}_{k+1}\|_{\mathbb{F}}^2 + 2\|\nabla g(\dot{\mathbf{W}}_k)\|_{\mathbb{F}}^2 \leq 2(q_2 + L_g)^2 \|\Delta \dot{\mathbf{W}}_{k+1}\|_{\mathbb{F}}^2 + 2\|\nabla g(\dot{\mathbf{W}}_{k+1})\|_{\mathbb{F}}^2$. It follows that:

$$-\frac{1}{2\beta} \|\dot{\mathbf{\Lambda}}_{k+1}\|_{\mathbb{F}}^2 \geq -\theta_3 \|\nabla g(\dot{\mathbf{W}}_{k+1})\|_{\mathbb{F}}^2 - \theta_4 \|\Delta \dot{\mathbf{W}}_{k+1}\|_{\mathbb{F}}^2 - \theta_5 \|\mathcal{B}^\# \Delta \dot{\mathbf{\Lambda}}_{k+1}\|_{\mathbb{F}}^2, \quad (34)$$

where

$$\theta_3 := \frac{1}{\beta \rho(\mu) \lambda_{\mathcal{B}^\# \mathcal{B}}}, \quad \theta_4 := \frac{(q_2 + L_g)^2}{\beta \rho(\mu) \lambda_{\mathcal{B}^\# \mathcal{B}}}, \quad \theta_5 := \frac{|1 - \mu|}{2\beta \mu^2 \lambda_{\mathcal{B}^\# \mathcal{B}}}.$$

Using Inequalities (34) and (32), we obtain

$$\begin{aligned}
& f(\dot{\mathbf{X}}_{k+1}) + \frac{1}{2\tau^2} \|\mathcal{P}_\Omega(\mathcal{A}(\dot{\mathbf{X}}_k)) - \mathcal{P}_\Omega(\dot{\mathbf{Y}})\|_{\mathbb{F}}^2 + \frac{\beta}{2} \left\| \mathcal{C}(\dot{\mathbf{X}}_{k+1}) + \mathcal{B}(\dot{\mathbf{W}}_{k+1}) - \dot{\mathbf{B}} + \frac{\dot{\mathbf{\Lambda}}_{k+1}}{\beta} \right\|_{\mathbb{F}}^2 \\
& + a(\|\Delta\dot{\mathbf{X}}_{k+1}\|_{\mathbb{F}}^2 + \|\Delta\dot{\mathbf{\Lambda}}_{k+1}\|_{\mathbb{F}}^2) + (r\theta_0 + a - \theta_4)\|\Delta\dot{\mathbf{W}}_{k+1}\|_{\mathbb{F}}^2 + (r\theta_2 - \theta_5)\|\mathcal{B}^\# \Delta\dot{\mathbf{\Lambda}}_{k+1}\|_{\mathbb{F}}^2 \\
& \leq \mathcal{R}_{k_0} - \inf_{\dot{\mathbf{W}}} \left\{ g(\dot{\mathbf{W}}) - \theta_3 \|\nabla g(\dot{\mathbf{W}})\|_{\mathbb{F}}^2 \right\}.
\end{aligned} \tag{35}$$

According to (19) in Assumption A2, setting $\dot{\mathbf{W}}_1 = \dot{\mathbf{W}} - \delta \nabla g(\dot{\mathbf{W}})$ and $\dot{\mathbf{W}}_2 = \dot{\mathbf{W}}$, it follows that $g(\dot{\mathbf{W}}_k - \delta \nabla g(\dot{\mathbf{W}}_k)) \leq g(\dot{\mathbf{W}}_k) - (\delta - \frac{L_g \delta^2}{2}) \|\nabla g(\dot{\mathbf{W}}_k)\|_{\mathbb{F}}^2$. Since g is bounded from below, there exist M such that

$$-M < \inf \left\{ g(\dot{\mathbf{W}}) - (\delta - \frac{L_g \delta^2}{2}) \|\nabla g(\dot{\mathbf{W}})\|_{\mathbb{F}}^2 : \dot{\mathbf{W}} \in \mathbb{H}^{m \times n} \right\}. \tag{36}$$

We choose $\delta = \frac{1}{L_g}$. According to Assumption A5, we have $\theta_3 < \frac{1}{2L_g} = \delta - \frac{L_g \delta^2}{2}$. Since $r > 1$ and $\mu \in (0, 2)$, according to the definition of $\theta_0, \theta_2, \theta_4$ and θ_5 , it holds that $r\theta_2 - \theta_5 > 0$ and $r\theta_0 + a - \theta_4 > 0$. It follows from (35) that

$$\begin{aligned}
& f(\dot{\mathbf{X}}_{k+1}) + \frac{1}{2\tau^2} \|\mathcal{P}_\Omega(\mathcal{A}(\dot{\mathbf{X}}_k)) - \mathcal{P}_\Omega(\dot{\mathbf{Y}})\|_{\mathbb{F}}^2 \\
& + \frac{\beta}{2} \left\| \mathcal{C}(\dot{\mathbf{X}}_{k+1}) + \mathcal{B}(\dot{\mathbf{W}}_{k+1}) - \dot{\mathbf{B}} + \frac{\dot{\mathbf{\Lambda}}_{k+1}}{\beta} \right\|_{\mathbb{F}}^2 + a(\|\Delta\dot{\mathbf{X}}_{k+1}\|_{\mathbb{F}}^2 + \|\Delta\dot{\mathbf{\Lambda}}_{k+1}\|_{\mathbb{F}}^2) < \mathcal{R}_{k_0} + M.
\end{aligned} \tag{37}$$

Since f is coercive, the sequence $\{\dot{\mathbf{X}}_k\}_{k \geq k_0}$ is bounded and hence $\{\mathcal{C}\dot{\mathbf{X}}_k\}_{k \geq k_0}$ is bounded. According to (37), $\Delta\dot{\mathbf{\Lambda}}_{k+1}$ is bounded. By the $\dot{\mathbf{\Lambda}}$ update in (17), we have $\mathcal{B}\dot{\mathbf{W}}_{k+1} = \frac{1}{\beta\mu} \Delta\dot{\mathbf{\Lambda}}_{k+1} - \mathcal{C}\dot{\mathbf{X}}_{k+1} + \dot{\mathbf{B}}$. Since $\{\mathcal{C}\dot{\mathbf{X}}_k\}_{k \geq k_0}$ is bounded and $\mathcal{B}^\# \mathcal{B}$ is full rank, it follows that $\{\dot{\mathbf{W}}_k\}_{k \geq k_0}$ is bounded. From the fact that $\frac{\beta}{2} \left\| \mathcal{C}(\dot{\mathbf{X}}_{k+1}) + \mathcal{B}(\dot{\mathbf{W}}_{k+1}) - \dot{\mathbf{B}} + \frac{\dot{\mathbf{\Lambda}}_{k+1}}{\beta} \right\|_{\mathbb{F}}^2$ is bounded, it follows that $\{\dot{\mathbf{\Lambda}}_k\}_{k \geq k_0}$ is bounded. As a consequence, $\{\dot{\mathbf{X}}_k\}_{k \geq 1}, \{\dot{\mathbf{W}}_k\}_{k \geq 1}, \{\dot{\mathbf{\Lambda}}_k\}_{k \geq 1}$ is bounded. \square

Using Theorem 4.1, we have the following convergence result of \mathcal{R}_k .

Lemma 4.5. *Suppose Assumption 4.1 holds. The sequence $\{\mathcal{R}_k\}_{k \geq 1}$ is bounded from below and converges.*

Proof. It follows from Theorem 4.1 that $\{(\dot{\mathbf{X}}_k, \dot{\mathbf{W}}_k, \dot{\mathbf{\Lambda}}_k)\}_{k \geq 1}$ is bounded. Since \mathcal{L}_β is continuous respect to $\dot{\mathbf{X}}_k, \dot{\mathbf{W}}_k, \dot{\mathbf{\Lambda}}_k$, it follows that $\mathcal{L}_\beta(\dot{\mathbf{X}}_k, \dot{\mathbf{W}}_k, \dot{\mathbf{\Lambda}}_k)$ is bounded from below. Hence \mathcal{R}_k is bounded from below. According to Assumption 4.1 and (31), $\{\mathcal{R}_k\}_{k \geq 1}$ is monotonically decreasing. As a consequence, $\{\mathcal{R}_k\}_{k \geq 1}$ is bounded from below and converges. \square

The following convergence result of sequence $\{\dot{\mathbf{X}}_k, \dot{\mathbf{W}}_k, \dot{\mathbf{\Lambda}}_k\}$ is given by Lemma 4.5.

Theorem 4.2. *Suppose Assumption 4.1 holds. It follows that*

$$\lim_{k \rightarrow \infty} \|\Delta\dot{\mathbf{W}}_k\|_{\mathbb{F}} = 0, \lim_{k \rightarrow \infty} \|\Delta\dot{\mathbf{X}}_k\|_{\mathbb{F}} = 0, \lim_{k \rightarrow \infty} \|\Delta\dot{\mathbf{\Lambda}}_k\|_{\mathbb{F}} = 0.$$

Proof. According to Theorem 4.1, summing up (31) from k_0 to $K \geq k_0$, the following inequality holds

$$\sum_{k=k_0}^K \|\Delta \dot{\mathbf{W}}_{k+1}\|_{\mathbb{F}}^2 + \|\Delta \dot{\mathbf{X}}_{k+1}\|_{\mathbb{F}}^2 + \|\Delta \dot{\mathbf{\Lambda}}_{k+1}\|_{\mathbb{F}}^2 < \frac{1}{a}(\mathcal{R}_{k_0} - \inf_{k \geq 1} \mathcal{R}_k).$$

According to Lemma 4.5, it follows that $-\infty < \inf_{k \geq 1} \mathcal{R}_k$. Let $K \rightarrow +\infty$, since $\{(\dot{\mathbf{X}}_k, \dot{\mathbf{W}}_k, \dot{\mathbf{\Lambda}}_k)\}_{k \geq 0}$ is bounded, then \mathcal{R}_{k_0} is bounded and hence $\sum_{k \geq 0} \|\Delta \dot{\mathbf{W}}_{k+1}\|_{\mathbb{F}}^2 + \|\Delta \dot{\mathbf{X}}_{k+1}\|_{\mathbb{F}}^2 + \|\Delta \dot{\mathbf{\Lambda}}_{k+1}\|_{\mathbb{F}}^2 < \infty$, which completes the proof. \square

Theorem 4.2 has proven the limiting behavior of $\|\Delta \dot{\mathbf{W}}_k\|_{\mathbb{F}}$, $\|\Delta \dot{\mathbf{X}}_k\|_{\mathbb{F}}$ and $\|\Delta \dot{\mathbf{\Lambda}}_k\|_{\mathbb{F}}$, which will be used to prove the limiting behavior of \mathcal{R}_k . We next prove that the subgradient of $\mathcal{L}_\beta(\dot{\mathbf{X}}, \dot{\mathbf{W}}, \dot{\mathbf{\Lambda}})$ can be bounded by $\Delta \dot{\mathbf{X}}_{k+1}$, $\Delta \dot{\mathbf{W}}_{k+1}$ and $\Delta \dot{\mathbf{\Lambda}}_{k+1}$.

Lemma 4.6 (Subgradient bound). *Suppose that Assumption A2 holds. Let $\{(\dot{\mathbf{X}}_k, \dot{\mathbf{W}}_k, \dot{\mathbf{\Lambda}}_k)\}_{k \geq 0}$ be a sequence generated by (17). Then $\tilde{\mathbf{D}}_{k+1} := (\dot{\mathbf{D}}_{\dot{\mathbf{X}}_{k+1}}, \dot{\mathbf{D}}_{\dot{\mathbf{W}}_{k+1}}, \dot{\mathbf{D}}_{\dot{\mathbf{\Lambda}}_{k+1}}) \in \partial \mathcal{L}_\beta(\dot{\mathbf{X}}_{k+1}, \dot{\mathbf{W}}_{k+1}, \dot{\mathbf{\Lambda}}_{k+1})$, where*

$$\begin{aligned} \dot{\mathbf{D}}_{\dot{\mathbf{X}}_{k+1}} &:= \mathcal{C}^\# \Delta \dot{\mathbf{\Lambda}}_{k+1} - L_{2,k} \Delta \dot{\mathbf{X}}_{k+1} - \beta \mathcal{C}^\# \mathcal{B} \Delta \dot{\mathbf{W}}_{k+1}, & \dot{\mathbf{D}}_{\dot{\mathbf{\Lambda}}_{k+1}} &:= \frac{1}{\beta \mu} \Delta \dot{\mathbf{\Lambda}}_{k+1}, \\ \dot{\mathbf{D}}_{\dot{\mathbf{W}}_{k+1}} &:= \nabla g(\dot{\mathbf{W}}_{k+1}) - \nabla g(\dot{\mathbf{W}}_k) + \mathcal{B}^\# \Delta \dot{\mathbf{\Lambda}}_{k+1} - L_{1,k} \Delta \dot{\mathbf{W}}_{k+1}. \end{aligned}$$

Furthermore, there exists $\rho > 0$ such that

$$\|\tilde{\mathbf{D}}_{k+1}\| \leq \pi \left(\|\Delta \dot{\mathbf{W}}_{k+1}\|_{\mathbb{F}} + \|\Delta \dot{\mathbf{X}}_{k+1}\|_{\mathbb{F}} + \|\Delta \dot{\mathbf{\Lambda}}_{k+1}\|_{\mathbb{F}} \right),$$

where

$$\pi := \max \left\{ q_1, \beta \|\mathcal{C}\| \|\mathcal{B}\| + q_2 + L_g, \|\mathcal{C}\| + \|\mathcal{B}\| + \frac{1}{\beta \mu} \right\}. \quad (38)$$

Proof. According to the optimality condition of the update of $\dot{\mathbf{X}}_{k+1}$, it follows that

$$-\frac{1}{\tau^2} \mathcal{A}^\# \mathcal{P}_\Omega^\# (\mathcal{P}_\Omega (\mathcal{A} \dot{\mathbf{X}}_{k+1} - \dot{\mathbf{Y}})) - \beta \mathcal{C}^\# (\mathcal{C}(\dot{\mathbf{X}}_{k+1}) + \mathcal{B}(\dot{\mathbf{W}}_k) - \dot{\mathbf{B}} + \dot{\mathbf{\Lambda}}_k / \beta) - L_{1,k} \Delta \dot{\mathbf{X}}_{k+1} \in \partial f(\dot{\mathbf{X}}_{k+1}),$$

which yields

$$\dot{\mathbf{D}}_{\dot{\mathbf{X}}_{k+1}} = -\mathcal{C}^\# \Delta \dot{\mathbf{\Lambda}}_{k+1} - L_{1,k} \Delta \dot{\mathbf{X}}_{k+1} + \beta \mathcal{C}^\# \mathcal{B} \Delta \dot{\mathbf{W}}_{k+1} \in \partial_{\dot{\mathbf{X}}} \mathcal{L}_\beta(\dot{\mathbf{X}}_{k+1}, \dot{\mathbf{W}}_{k+1}, \dot{\mathbf{\Lambda}}_{k+1}). \quad (39)$$

According to the optimality condition of the update of $\dot{\mathbf{W}}_{k+1}$, the following equality holds:

$$\nabla g(\dot{\mathbf{W}}_k) + \beta \mathcal{B}^\# (\mathcal{C} \dot{\mathbf{X}}_{k+1} - \mathcal{B} \dot{\mathbf{W}}_{k+1} - \dot{\mathbf{B}} + \dot{\mathbf{\Lambda}}_k / \beta) + L_{2,k} \Delta \dot{\mathbf{W}}_{k+1} = 0. \quad (40)$$

It follows from (40) and the update of $\dot{\mathbf{\Lambda}}_{k+1}$ that

$$\begin{aligned} \dot{\mathbf{D}}_{\dot{\mathbf{W}}_{k+1}} &= \nabla g(\dot{\mathbf{W}}_{k+1}) - \nabla g(\dot{\mathbf{W}}_k) + \mathcal{B}^\# \Delta \dot{\mathbf{\Lambda}}_{k+1} - L_{2,k} \Delta \dot{\mathbf{W}}_{k+1} \in \partial_{\dot{\mathbf{W}}} \mathcal{L}_\beta(\dot{\mathbf{X}}_{k+1}, \dot{\mathbf{W}}_{k+1}, \dot{\mathbf{\Lambda}}_{k+1}). \\ \dot{\mathbf{D}}_{\dot{\mathbf{\Lambda}}_{k+1}} &= \frac{1}{\beta \mu} \Delta \dot{\mathbf{\Lambda}}_{k+1} \in \partial_{\dot{\mathbf{\Lambda}}} \mathcal{L}_\beta(\dot{\mathbf{X}}_{k+1}, \dot{\mathbf{W}}_{k+1}, \dot{\mathbf{\Lambda}}_{k+1}). \end{aligned} \quad (41)$$

Combining (39), (41), we obtain

$$\begin{aligned}\|\dot{\mathbf{D}}_{\dot{\mathbf{X}}_{k+1}}\| &\leq \|\mathcal{C}\|\|\Delta\dot{\mathbf{\Lambda}}_{k+1}\|_{\mathbb{F}} + q_1\|\Delta\dot{\mathbf{X}}_{k+1}\|_{\mathbb{F}} + \beta\|\mathcal{C}\|\|\mathcal{B}\|\|\Delta\dot{\mathbf{W}}_{k+1}\|_{\mathbb{F}}, \\ \|\dot{\mathbf{D}}_{\dot{\mathbf{W}}_{k+1}}\| &\leq \|\mathcal{B}\|\|\Delta\dot{\mathbf{\Lambda}}_{k+1}\|_{\mathbb{F}} + (q_2 + L_g)\|\Delta\dot{\mathbf{W}}_{k+1}\|_{\mathbb{F}}, \quad \|\dot{\mathbf{D}}_{\dot{\mathbf{\Lambda}}_{k+1}}\| = \frac{1}{\beta\mu}\|\Delta\dot{\mathbf{\Lambda}}_{k+1}\|_{\mathbb{F}}.\end{aligned}$$

Therefore, the following inequality holds:

$$\|\|\tilde{\mathbf{D}}_{k+1}\|\| \leq \|\dot{\mathbf{D}}_{\dot{\mathbf{W}}_{k+1}}\|_{\mathbb{F}} + \|\dot{\mathbf{D}}_{\dot{\mathbf{X}}_{k+1}}\|_{\mathbb{F}} + \|\dot{\mathbf{D}}_{\dot{\mathbf{\Lambda}}_{k+1}}\|_{\mathbb{F}} \leq \rho(\|\Delta\dot{\mathbf{X}}_{k+1}\|_{\mathbb{F}} + \|\Delta\dot{\mathbf{W}}_{k+1}\|_{\mathbb{F}} + \|\Delta\dot{\mathbf{\Lambda}}_{k+1}\|_{\mathbb{F}}), \quad (42)$$

which completes the proof. \square

Lemma 4.7. *Suppose that Assumption 4.1 holds. Any limit point $(\dot{\mathbf{X}}_*, \dot{\mathbf{W}}_*, \dot{\mathbf{\Lambda}}_*)$ of the sequence $\{(\dot{\mathbf{X}}_k, \dot{\mathbf{W}}_k, \dot{\mathbf{\Lambda}}_k)\}_{j \geq 0}$ generated by (17) is a stationary point of $\mathcal{L}_\beta(\dot{\mathbf{X}}, \dot{\mathbf{W}}; \dot{\mathbf{\Lambda}})$, i.e.*

$$0 = \partial f(\dot{\mathbf{X}}_*) + \frac{1}{\tau^2} \mathcal{A}^\# \mathcal{P}_\Omega^\# (\mathcal{P}_\Omega(\mathcal{A}\dot{\mathbf{X}}_{k+1} - \dot{\mathbf{Y}})) + \mathcal{C}^\# \dot{\mathbf{\Lambda}}_*, \quad 0 \in \partial g(\dot{\mathbf{W}}_*) + \mathcal{B}^\# \dot{\mathbf{\Lambda}}_*, \quad \mathcal{C}\dot{\mathbf{X}}_* + \mathcal{B}\dot{\mathbf{W}}_* = \dot{\mathbf{B}}.$$

Proof. Let $\{(\dot{\mathbf{X}}_{k_j}, \dot{\mathbf{W}}_{k_j}, \dot{\mathbf{\Lambda}}_{k_j})\}_{j \geq 0}$ be a subsequence of $\{(\dot{\mathbf{X}}_k, \dot{\mathbf{W}}_k, \dot{\mathbf{\Lambda}}_k)\}_{k \geq 0}$ such that $(\dot{\mathbf{X}}_*, \dot{\mathbf{W}}_*, \dot{\mathbf{\Lambda}}_*) = \lim_{j \rightarrow \infty} (\dot{\mathbf{X}}_{k_j}, \dot{\mathbf{W}}_{k_j}, \dot{\mathbf{\Lambda}}_{k_j})$. By the continuity of \mathcal{L}_β , $\mathcal{L}_\beta(\dot{\mathbf{X}}_{k_j}, \dot{\mathbf{W}}_{k_j}, \dot{\mathbf{\Lambda}}_{k_j}) \rightarrow \mathcal{L}_\beta(\dot{\mathbf{X}}_*, \dot{\mathbf{W}}_*, \dot{\mathbf{\Lambda}}_*)$ as $j \rightarrow \infty$. Let $\dot{\mathbf{D}}_{k_j} \in \partial \mathcal{L}_\beta(\dot{\mathbf{X}}_{k_j}, \dot{\mathbf{W}}_{k_j}, \dot{\mathbf{\Lambda}}_{k_j})$ and according to Lemma 4.6, it follows that $\|\dot{\mathbf{D}}_{k_j}\|_{\mathbb{F}} \leq \rho(\|\Delta\dot{\mathbf{W}}_{k_j}\|_{\mathbb{F}} + \|\Delta\dot{\mathbf{X}}_{k_j}\|_{\mathbb{F}} + \|\Delta\dot{\mathbf{\Lambda}}_{k_j}\|_{\mathbb{F}})$. According to Theorem 4.2, it follows that $\dot{\mathbf{D}}_{k_j} \rightarrow 0$. By the closeness criterion of the limiting sub-differential, $(\dot{\mathbf{X}}_*, \dot{\mathbf{W}}_*, \dot{\mathbf{\Lambda}}_*) \in \text{crit } \mathcal{L}_\beta(\dot{\mathbf{X}}, \dot{\mathbf{W}}; \dot{\mathbf{\Lambda}})$. The proof is completed. \square

The following Lemma states the behavior of limit points of $\{\dot{\mathbf{X}}_k, \dot{\mathbf{W}}_k, \dot{\mathbf{\Lambda}}_k\}$.

Lemma 4.8. *Suppose Assumption 4.1 holds. If $(\dot{\mathbf{X}}_*, \dot{\mathbf{W}}_*, \dot{\mathbf{\Lambda}}_*)$ is a limit point of a converging subsequence $\{\dot{\mathbf{X}}_{k_j}, \dot{\mathbf{W}}_{k_j}, \dot{\mathbf{\Lambda}}_{k_j}\}$, then it follows that*

$$\lim_{j \rightarrow \infty} \mathcal{R}_{k_j} = \mathcal{R}(\dot{\mathbf{X}}_*, \dot{\mathbf{W}}_*, \dot{\mathbf{\Lambda}}_*, \dot{\mathbf{W}}_*, \dot{\mathbf{\Lambda}}_*) = \mathcal{L}_\beta(\dot{\mathbf{X}}_*, \dot{\mathbf{W}}_*, \dot{\mathbf{\Lambda}}_*) = g(\dot{\mathbf{W}}_*) + f(\dot{\mathbf{X}}_*) + \frac{1}{2\tau^2} \|\mathcal{P}_\Omega(\mathcal{A}(\dot{\mathbf{X}}_*)) - \mathcal{P}_\Omega(\dot{\mathbf{Y}})\|_{\mathbb{F}}^2.$$

Proof. Let $\{(\dot{\mathbf{X}}_{k_j}, \dot{\mathbf{W}}_{k_j}, \dot{\mathbf{\Lambda}}_{k_j})\}_{j \geq 0}$ be a subsequence generated by (17) such that $(\dot{\mathbf{X}}_{k_j}, \dot{\mathbf{W}}_{k_j}, \dot{\mathbf{\Lambda}}_{k_j}) \rightarrow (\dot{\mathbf{X}}_*, \dot{\mathbf{W}}_*, \dot{\mathbf{\Lambda}}_*)$ as $j \rightarrow \infty$. According to Lemma 4.2, $\|\Delta\dot{\mathbf{X}}_{k_j}\|_{\mathbb{F}} \rightarrow 0$ and $\|\mathcal{C}^\# \Delta\dot{\mathbf{\Lambda}}_{k_j}\|_{\mathbb{F}} \leq \|\mathcal{C}\|\|\Delta\dot{\mathbf{\Lambda}}_{k_j}\|_{\mathbb{F}} \rightarrow 0$ when $j \rightarrow \infty$. According to the definition of \mathcal{R}_k , it follows that

$$\lim_{j \rightarrow \infty} \mathcal{R}_{k_j} = \lim_{j \rightarrow \infty} \mathcal{L}_\beta(\dot{\mathbf{X}}_{k_j}, \dot{\mathbf{W}}_{k_j}, \dot{\mathbf{\Lambda}}_{k_j}).$$

Since $\|\Delta\dot{\mathbf{\Lambda}}_{k_j+1}\|_{\mathbb{F}} \rightarrow 0$ as $j \rightarrow \infty$, $\|\mathcal{C}\dot{\mathbf{X}}_{k_j} + \mathcal{B}\dot{\mathbf{W}}_{k_j} - \dot{\mathbf{B}}\|_{\mathbb{F}} \rightarrow 0$. According to the definition of \mathcal{L}_β and the fact that $\{\dot{\mathbf{\Lambda}}_{k_j}\}_{j \geq 0}$ is a bounded sequence we also have $\langle \dot{\mathbf{\Lambda}}_{k_j}, \mathcal{C}\dot{\mathbf{X}}_{k_j} + \mathcal{B}\dot{\mathbf{W}}_{k_j} - \dot{\mathbf{B}} \rangle \rightarrow 0$ as $j \rightarrow \infty$. According to the fact that f is continuous, it follows that:

$$\begin{aligned}\lim_{j \rightarrow \infty} \mathcal{R}(\dot{\mathbf{X}}_{k_j}, \dot{\mathbf{W}}_{k_j}, \dot{\mathbf{\Lambda}}_{k_j}, \dot{\mathbf{W}}_{k_j}, \dot{\mathbf{\Lambda}}_{k_j}) &= \lim_{j \rightarrow \infty} \mathcal{L}_\beta(\dot{\mathbf{X}}_{k_j}, \dot{\mathbf{W}}_{k_j}, \dot{\mathbf{\Lambda}}_{k_j}) \\ &= f(\dot{\mathbf{X}}_*) + g(\dot{\mathbf{W}}_*) + \frac{1}{2\tau^2} \|\mathcal{P}_\Omega(\mathcal{A}(\dot{\mathbf{X}}_*)) - \mathcal{P}_\Omega(\dot{\mathbf{Y}})\|_{\mathbb{F}}^2.\end{aligned}$$

\square

Theorem 4.3 (Properties of limit point set). *Suppose Assumption 4.1 holds. Sequence $\{(\dot{\mathbf{X}}_k, \dot{\mathbf{W}}_k, \dot{\mathbf{\Lambda}}_k)\}_{k \geq 0}$ generated by (17) satisfies the following properties:*

1. *The limit point set of the sequence $\{(\dot{\mathbf{X}}_k, \dot{\mathbf{W}}_k, \dot{\mathbf{\Lambda}}_k)\}$, denoted by $\omega\left(\{(\dot{\mathbf{X}}_k, \dot{\mathbf{W}}_k, \dot{\mathbf{\Lambda}}_k)\}_{k \geq 0}\right)$ is nonempty, and compact.*
2. $\lim_{k \rightarrow \infty} \text{dist}\left[(\dot{\mathbf{X}}_k, \dot{\mathbf{W}}_k, \dot{\mathbf{\Lambda}}_k), \omega\left(\{(\dot{\mathbf{X}}_k, \dot{\mathbf{W}}_k, \dot{\mathbf{\Lambda}}_k)\}_{k \geq 0}\right)\right] = 0.$
3. $\omega\left(\{(\dot{\mathbf{X}}_k, \dot{\mathbf{W}}_k, \dot{\mathbf{\Lambda}}_k)\}_{k \geq 0}\right) \subseteq \text{crit } \mathcal{L}_\beta.$

Proof. Since $\{(\dot{\mathbf{X}}_k, \dot{\mathbf{W}}_k, \dot{\mathbf{\Lambda}}_k)\}_{k \geq 0}$ is bounded by Theorem 4.1. There exists at least one limit point of $\{(\dot{\mathbf{X}}_k, \dot{\mathbf{W}}_k, \dot{\mathbf{\Lambda}}_k)\}_{k \geq 0}$ and $\omega\left(\{(\dot{\mathbf{X}}_k, \dot{\mathbf{W}}_k, \dot{\mathbf{\Lambda}}_k)\}_{k \geq 0}\right)$ is bounded. According to [27, Chapter 2, Exercise 6], it follows that $\omega\left(\{(\dot{\mathbf{X}}_k, \dot{\mathbf{W}}_k, \dot{\mathbf{\Lambda}}_k)\}_{k \geq 0}\right)$ is closed. Hence $\omega\left(\{(\dot{\mathbf{X}}_k, \dot{\mathbf{W}}_k, \dot{\mathbf{\Lambda}}_k)\}_{k \geq 0}\right)$ is nonempty and compact. As a consequence, $\lim_{k \rightarrow \infty} \text{dist}\left[(\dot{\mathbf{X}}_k, \dot{\mathbf{W}}_k, \dot{\mathbf{\Lambda}}_k), \omega\left(\{(\dot{\mathbf{X}}_k, \dot{\mathbf{W}}_k, \dot{\mathbf{\Lambda}}_k)\}_{k \geq 0}\right)\right] = 0.$ It follows from Lemma 4.7 that $\omega\left(\{(\dot{\mathbf{X}}_k, \dot{\mathbf{W}}_k, \dot{\mathbf{\Lambda}}_k)\}_{k \geq 0}\right) \subseteq \text{crit } \mathcal{L}_\beta,$ which completes the proof. \square

Lemma 4.9. *Suppose that the Assumption 4.1 holds. Let $\{(\dot{\mathbf{X}}_k, \dot{\mathbf{W}}_k, \dot{\mathbf{\Lambda}}_k)\}_{k \geq 0}$ be a sequence generated by (17). Define*

$$\begin{aligned} \dot{\mathbf{S}}_{\dot{\mathbf{X}}_k} &:= \dot{\mathbf{D}}_{\dot{\mathbf{X}}_k}, & \dot{\mathbf{S}}_{\dot{\mathbf{W}}_k} &:= \dot{\mathbf{D}}_{\dot{\mathbf{W}}_k} + 2r\theta_0\Delta\dot{\mathbf{W}}_k, & \dot{\mathbf{S}}_{\dot{\mathbf{\Lambda}}_k} &:= \dot{\mathbf{D}}_{\dot{\mathbf{\Lambda}}_k} + 2r\theta_2\mathcal{B}\mathcal{B}^\# \Delta\dot{\mathbf{\Lambda}}_k, \\ \dot{\mathbf{S}}_{\dot{\mathbf{W}}'_k} &:= -2r\theta_0\Delta\dot{\mathbf{W}}_k, & \dot{\mathbf{S}}_{\dot{\mathbf{\Lambda}}'_k} &:= -2\theta_2\mathcal{B}\mathcal{B}^\# \Delta\dot{\mathbf{\Lambda}}_k \end{aligned}$$

where $(\dot{\mathbf{D}}_{\dot{\mathbf{X}}_k}, \dot{\mathbf{D}}_{\dot{\mathbf{W}}_k}, \dot{\mathbf{D}}_{\dot{\mathbf{\Lambda}}_k}) \in \partial\mathcal{L}_\beta(\dot{\mathbf{X}}_k, \dot{\mathbf{W}}_k, \dot{\mathbf{\Lambda}}_k).$ Then

$$\tilde{\mathbf{S}}_k := (\dot{\mathbf{S}}_{\dot{\mathbf{X}}_k}, \dot{\mathbf{S}}_{\dot{\mathbf{W}}_k}, \dot{\mathbf{S}}_{\dot{\mathbf{\Lambda}}_k}, \dot{\mathbf{S}}_{\dot{\mathbf{W}}'_k}, \dot{\mathbf{S}}_{\dot{\mathbf{\Lambda}}'_k}) \in \partial\mathcal{R}(\dot{\mathbf{X}}_k, \dot{\mathbf{W}}_k, \dot{\mathbf{\Lambda}}_k, \dot{\mathbf{W}}_{k-1}, \dot{\mathbf{\Lambda}}_{k-1})$$

for $k \geq 1,$ and it holds that

$$\|\tilde{\mathbf{S}}_k\| \leq \tilde{\pi} \left(\|\Delta\dot{\mathbf{X}}_k\|_F + \|\Delta\dot{\mathbf{W}}_k\|_F + \|\Delta\dot{\mathbf{\Lambda}}_k\|_F \right), \quad (43)$$

where

$$\tilde{\pi} = \sqrt{3}\pi + 4r \max\{\theta_0, \theta_2\|\mathcal{B}\|^2\}, \quad (44)$$

$r > 1,$ π is given in (38).

Proof. Let $k \geq 1$ fixed, and $(\dot{\mathbf{D}}_{\dot{\mathbf{X}}_k}, \dot{\mathbf{D}}_{\dot{\mathbf{W}}_k}, \dot{\mathbf{D}}_{\dot{\mathbf{\Lambda}}_k}) \in \partial\mathcal{L}_\beta(\dot{\mathbf{X}}_k, \dot{\mathbf{W}}_k, \dot{\mathbf{\Lambda}}_k).$ By taking partial derivatives of \mathcal{R}_k with respect to $\dot{\mathbf{X}}, \dot{\mathbf{W}}, \dot{\mathbf{\Lambda}}, \dot{\mathbf{W}}', \dot{\mathbf{\Lambda}}'$ we obtain

$$\begin{aligned} \dot{\mathbf{S}}_{\dot{\mathbf{X}}_k} &:= \partial_{\dot{\mathbf{X}}}\mathcal{R}(\dot{\mathbf{X}}_k, \dot{\mathbf{W}}_k, \dot{\mathbf{\Lambda}}_k, \dot{\mathbf{W}}_{k-1}, \dot{\mathbf{\Lambda}}_{k-1}) = \partial_{\dot{\mathbf{X}}}\mathcal{L}_\beta(\dot{\mathbf{X}}_k, \dot{\mathbf{W}}_k, \dot{\mathbf{\Lambda}}_k) = \dot{\mathbf{D}}_{\dot{\mathbf{X}}_k}, \\ \dot{\mathbf{S}}_{\dot{\mathbf{W}}_k} &:= \nabla_{\dot{\mathbf{W}}}\mathcal{R}(\dot{\mathbf{X}}_k, \dot{\mathbf{W}}_k, \dot{\mathbf{\Lambda}}_k, \dot{\mathbf{W}}_{k-1}, \dot{\mathbf{\Lambda}}_{k-1}) = \nabla_{\dot{\mathbf{W}}}\mathcal{L}_\beta(\dot{\mathbf{X}}_k, \dot{\mathbf{W}}_k, \dot{\mathbf{\Lambda}}_k) + 2r\theta_0\Delta\dot{\mathbf{W}}_k = \dot{\mathbf{D}}_{\dot{\mathbf{W}}_k} + 2r\theta_0\Delta\dot{\mathbf{W}}_k, \\ \dot{\mathbf{S}}_{\dot{\mathbf{\Lambda}}_k} &:= \nabla_{\dot{\mathbf{\Lambda}}}\mathcal{R}(\dot{\mathbf{X}}_k, \dot{\mathbf{W}}_k, \dot{\mathbf{\Lambda}}_k, \dot{\mathbf{W}}_{k-1}, \dot{\mathbf{\Lambda}}_{k-1}) = \nabla_{\dot{\mathbf{\Lambda}}}\mathcal{L}_\beta(\dot{\mathbf{X}}_k, \dot{\mathbf{W}}_k, \dot{\mathbf{\Lambda}}_k) + 2r\theta_2\mathcal{B}\mathcal{B}^\# \Delta\dot{\mathbf{\Lambda}}_k = \dot{\mathbf{D}}_{\dot{\mathbf{\Lambda}}_k} + 2r\theta_2\mathcal{B}\mathcal{B}^\# \Delta\dot{\mathbf{\Lambda}}_k, \end{aligned}$$

$$\begin{aligned}\dot{\mathbf{S}}_{\dot{\mathbf{W}}'_k} &:= \nabla_{\dot{\mathbf{W}}'} \mathcal{R}(\dot{\mathbf{X}}_k, \dot{\mathbf{W}}_k, \dot{\mathbf{\Lambda}}_k, \dot{\mathbf{W}}_{k-1}, \dot{\mathbf{\Lambda}}_{k-1}) = -2r\theta_0 \Delta \dot{\mathbf{W}}_k, \\ \dot{\mathbf{S}}_{\dot{\mathbf{\Lambda}}'_k} &:= \nabla_{\dot{\mathbf{\Lambda}}'} \mathcal{R}(\dot{\mathbf{X}}_k, \dot{\mathbf{W}}_k, \dot{\mathbf{\Lambda}}_k, \dot{\mathbf{W}}_{k-1}, \dot{\mathbf{\Lambda}}_{k-1}) = -2r\theta_2 \mathcal{B} \mathcal{B}^\# \Delta \dot{\mathbf{\Lambda}}_k.\end{aligned}$$

By the triangle inequality, we obtain

$$\begin{aligned}\|\dot{\mathbf{S}}_{\dot{\mathbf{X}}_k}\|_{\mathbb{F}} &= \|\dot{\mathbf{D}}_{\dot{\mathbf{X}}_k}\|_{\mathbb{F}}, \quad \|\dot{\mathbf{S}}_{\dot{\mathbf{W}}_k}\|_{\mathbb{F}} \leq \|\dot{\mathbf{D}}_{\dot{\mathbf{W}}_k}\|_{\mathbb{F}} + 2r\theta_0 \|\Delta \dot{\mathbf{W}}_k\|_{\mathbb{F}}, \\ \|\dot{\mathbf{S}}_{\dot{\mathbf{\Lambda}}_k}\|_{\mathbb{F}} &\leq \|\dot{\mathbf{D}}_{\dot{\mathbf{\Lambda}}_k}\|_{\mathbb{F}} + 2r\theta_2 \|\mathcal{B}\|^2 \|\Delta \dot{\mathbf{\Lambda}}_k\|_{\mathbb{F}}, \quad \|\dot{\mathbf{S}}_{\dot{\mathbf{W}}'_k}\|_{\mathbb{F}} = 2r\theta_0 \|\Delta \dot{\mathbf{W}}_k\|_{\mathbb{F}}, \quad \|\dot{\mathbf{S}}_{\dot{\mathbf{\Lambda}}'_k}\|_{\mathbb{F}} = 2r\theta_2 \|\mathcal{B}\|^2 \|\Delta \dot{\mathbf{\Lambda}}_k\|_{\mathbb{F}}.\end{aligned}$$

By Lemma 4.6, it follows that

$$\begin{aligned}|\|\tilde{\dot{\mathbf{S}}}_k||| &\leq \|\dot{\mathbf{S}}_{\dot{\mathbf{X}}_k}\|_{\mathbb{F}} + \|\dot{\mathbf{S}}_{\dot{\mathbf{W}}_k}\|_{\mathbb{F}} + \|\dot{\mathbf{S}}_{\dot{\mathbf{\Lambda}}_k}\|_{\mathbb{F}} + \|\dot{\mathbf{S}}_{\dot{\mathbf{W}}'_k}\|_{\mathbb{F}} + \|\dot{\mathbf{S}}_{\dot{\mathbf{\Lambda}}'_k}\|_{\mathbb{F}} \\ &\leq \|\dot{\mathbf{D}}_{\dot{\mathbf{X}}_k}\|_{\mathbb{F}} + \|\dot{\mathbf{D}}_{\dot{\mathbf{W}}_k}\|_{\mathbb{F}} + \|\dot{\mathbf{D}}_{\dot{\mathbf{\Lambda}}_k}^k\|_{\mathbb{F}} + 4r\theta_0 \|\Delta \dot{\mathbf{W}}_k\|_{\mathbb{F}} + 4r\theta_2 \|\mathcal{B}\|^2 \|\Delta \dot{\mathbf{\Lambda}}_k\|_{\mathbb{F}} \\ &\leq \sqrt{3} |\|\dot{\mathbf{D}}_k||| + 4r\theta_0 \|\Delta \dot{\mathbf{W}}_k\|_{\mathbb{F}} + 4r\theta_2 \|\mathcal{B}\|^2 \|\Delta \dot{\mathbf{\Lambda}}_k\|_{\mathbb{F}} \\ &\leq \sqrt{3}\rho \|\Delta \dot{\mathbf{X}}_k\|_{\mathbb{F}} + (\sqrt{3}\rho + 4r\theta_0) \|\Delta \dot{\mathbf{W}}_k\|_{\mathbb{F}} + (\sqrt{3}\rho + 4r\theta_2 \|\mathcal{B}\|^2) \|\Delta \dot{\mathbf{\Lambda}}_k\|_{\mathbb{F}},\end{aligned}$$

which completes the proof. \square

We next prove the limiting behavior of \mathcal{R}_k , the detailed proof is similar to Theorem 4.3 and we omit it.

Lemma 4.10. *Suppose the Assumption 4.1 holds. If $\{(\dot{\mathbf{X}}_k, \dot{\mathbf{W}}_k, \dot{\mathbf{\Lambda}}_k)\}_{k \geq 0}$ is a sequence generated by Algorithm 1, then the following statements hold.*

(i) *The set $\Gamma := \omega\left(\{(\dot{\mathbf{X}}_k, \dot{\mathbf{W}}_k, \dot{\mathbf{\Lambda}}_k, \dot{\mathbf{W}}_{k-1}, \dot{\mathbf{\Lambda}}_{k-1})\}_{k \geq 1}\right)$ is nonempty, and compact.*

(ii) $\Gamma \subseteq \{(\dot{\mathbf{X}}, \dot{\mathbf{W}}, \dot{\mathbf{\Lambda}}, \dot{\mathbf{W}}, \dot{\mathbf{\Lambda}}) \in \mathbb{R}^n \times \mathbb{R}^m \times \mathbb{R}^p \times \mathbb{R}^m \times \mathbb{R}^p : (\dot{\mathbf{X}}, \dot{\mathbf{W}}, \dot{\mathbf{\Lambda}}) \in \text{crit}(\mathcal{L}_\beta)\}$.

(iii) $\lim_{k \rightarrow \infty} \text{dist}\left[(\dot{\mathbf{X}}_k, \dot{\mathbf{W}}_k, \dot{\mathbf{\Lambda}}_k, \dot{\mathbf{W}}_{k-1}, \dot{\mathbf{\Lambda}}_{k-1}), \Gamma\right] = 0$.

(iv) *The sequences $\{\mathcal{R}_k\}_{k \geq 0}$, $\{\mathcal{L}_\beta(\dot{\mathbf{X}}_k, \dot{\mathbf{W}}_k, \dot{\mathbf{\Lambda}}_k)\}_{k \geq 0}$ approach to the same limit and if $(\dot{\mathbf{X}}_*, \dot{\mathbf{W}}_*, \dot{\mathbf{\Lambda}}_*, \dot{\mathbf{W}}_*, \dot{\mathbf{\Lambda}}_*) \in \Gamma$, then*

$$\mathcal{R}(\dot{\mathbf{X}}_*, \dot{\mathbf{W}}_*, \dot{\mathbf{\Lambda}}_*, \dot{\mathbf{W}}_*, \dot{\mathbf{\Lambda}}_*) = \mathcal{L}_\beta(\dot{\mathbf{X}}_*, \dot{\mathbf{W}}_*, \dot{\mathbf{\Lambda}}_*) = g(\dot{\mathbf{W}}_*) + f(\dot{\mathbf{X}}_*) + \frac{1}{2\tau^2} \|\mathcal{P}_\Omega(\mathcal{A}(\dot{\mathbf{X}}_*)) - \mathcal{P}_\Omega(\dot{\mathbf{Y}})\|_{\mathbb{F}}^2.$$

Proof. The results follow immediately from Theorem 4.1, 4.2 and Lemma 4.9. \square

The following convergence result of the whole sequence, established under the Kurdyka-Łojasiewicz property, follows from [36, Theorem 2]. The difference lies in the construction of \mathcal{R}_k . The proofs are given for completeness.

Theorem 4.4 (Global Convergence). *Suppose that Assumption 4.1 holds and \mathcal{R} defined in (30) satisfies the KL property on the limit point set Γ , i.e. for every $\dot{\mathbf{V}}_* = (\dot{\mathbf{X}}_*, \dot{\mathbf{W}}_*, \dot{\mathbf{\Lambda}}_*, \dot{\mathbf{W}}_*, \dot{\mathbf{\Lambda}}_*) \in \Gamma$,*

there exists $\varepsilon > 0$ and desingularizing function $\psi : [0, \eta] \rightarrow [0, \infty)$, for some $\eta \in [0, \infty)$ such that for all $\dot{\mathbf{V}} = (\dot{\mathbf{X}}, \dot{\mathbf{W}}, \dot{\mathbf{\Lambda}}, \dot{\mathbf{W}}', \dot{\mathbf{\Lambda}}')$ in the following set:

$$\mathcal{S} := \{\dot{\mathbf{V}} : \text{dist}(\dot{\mathbf{V}}, \Gamma) < \varepsilon \text{ and } \mathcal{R}(\dot{\mathbf{V}}^*) < \mathcal{R}(\dot{\mathbf{V}}) < \mathcal{R}(\dot{\mathbf{V}}^*) + \eta\}, \quad (45)$$

the inequality

$$\psi'(\mathcal{R}(\dot{\mathbf{V}}) - \mathcal{R}(\dot{\mathbf{V}}^*)) \text{dist}(0, \partial \mathcal{R}(\dot{\mathbf{V}})) \geq 1 \quad (46)$$

holds, then $\{\dot{\mathbf{T}}_k\}_{k \geq 0} := \{(\dot{\mathbf{X}}_k, \dot{\mathbf{W}}_k, \dot{\mathbf{\Lambda}}_k)\}_{k \geq 0}$ satisfies the finite length property: $\sum_{k=0}^{\infty} \|\dot{\mathbf{X}}_k\|_{\mathbb{F}} + \|\dot{\mathbf{W}}_k\|_{\mathbb{F}} + \|\dot{\mathbf{\Lambda}}_k\|_{\mathbb{F}} < \infty$, and consequently converges to a stationary point of (15).

Proof. According to Lemma 4.5, $\lim_{k \rightarrow \infty} \mathcal{R}_k := \mathcal{R}_{\infty}$. It follows that the sequence $\{\mathcal{E}_k\}_{k \geq k_0}$ defined by

$$\mathcal{E}_k := \mathcal{R}_k - \mathcal{R}_{\infty},$$

is non-negative, monotonically decreasing, and converges to 0. We consider the following two cases:

Case 1. There exists $k_1 \geq k_0$ such that $\mathcal{E}_{k_1} = 0$. Hence $\mathcal{E}_k = 0$ for all $k \geq k_1$ and, it follows that $\|\Delta \dot{\mathbf{X}}_{k+1}\|_{\mathbb{F}}^2 + \|\Delta \dot{\mathbf{W}}_{k+1}\|_{\mathbb{F}}^2 + \|\Delta \dot{\mathbf{\Lambda}}_{k+1}\|_{\mathbb{F}}^2 \leq \frac{1}{a}(\mathcal{E}_k - \mathcal{E}_{k+1}) = 0$, $\forall k \geq k_1$ by (31). This gives rise to

$$\sum_{k \geq 0} \left(\|\Delta \dot{\mathbf{X}}_{k+1}\|_{\mathbb{F}} + \|\Delta \dot{\mathbf{W}}_{k+1}\|_{\mathbb{F}} + \|\Delta \dot{\mathbf{\Lambda}}_{k+1}\|_{\mathbb{F}} \right) \leq \sum_{k=1}^{k_1} \left(\|\Delta \dot{\mathbf{X}}_k\|_{\mathbb{F}} + \|\Delta \dot{\mathbf{W}}_k\|_{\mathbb{F}} + \|\Delta \dot{\mathbf{\Lambda}}_k\|_{\mathbb{F}} \right) < +\infty.$$

The latter conclusion is due to the fact that the sequence is bounded from Theorem 4.1.

Case 2. The error sequence $\mathcal{E}_k = \mathcal{R}_k - \mathcal{R}_{\infty} > 0$ for all $k \geq k_0$. Then by (31), it follows that

$$\|\Delta \dot{\mathbf{T}}_{k+1}\|_{\mathbb{F}}^2 = \|\Delta \dot{\mathbf{X}}_{k+1}\|_{\mathbb{F}}^2 + \|\Delta \dot{\mathbf{W}}_{k+1}\|_{\mathbb{F}}^2 + \|\Delta \dot{\mathbf{\Lambda}}_{k+1}\|_{\mathbb{F}}^2 \leq \frac{1}{a}(\mathcal{E}_k - \mathcal{E}_{k+1}), \quad \forall k \geq k_0. \quad (47)$$

By Lemma 4.10, Γ is nonempty, compact. Furthermore, \mathcal{R}_k takes on a constant value \mathcal{R}_{∞} on Γ .

Since the sequence $\{\mathcal{R}_k\}_{k \geq k_0}$ is monotonically decreasing to \mathcal{R}_{∞} , there exists $k_1 \geq k_0 \geq 1$ such that

$$\mathcal{R}_{\infty} < \mathcal{R}_k < \mathcal{R}_{\infty} + \eta, \quad \forall k \geq k_1.$$

By Theorem 4.10, it follows that $\lim_{k \rightarrow \infty} \text{dist}\left[(\dot{\mathbf{X}}_k, \dot{\mathbf{W}}_k, \dot{\mathbf{\Lambda}}_k, \dot{\mathbf{W}}_{k-1}, \dot{\mathbf{X}}_{k-1}), \Gamma\right] = 0$. Thus there exists $k_2 \geq 1$ such that

$$\text{dist}\left[(\dot{\mathbf{X}}_k, \dot{\mathbf{W}}_k, \dot{\mathbf{\Lambda}}_k, \dot{\mathbf{W}}_{k-1}, \dot{\mathbf{X}}_{k-1}), \Gamma\right] < \varepsilon, \quad \forall k \geq k_2.$$

Let $\tilde{k} = \max\{k_1, k_2, 3\}$. It follows that $(\dot{\mathbf{X}}_k, \dot{\mathbf{W}}_k, \dot{\mathbf{\Lambda}}_k, \dot{\mathbf{W}}_{k-1}, \dot{\mathbf{X}}_{k-1}) \in \mathcal{S}$ for $k \geq \tilde{k}$, where \mathcal{S} defined in (45). Thus, we have

$$\psi'(\mathcal{E}_k) \cdot \text{dist}\left(0, \partial \mathcal{R}_k\right) \geq 1. \quad (48)$$

Since ψ is concave, it holds that $\psi(\mathcal{E}_k) - \psi(\mathcal{E}_{k+1}) \geq \psi'(\mathcal{E}_k)(\mathcal{E}_k - \mathcal{E}_{k+1})$. Together with (47) and (48), it follows that

$$\begin{aligned} \|\Delta \dot{\mathbf{T}}_{k+1}\|_{\mathbb{F}}^2 &\leq \psi'(\mathcal{E}_k) \|\Delta \dot{\mathbf{T}}_{k+1}\|_{\mathbb{F}}^2 \cdot \text{dist}(0, \partial \mathcal{R}_k) \\ &\leq \frac{1}{a} \psi'(\mathcal{E}_k) (\mathcal{E}_k - \mathcal{E}_{k+1}) \cdot \text{dist}(0, \partial \mathcal{R}_k) \end{aligned}$$

$$\leq \frac{1}{a} \left(\psi(\mathcal{E}_k) - \psi(\mathcal{E}_{k+1}) \right) \cdot \text{dist}(0, \partial\mathcal{R}_k).$$

By the arithmetic mean-geometric mean inequality, for any $\gamma > 0$, we have

$$\|\Delta \dot{\mathbf{T}}_{k+1}\|_{\mathbb{F}} \leq \frac{\gamma}{2a} \left(\psi(\mathcal{E}_k) - \psi(\mathcal{E}_{k+1}) \right) + \frac{1}{2\gamma} \text{dist}(0, \partial\mathcal{R}_k).$$

It follows that

$$\|\Delta \dot{\mathbf{X}}_{k+1}\|_{\mathbb{F}} + \|\Delta \dot{\mathbf{W}}_{k+1}\|_{\mathbb{F}} + \|\Delta \dot{\mathbf{A}}_{k+1}\|_{\mathbb{F}} \leq \frac{\sqrt{3}\gamma}{2a} \left(\psi(\mathcal{E}_k) - \psi(\mathcal{E}_{k+1}) \right) + \frac{\sqrt{3}}{2\gamma} \text{dist}(0, \partial\mathcal{R}_k). \quad (49)$$

Then according to Lemma 4.9, we obtain

$$\|\Delta \dot{\mathbf{X}}_{k+1}\|_{\mathbb{F}} + \|\Delta \dot{\mathbf{W}}_{k+1}\|_{\mathbb{F}} + \|\Delta \dot{\mathbf{A}}_{k+1}\|_{\mathbb{F}} \leq \frac{\sqrt{3}\gamma}{2a} \left(\psi(\mathcal{E}_k) - \psi(\mathcal{E}_{k+1}) \right) + \frac{\sqrt{3}\tilde{\rho}}{2\gamma} \left(\|\Delta \dot{\mathbf{X}}_k\|_{\mathbb{F}} + \|\Delta \dot{\mathbf{W}}_k\|_{\mathbb{F}} + \|\Delta \dot{\mathbf{A}}_k\|_{\mathbb{F}} \right). \quad (50)$$

According to the equality $\sum_{k=\underline{k}}^K \|\Delta \dot{\mathbf{X}}_k\|_{\mathbb{F}} = \sum_{k=\underline{k}}^K \|\Delta \dot{\mathbf{X}}_{k+1}\|_{\mathbb{F}} + \|\Delta \dot{\mathbf{X}}_{\underline{k}}\|_{\mathbb{F}} - \|\Delta \dot{\mathbf{X}}_K\|_{\mathbb{F}}$, we choose $\gamma > 0$ large enough such that $1 > \sqrt{3}\tilde{\rho}/2\gamma$, and let $\delta_0 = 1 - \frac{\sqrt{3}\tilde{\rho}}{2\gamma}$. Summing up (50) from $k = \underline{k} \geq \tilde{k}$ to $K \geq \underline{k}$ gives

$$\begin{aligned} \delta_0 \left(\sum_{k=\underline{k}}^K \|\Delta \dot{\mathbf{X}}_{k+1}\|_{\mathbb{F}} + \|\Delta \dot{\mathbf{W}}_{k+1}\|_{\mathbb{F}} + \|\Delta \dot{\mathbf{A}}_{k+1}\|_{\mathbb{F}} \right) &\leq \frac{\sqrt{3}\gamma}{2a} \left(\psi(\mathcal{E}_k) - \psi(\mathcal{E}_{K+1}) \right) \\ &+ \frac{\sqrt{3}\tilde{\rho}}{2\gamma} \left(\|\Delta \dot{\mathbf{X}}_{\underline{k}}\|_{\mathbb{F}} + \|\Delta \dot{\mathbf{W}}_{\underline{k}}\|_{\mathbb{F}} + \|\Delta \dot{\mathbf{A}}_{\underline{k}}\|_{\mathbb{F}} \right) - \frac{\sqrt{3}\tilde{\rho}}{2\gamma} \left(\|\Delta \dot{\mathbf{X}}_K\|_{\mathbb{F}} + \|\Delta \dot{\mathbf{W}}_K\|_{\mathbb{F}} + \|\Delta \dot{\mathbf{A}}_K\|_{\mathbb{F}} \right). \end{aligned}$$

Recall that \mathcal{E}_k is monotonically decreasing and $\psi(\mathcal{E}_k) \geq \psi(\mathcal{E}_{k+1}) > 0$, it follows that

$$\sum_{k=\underline{k}}^K \|\Delta \dot{\mathbf{X}}_{k+1}\|_{\mathbb{F}} + \|\Delta \dot{\mathbf{W}}_{k+1}\|_{\mathbb{F}} + \|\Delta \dot{\mathbf{A}}_{k+1}\|_{\mathbb{F}} \leq \frac{\sqrt{3}\gamma}{2a\delta_0} \psi(\mathcal{E}_{\underline{k}}) + \frac{\sqrt{3}\tilde{\rho}}{2\gamma\delta_0} \left(\|\Delta \dot{\mathbf{X}}_{\underline{k}}\|_{\mathbb{F}} + \|\Delta \dot{\mathbf{W}}_{\underline{k}}\|_{\mathbb{F}} + \|\Delta \dot{\mathbf{A}}_{\underline{k}}\|_{\mathbb{F}} \right).$$

The right hand side of this inequality is bounded for any $K \geq \underline{k}$. Let $K \rightarrow \infty$ and we obtain

$$\sum_{k \geq \underline{k}} \|\Delta \dot{\mathbf{X}}_{k+1}\|_{\mathbb{F}} + \|\Delta \dot{\mathbf{W}}_{k+1}\|_{\mathbb{F}} + \|\Delta \dot{\mathbf{A}}_{k+1}\|_{\mathbb{F}} \leq \frac{\sqrt{3}\gamma}{2a\delta_0} \psi(\mathcal{E}_{\underline{k}}) + \frac{\sqrt{3}\tilde{\rho}}{2\gamma\delta_0} \left(\|\Delta \dot{\mathbf{X}}_{\underline{k}}\|_{\mathbb{F}} + \|\Delta \dot{\mathbf{W}}_{\underline{k}}\|_{\mathbb{F}} + \|\Delta \dot{\mathbf{A}}_{\underline{k}}\|_{\mathbb{F}} \right). \quad (51)$$

Since $\{(\dot{\mathbf{X}}_k, \dot{\mathbf{W}}_k, \dot{\mathbf{A}}_k)\}_{k \geq 0}$ is a bounded sequence, for any $\underline{k} \in \mathbb{N}_+$, it follows that

$$\lambda(\underline{k}) := \sum_{k=1}^{\underline{k}} \|\Delta \dot{\mathbf{X}}_k\|_{\mathbb{F}} + \|\Delta \dot{\mathbf{W}}_k\|_{\mathbb{F}} + \|\Delta \dot{\mathbf{A}}_k\|_{\mathbb{F}} < +\infty. \quad (52)$$

By combining (51) and (52), we conclude that $\sum_{k \geq 0} \|\Delta \dot{\mathbf{X}}_{k+1}\|_{\mathbb{F}} + \|\Delta \dot{\mathbf{W}}_{k+1}\|_{\mathbb{F}} + \|\Delta \dot{\mathbf{A}}_{k+1}\|_{\mathbb{F}}$ is finite.

Note that for any $p, q, K \in \mathbb{N}_+$ where $q \geq p > 0$, it follows that:

$$\begin{aligned} \|\dot{\mathbf{T}}_q - \dot{\mathbf{T}}_p\|_{\mathbb{F}} &= \left\| \sum_{k=p}^{q-1} \Delta \dot{\mathbf{T}}_{k+1} \right\|_{\mathbb{F}} \leq \sum_{k=p}^{q-1} \|\Delta \dot{\mathbf{T}}_{k+1}\|_{\mathbb{F}} \\ &\leq \sum_{k=p}^{q-1} \left(\|\Delta \dot{\mathbf{X}}_{k+1}\|_{\mathbb{F}} + \|\Delta \dot{\mathbf{W}}_{k+1}\|_{\mathbb{F}} + \|\Delta \dot{\mathbf{A}}_{k+1}\|_{\mathbb{F}} \right) \end{aligned}$$

$$\leq \sum_{k \geq 0} \|\Delta \dot{\mathbf{X}}_{k+1}\|_F + \|\Delta \dot{\mathbf{W}}_{k+1}\|_F + \|\Delta \dot{\mathbf{\Lambda}}_{k+1}\|_F < \infty.$$

This implies that $\{\dot{\mathbf{T}}_k\}_{k \geq 0} = \{(\dot{\mathbf{X}}_k, \dot{\mathbf{W}}_k, \dot{\mathbf{\Lambda}}_k)\}_{k \geq 0}$ is a Cauchy sequence and hence converges. Moreover, by Theorem 4.3, it converges to a stationary point. \square

Corollary 4.1. *Suppose the penalty parameter β is large enough, and $L_{1,k}, L_{2,k}$ are set as given constants for all k such that (20) and Assumption (A5) hold, then the sequence $\{(\dot{\mathbf{X}}_k, \dot{\mathbf{W}}_k, \dot{\mathbf{\Lambda}}_k)\}_{k \geq 0}$ generated by Algorithm 1 converges to a stationary point of SLRQA (2).*

Proof. It follows directly from the definition of SLRQA (2) that Assumption A1, A2 and A3 are all satisfied. Since (20) and Assumption (A5) hold, Assumption A4, A5 are also satisfied. Furthermore, the Huber function and Frobenius norm are semi-algebraic [3, Example 2]. From [28, Appendix, Lemma 4], it follows that the nuclear norm is also a semi-algebraic function. Since ϕ is a semi-algebraic function and the fact that the composition and sum of semi-algebraic functions are also semi-algebraic, we can conclude that \mathcal{R} is semi-algebraic and the KL-inequality 46 holds since any proper closed semi-algebraic function satisfies the KL-inequality [3, Theorem 3]. It follows from Theorem 4.4 that the sequence $\{(\dot{\mathbf{X}}_k, \dot{\mathbf{W}}_k, \dot{\mathbf{\Lambda}}_k)\}_{k \geq 0}$ generated by Algorithm 1 converges to a stationary point of SLRQA (2), which completes the proof. \square

5 An Algorithm for SLRQA-NF model

In this section, we propose the PL-ADMM-NF algorithm to solve SLRQA-NF (4) which is summarized in Algorithm 3. It is noted that SLRQA-NF is a model of the limiting case of SLRQA. The linearization technique is applied to the update of $\dot{\mathbf{W}}$. Each iteration of PL-ADMM-NF consists of minimizing the augmented Lagrange function with respect to $\dot{\mathbf{W}}$ variable after linearization, minimizing the augmented Lagrange function with respect to $\dot{\mathbf{X}}$ variable, and updating the multiplier.

The augmented Lagrangian function of SLRQA-NF (4) is given by:

$$\begin{aligned} \tilde{\mathcal{L}}_\beta(\dot{\mathbf{Z}}, \dot{\mathbf{W}}, \dot{\mathbf{\Lambda}}_1, \dot{\mathbf{\Lambda}}_2) &= \sum_i \phi(\sigma_i(\dot{\mathbf{Z}}), \gamma) + \lambda p(\dot{\mathbf{W}}) + \langle \dot{\mathbf{\Lambda}}_1, \dot{\mathbf{Z}} - \dot{\mathbf{W}} \rangle \\ &+ \frac{\beta}{2} \|\dot{\mathbf{Z}} - \dot{\mathbf{W}}\|_F^2 + \langle \dot{\mathbf{\Lambda}}_2, \mathcal{P}_\Omega(\mathcal{AW}^\#(\dot{\mathbf{W}})) - \mathcal{P}_\Omega(\dot{\mathbf{Y}}) \rangle + \frac{\beta}{2} \|\mathcal{P}_\Omega(\mathcal{AW}^\#(\dot{\mathbf{W}})) - \mathcal{P}_\Omega(\dot{\mathbf{Y}})\|_F^2 \\ &= \sum_i \phi(\sigma_i(\dot{\mathbf{Z}}), \gamma) + \lambda p(\dot{\mathbf{W}}) + \frac{\beta}{2} \|\dot{\mathbf{Z}} - \dot{\mathbf{W}} + \frac{1}{\beta} \dot{\mathbf{\Lambda}}_1\|_F^2 \\ &+ \frac{\beta}{2} \|\mathcal{P}_\Omega(\mathcal{AW}^\#(\dot{\mathbf{W}})) - \mathcal{P}_\Omega(\dot{\mathbf{Y}}) + \frac{1}{\beta} \dot{\mathbf{\Lambda}}_2\|_F^2 - \frac{1}{2\beta} \|\dot{\mathbf{\Lambda}}_1\|_F^2 - \frac{1}{2\beta} \|\dot{\mathbf{\Lambda}}_2\|_F^2, \end{aligned} \tag{53}$$

where $\beta > 0$ is the penalty parameter, $\dot{\mathbf{\Lambda}}_1, \dot{\mathbf{\Lambda}}_2 \in \mathbb{H}^{m \times n}$ are the Lagrange multipliers.

In Algorithm 3, the subproblem of $\dot{\mathbf{Z}}$ in Step 3 is the proximal ADMM step i.e. the minimization of $\tilde{\mathcal{L}}_\beta(\dot{\mathbf{Z}}, \dot{\mathbf{W}}, \dot{\mathbf{\Lambda}}_1, \dot{\mathbf{\Lambda}}_2)$ for fixed $\dot{\mathbf{W}}_k, \dot{\mathbf{\Lambda}}_{1,k}, \dot{\mathbf{\Lambda}}_{2,k}$ plus a proximal term $\frac{L_{1,k}}{2} \|\dot{\mathbf{Z}} - \dot{\mathbf{Z}}_k\|_F^2$. Since the subproblem is equivalent to

$$\min_{\dot{\mathbf{Z}}} \sum_i \phi(\sigma_i(\dot{\mathbf{Z}}), \gamma) + \frac{\beta + L_{1,k}}{2} \left\| \dot{\mathbf{Z}} - \frac{1}{\beta + L_{1,k}} \left(\beta \dot{\mathbf{W}}_k + \dot{\mathbf{\Lambda}}_{1,k} + L_{1,k} \dot{\mathbf{Z}}_k \right) \right\|_F^2,$$

Algorithm 3 PL-ADMM-NF algorithm for SLRQA-NF in (4)

Input: Corrupted images $\dot{\mathbf{Y}}$; two parameters $\mu \in (0, 2)$ and $\beta > 0$; a tolerance $\eta > 0$; a sequence of regularization parameters $\{L_{1,k}\}$ satisfying $\sup_{k \geq 0} L_{1,k} < \infty$ and $\inf_{k > 0} L_{1,k} > 0$.

Output: Recovered $\dot{\mathbf{Z}}_*$.

1: Set $\dot{\mathbf{Z}}_0 = \mathbf{0}$, $\dot{\mathbf{W}}_0 = \mathbf{0}$, $\dot{\mathbf{\Lambda}}_{1,0} = \mathbf{0}$, $\dot{\mathbf{\Lambda}}_{2,0} = \mathbf{0}$.

2: **for** $k = 0, 1, 2, \dots$ **do**

3: $\dot{\mathbf{Z}}$ subproblem:

$$\dot{\mathbf{Z}}_{k+1} \in \arg \min_{\dot{\mathbf{Z}}} \sum_i \phi(\sigma_i(\dot{\mathbf{Z}}), \gamma) + \langle \dot{\mathbf{\Lambda}}_{1,k}, \dot{\mathbf{Z}} - \dot{\mathbf{W}}_k \rangle + \frac{\beta}{2} \|\dot{\mathbf{Z}} - \dot{\mathbf{W}}_k\|_{\mathbb{F}}^2 + \frac{L_{1,k}}{2} \|\dot{\mathbf{Z}} - \dot{\mathbf{Z}}_k\|_{\mathbb{F}}^2;$$

4: $\dot{\mathbf{W}}$ subproblem:

$$\begin{aligned} \dot{\mathbf{W}}_{k+1} = \arg \min_{\dot{\mathbf{W}}} & \lambda \langle \nabla p(\dot{\mathbf{W}}_k), \dot{\mathbf{W}} - \dot{\mathbf{W}}_k \rangle + \beta \left\langle \dot{\mathbf{W}}_k - \dot{\mathbf{Z}}_{k+1} + \frac{1}{\beta} \dot{\mathbf{\Lambda}}_{1,k}, \dot{\mathbf{W}} - \dot{\mathbf{W}}_k \right\rangle \\ & + \beta \left\langle \mathcal{W}\mathcal{A}^\#(\mathcal{P}_\Omega(\mathcal{A}\mathcal{W}^\#(\dot{\mathbf{W}}_k) - \dot{\mathbf{Y}}) + \frac{1}{\beta} \dot{\mathbf{\Lambda}}_{2,k}, \dot{\mathbf{W}} - \dot{\mathbf{W}}_k \right\rangle + \frac{\beta\eta}{2} \|\dot{\mathbf{W}} - \dot{\mathbf{W}}_k\|_{\mathbb{F}}^2; \end{aligned}$$

5: $\dot{\mathbf{\Lambda}}_{1,k+1} = \dot{\mathbf{\Lambda}}_{1,k} + \mu\beta \cdot (\dot{\mathbf{Z}}_{k+1} - \dot{\mathbf{W}}_{k+1})$;

6: $\dot{\mathbf{\Lambda}}_{2,k+1} = \dot{\mathbf{\Lambda}}_{2,k} + \mu\beta \cdot \mathcal{P}_\Omega(\mathcal{A}\mathcal{W}^\#(\dot{\mathbf{W}}_{k+1}) - \dot{\mathbf{Y}})$;

7: **if** $\|\dot{\mathbf{Z}}_{k+1} - \dot{\mathbf{W}}_{k+1}\|_{\mathbb{F}} + \|\mathcal{P}_\Omega(\mathcal{A}\mathcal{W}^\#(\dot{\mathbf{W}}_{k+1})) - \mathcal{P}_\Omega(\dot{\mathbf{Y}})\|_{\mathbb{F}} < \eta$ **then**

8: $\dot{\mathbf{Z}}_* = \dot{\mathbf{Z}}_{k+1}$; **break**

9: **end if**

10: **end for**

Algorithm 2 can also be used to obtain $\dot{\mathbf{Z}}_{k+1}$.

In Step 4 of Algorithm 3, $\dot{\mathbf{W}}$, according to the linearization strategy in [21], a proximal gradient method is used in Step 4 to linearize the second order term. The penalty parameter of the second order term is denoted by $\beta\eta$. To be specific, the quadratic term $\frac{\beta}{2} \|\dot{\mathbf{W}} - \dot{\mathbf{Z}} - \frac{1}{\beta} \dot{\mathbf{\Lambda}}_1\|_{\mathbb{F}}^2 + \frac{\beta}{2} \|\mathcal{P}_\Omega(\mathcal{A}\mathcal{W}^\#(\dot{\mathbf{W}})) - \mathcal{P}_\Omega(\dot{\mathbf{Y}})\|_{\mathbb{F}}^2$ in $\tilde{\mathcal{L}}_\beta(\dot{\mathbf{Z}}, \dot{\mathbf{W}}, \dot{\mathbf{\Lambda}}_1, \dot{\mathbf{\Lambda}}_2)$ is replaced by the linearized term plus a regularized term $\beta \left\langle \dot{\mathbf{W}}_k - \dot{\mathbf{Z}}_{k+1} - \frac{1}{\beta} \dot{\mathbf{\Lambda}}_{1,k}, \dot{\mathbf{W}} - \dot{\mathbf{W}}_k \right\rangle + \beta \left\langle \mathcal{W}\mathcal{A}^\#(\mathcal{P}_\Omega(\mathcal{A}\mathcal{W}^\#(\dot{\mathbf{W}}_k) - \dot{\mathbf{Y}}) + \frac{1}{\beta} \dot{\mathbf{\Lambda}}_{2,k}, \dot{\mathbf{W}} - \dot{\mathbf{W}}_k \right\rangle$. Hence, the update of $\dot{\mathbf{W}}_{k+1}$ is given by

$$\dot{\mathbf{W}}_{k+1} = \dot{\mathbf{W}}_k - \frac{\mathcal{W}\mathcal{A}^\#(\mathcal{P}_\Omega(\mathcal{A}\mathcal{W}^\#(\dot{\mathbf{W}}_k) - \dot{\mathbf{Y}}) + \frac{1}{\beta} \dot{\mathbf{\Lambda}}_{2,k}) + \dot{\mathbf{W}}_k - \dot{\mathbf{Z}}_{k+1} - \frac{1}{\beta} \dot{\mathbf{\Lambda}}_{1,k}}{\eta} - \frac{\lambda}{\beta\eta} \nabla p(\dot{\mathbf{W}}_k). \quad (54)$$

Step 5 and 6 is used to update the Lagrange multipliers. Finally, the recovered image $\dot{\mathbf{X}}_*$ is given by $\dot{\mathbf{X}}_* = \mathcal{W}^\#(\dot{\mathbf{Z}}_*)$.

Remark 5.1. *{ The combination of two constraints in (4) with respect to $\dot{\mathbf{W}}$ and $\dot{\mathbf{Z}}$ can be represented by $(\mathbf{0}; \mathbf{I})$ and $(\mathbf{T}; \mathbf{I})$, where \mathbf{T} is the matrix form of $\mathcal{P}_\Omega(\mathcal{A}\mathcal{W}^\#)$. It follows that Assumption A3 is not satisfied. However, this assumption is essential in all known proofs for nonconvex ADMM*

and its variants [29, 36, 22] for the global convergence. Hence, existing techniques have difficulties proving the convergence of Algorithm 3. It is challenging to prove the global convergence result of variants of nonconvex ADMM without Assumption A3. We leave it as future works.}

6 Numerical experiment

In this section, color image denoising and image inpainting problems are respectively used to demonstrate the performance of SLRQA in (2) with Algorithm 1 and SLRQA-NF in (4) with Algorithm 3. In Section 6.1, we give the parameter setting for SLRQA and SLRQA-NF. In Section 6.2, we compare SLRQA and SLRQA-NF models based on quaternion and RGB representation to demonstrate the rationality of quaternion representation. Furthermore, in Section 6.3 and 6.4, comparisons of SLRQA and SLRQA-NF with other state-of-the-art methods are also presented to respectively show the superiority of SLRQA and SLRQA-NF. All the experiments are performed using MATLAB R2022b running on a desktop with an Intel Core R7-5800H CPU (3.90 GHz) and 16 GB of RAM. The codes are available at <https://github.com/dengzhanwang/SLRQA/tree/main>.

6.1 Problem description, parameter setting, and testing environment

The models for color image denoising and image inpainting are respectively given by

$$\min_{\dot{\mathbf{X}}, \dot{\mathbf{W}} \in \mathbb{H}^{m \times n}} \sum_i \phi(\sigma_i(\dot{\mathbf{X}}), \gamma) + \lambda p(\dot{\mathbf{W}}) + \frac{1}{2\tau^2} \|\dot{\mathbf{X}} - \dot{\mathbf{Y}}\|_{\mathbb{F}}^2, \quad \text{s.t. } \mathcal{W}(\dot{\mathbf{X}}) = \dot{\mathbf{W}}, \quad (55)$$

and

$$\min_{\dot{\mathbf{Z}}, \dot{\mathbf{W}} \in \mathbb{H}^{m \times n}} \sum_i \phi(\sigma_i(\dot{\mathbf{Z}}), \gamma) + \lambda p(\dot{\mathbf{W}}), \quad \text{s.t. } \mathcal{P}_{\Omega}(\mathcal{W}^{\#}(\dot{\mathbf{W}})) = \mathcal{P}_{\Omega}(\dot{\mathbf{Y}}), \quad \dot{\mathbf{Z}} = \dot{\mathbf{W}}, \quad (56)$$

where \mathcal{W} is the QDCT [12], $p(\dot{\mathbf{W}})$ is chosen as the Huber function, i.e., $(p(\dot{\mathbf{W}}))_{ij} = \frac{1}{2\delta} |\dot{\mathbf{W}}_{ij}|^2$ if $|\dot{\mathbf{W}}_{ij}| < \delta$; and $(p(\dot{\mathbf{W}}))_{ij} = |\dot{\mathbf{W}}_{ij}| - \frac{1}{2}\delta$ otherwise, $\delta > 0$ is a prescribed constant, and the function ϕ are chosen as the Schatten- γ , Laplace, or Weighted Schatten- γ functions. Note that the color image denoising problem (55) is the SLRQA in (2) with \mathcal{A} being identity, Ω being the entire indices of pixels, and p being the Huber function. The color image inpainting problem (56) is the SLRQA-NF in (4) with \mathcal{A} being identity and p being the Huber function. Problem (55) with the Schatten- γ , Laplace, and Weighted Schatten- γ functions for ϕ is respectively denoted by SLRQA-1, SLRQA-2, and SLRQA-3. Likewise, Problem (56) using the three options of ϕ is denoted by SLRQA-NF-1, SLRQA-NF-2, and SLRQA-NF-3.

The ten images in Figure 1 are used to generate simulation problems. Specifically, for image denoising, the noisy images $\dot{\mathbf{Y}}$ are obtained by adding additive white Gaussian noise with zero mean and variance τ^2 to the color images in Figure 1, and for image inpainting, each pixel of an image is chosen to be in the indices set Ω with the same probability $\chi \in (0, 1)$. Therefore, χ is also called the missing rate. The parameters τ , λ , and γ are specified later when reporting numerical results. Note that the parameters γ and λ depend on the choice of the surrogate function ϕ , the noise level, and whether the non-local self-similarity is used. The parameter δ is set depending on

the accuracy of the current iterate. Specifically, $\delta = 1$ if $\epsilon_k \geq 10^{-2}$, $\delta = 10^{-2}$ if $10^{-3} \leq \epsilon_k < 10^{-2}$, and $\delta = 10^{-4}$ otherwise, where $\epsilon_k = \|\dot{\mathbf{X}}_{k+1} - \dot{\mathbf{X}}_k\|_F + \|\dot{\mathbf{W}}_{k+1} - \dot{\mathbf{W}}_k\|_F + \|\mathcal{W}(\dot{\mathbf{X}}_{k+1}) - \dot{\mathbf{W}}_{k+1}\|_F$ in Algorithm 1 and $\epsilon_k = \|\dot{\mathbf{Z}}_{k+1} - \dot{\mathbf{W}}_{k+1}\|_F + \|\mathcal{P}_\Omega(\mathcal{W}^\#(\dot{\mathbf{W}}_{k+1})) - \mathcal{P}_\Omega(\dot{\mathbf{Y}})\|_F$ in Algorithm 3.

The parameters in Algorithm 1, 2 and 3 are set as $\mu = 1.1$, $\beta = 10$, $L_{1,k} = L_{2,k} = 1, \forall k$, $\eta_C = 10^{-10}$, and $\eta = 10^{-4}$. Note that $\eta_C = 10^{-10}$ is for the high accuracy of the $\dot{\mathbf{X}}$ or $\dot{\mathbf{Z}}$ -subproblem.

The `qtfm` [1] package is used for the quaternion computations except the QSVD. The QSVD of a quaternion matrix $\dot{\mathbf{X}} \in \mathbb{H}^{m \times n}$ is computed by taking the SVD of the complex adjoint form of $\dot{\mathbf{X}}$, which needs an SVD of a $2m \times 2n$ complex matrix and is more efficient. For the details, we refer to [10].

Peak Signal-to-Noise Ration (PSNR) and Structure Similarity (SSIM) [30] are chosen to measure the quality of the images recovered by all methods. Specifically, the PSNR of two color image \mathbf{X} and $\mathbf{Y} \in \mathbb{R}^{m \times n \times 3}$ is calculated as: $\text{PSNR}(\mathbf{X}, \mathbf{Y}) = 10 \log_{10} \frac{\text{peakval}}{\text{MSE}}$, where $\text{MSE} = \frac{1}{3mn} \sum_{i=1}^m \sum_{j=1}^n \sum_{k=1}^3 |\mathbf{X}_{i,j,k} - \mathbf{Y}_{i,j,k}|^2$, and *peakval* is taken from the range of the image data type. Furthermore, the SSIM of \mathbf{X} and \mathbf{Y} is given by

$$\text{SSIM}(\mathbf{X}_{ij}, \mathbf{Y}_{ij}) = \frac{1}{MN} \sum_{i=1}^M \sum_{j=1}^N \text{SSIM}(\mathbf{X}_{ij}, \mathbf{Y}_{ij}) \quad (57)$$

$$\text{SSIM}(\mathbf{X}_{ij}, \mathbf{Y}_{ij}) = l(\mathbf{X}_{ij}, \mathbf{Y}_{ij}) c(\mathbf{X}_{ij}, \mathbf{Y}_{ij}) s(\mathbf{X}_{ij}, \mathbf{Y}_{ij}), \quad (58)$$

where \mathbf{X}_{ij} and \mathbf{Y}_{ij} denote the local image patches, M and N denote the number of local patches along horizontal and vertical direction respectively, the three functions $l(\mathbf{X}_{ij}, \mathbf{Y}_{ij})$, $c(\mathbf{X}_{ij}, \mathbf{Y}_{ij})$, and $s(\mathbf{X}_{ij}, \mathbf{Y}_{ij})$ respectively denote luminance item, contrast item, and structure item, and they are defined as follows:

$$l(\mathbf{X}_{ij}, \mathbf{Y}_{ij}) = \frac{2\mu_{\mathbf{X}_{ij}}\mu_{\mathbf{Y}_{ij}} + C_1}{\mu_{\mathbf{X}_{ij}}^2 + \mu_{\mathbf{Y}_{ij}}^2 + C_1}, \quad c(\mathbf{X}_{ij}, \mathbf{Y}_{ij}) = \frac{2\sigma_{\mathbf{X}_{ij}}\sigma_{\mathbf{Y}_{ij}} + C_2}{\sigma_{\mathbf{X}_{ij}}^2 + \sigma_{\mathbf{Y}_{ij}}^2 + C_2}, \quad s(\mathbf{X}_{ij}, \mathbf{Y}_{ij}) = \frac{\sigma_{\mathbf{X}_{ij}\mathbf{Y}_{ij}} + C_3}{\beta_{\mathbf{X}_{ij}}\sigma_{\mathbf{Y}_{ij}} + C_3}, \quad (59)$$

with $\mu_{\mathbf{X}_{ij}}, \mu_{\mathbf{Y}_{ij}}, \sigma_{\mathbf{X}_{ij}}, \sigma_{\mathbf{Y}_{ij}}, \sigma_{\mathbf{X}_{ij}\mathbf{Y}_{ij}}, C_1, C_2$ and C_3 being the mean, standard deviation and cross-covariance of image patches \mathbf{X}_{ij} and \mathbf{Y}_{ij} , $10^{-4}, 9 \times 10^{-4}$ and 4.5×10^{-4} respectively. MATLAB commands `psnr` and `ssim` are used to compute the PSNR and SSIM for color images. In general, the higher values the PSNR and SSIM are, the better the denoising quality is.

6.2 Quaternion and RGB representation

Simulation problems of image denoising in Section 6.2.1 and image inpainting in Section 6.2.2 are used to compare the performance of quaternion and RGB representations.

6.2.1 Image denoising

The parameter γ is set as 0.5 in SLRQA-1, SLRQA-2, and SLRQA-3. The parameter w in SLRQA-3 is chosen depending on the number of iteration k and the index i , i.e., $w_{i,k} = 20/(\sigma_i(\dot{\mathbf{X}}_{k-1}) + 10^{-4})$.

Note that the definition of ϕ for SLRQA-3 depends on the index i . Such dependency has been used in e.g., [10]. The multiple values of (λ, τ) are used, i.e., $(\lambda, \tau) = (0.01, 10), (0.3, 30),$ and $(0.5, 50)$.

The PSNR and SSIM values of SLRQA with quaternion and RGB representation are reported in Table 2. Furthermore, the comparison of the two representations for SLRQA-1 with different noise levels is shown in Figure 2. The figure and table show that SLRQA with quaternion representation achieves higher PSNR and SSIM compared with RGB representation in all cases. This observation coincides with the intuition that quaternion representation utilizes the information between channels to achieve better performance.

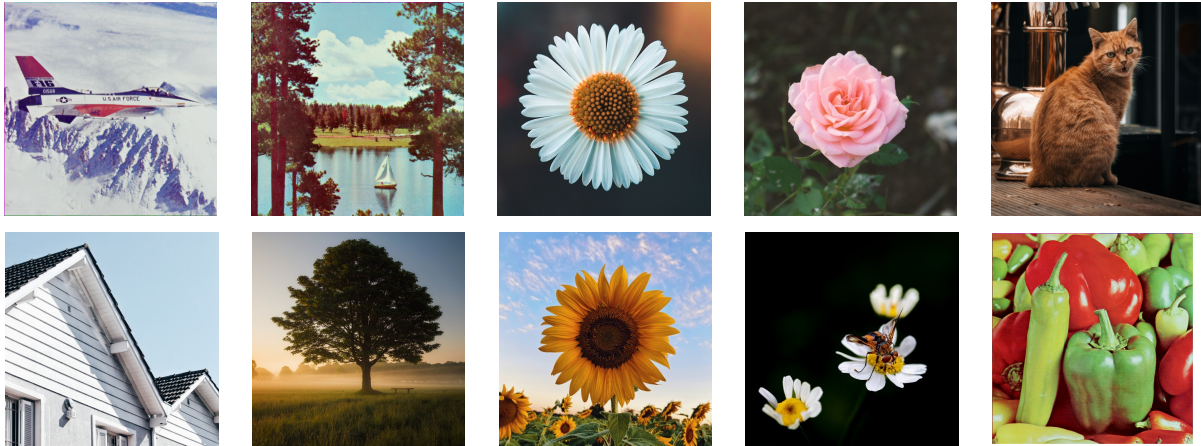


Figure 1: The 10 color images ($512 \times 512 \times 3$) for numerical experiments.

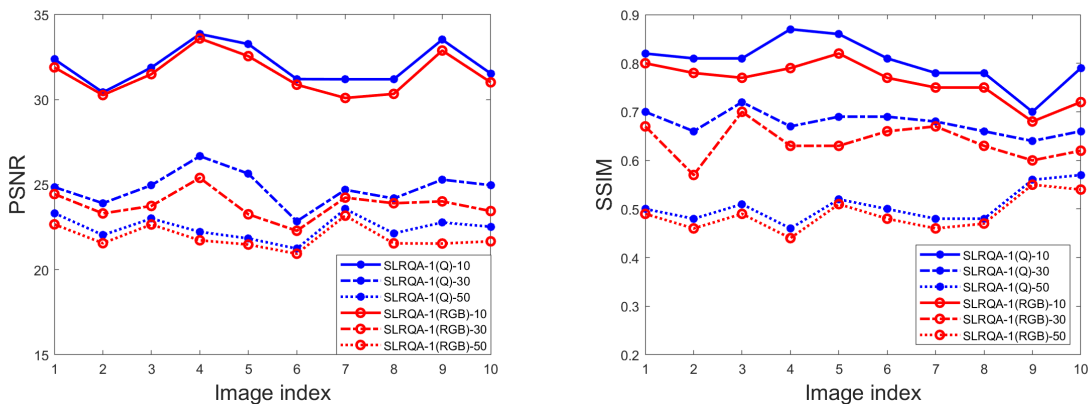


Figure 2: PSNR and SSIM comparison of SLRQA-1 using quaternion and RGB representation. In the legend, the suffix (Q) means that quaternion representation is used, and (RGB) means that RGB representation is used. The numbers 10, 30, and 50 denote the variance of the noise respectively.

Table 2: PSNR/SSIM values of SLRQA using the RGB and quaternion representations. “QR” denotes that the quaternion representation is used. **Bold** fonts denote the best performance on the same conditions.

Model \ Image		Image									
		Image1	Image2	Image3	Image4	Image5	Image6	Image7	Image8	Image9	Image10
SLRQA-1 $\tau = 10$	QR	32.38/0.82	30.43/0.81	31.89/0.81	33.86/0.87	33.27/0.86	31.21/0.81	31.20/0.78	31.20/0.78	33.53/0.70	31.54/0.79
	RGB	31.90/0.80	30.27/0.78	31.50/0.77	33.60/0.79	32.56/0.82	30.88/0.77	30.10/0.75	30.34/0.75	32.89/0.68	31.02/0.72
SLRQA-1 $\tau = 30$	QR	24.86/0.70	23.91/0.66	24.97/0.72	26.68/0.67	25.65/0.69	22.85/0.69	24.70/0.68	24.19/0.66	25.30/0.64	24.97/0.66
	RGB	23.55/0.67	20.71/0.57	23.65/0.70	25.10/0.63	23.26/0.63	21.29/0.66	22.74/0.67	23.91/0.63	24.02/0.60	23.45/0.62
SLRQA-1 $\tau = 50$	QR	23.33/0.50	22.04/0.48	23.01/0.51	22.23/0.46	21.84/0.52	21.24/0.50	23.57/0.48	22.14/0.48	22.78/0.56	22.53/0.57
	RGB	22.67/0.49	21.56/0.46	22.66/0.49	21.73/0.44	21.48/0.51	20.94/0.48	23.18/0.46	21.55/0.47	21.54/0.55	21.67/0.54
SLRQA-2 $\tau = 10$	QR	31.45/0.78	30.19/0.80	31.79/0.78	32.45/0.75	31.18/0.80	30.92/0.80	30.82/0.75	30.75/0.74	32.87/0.70	31.56/0.76
	RGB	31.20/0.77	30.72/0.80	31.46/0.78	31.91/0.72	31.04/0.80	30.57/0.79	30.20/0.74	30.35/0.72	31.40/0.67	30.32/0.72
SLRQA-2 $\tau = 30$	QR	24.30/0.61	22.77/0.64	25.21/0.64	22.74/0.57	25.32/0.58	21.72/0.64	24.39/0.68	24.06/0.62	25.45/0.68	25.02/0.70
	RGB	24.12/0.60	22.47/0.63	24.98/0.62	22.52/0.56	25.02/0.58	21.59/0.62	24.26/0.68	23.75/0.60	24.82/0.65	24.30/0.64
SLRQA-2 $\tau = 50$	QR	23.50/0.51	22.77/0.52	24.91/0.58	22.34/0.47	22.62/0.67	21.02/0.51	23.09/0.45	23.26/0.52	23.02/0.62	22.60/0.70
	RGB	23.27/0.51	21.96/0.52	24.76/0.57	22.03/0.46	21.88/0.65	20.94/0.51	22.88/0.45	22.90/0.51	22.32/0.60	22.12/0.65
SLRQA-3 $\tau = 10$	QR	32.86/0.81	31.20/0.82	32.03/0.84	30.36/0.75	32.50/0.87	30.77/0.76	31.10/0.80	31.92/0.76	33.89/0.73	31.87/0.82
	RGB	32.76/0.80	30.80/0.81	31.30/0.84	30.01/0.74	32.04/0.86	30.17/0.74	30.48/0.78	31.65/0.75	32.20/0.68	32.02/0.78
SLRQA-3 $\tau = 30$	QR	26.40/0.67	24.02/0.64	26.22/0.68	24.21/0.64	26.34/0.68	22.50/0.63	26.42/0.68	26.12/0.67	25.80/0.68	25.68/0.70
	RGB	25.32/0.66	23.78/0.63	26.18/0.67	23.82/0.64	25.89/0.67	22.13/0.61	24.26/0.68	26.05/0.66	24.79/0.62	25.03/0.67
SLRQA-3 $\tau = 50$	QR	23.90/0.51	22.06/0.45	24.99/0.60	23.51/0.49	22.72/0.65	22.00/0.53	23.92/0.53	24.32/0.56	23.04/0.63	23.10/0.65
	RGB	23.57/0.50	21.46/0.43	24.76/0.60	22.63/0.50	22.08/0.63	21.94/0.53	23.18/0.52	23.58/0.55	22.23/0.56	22.30/0.62

6.2.2 Image inpainting

The parameter γ is set as 0.7, 1, and 0.7 respectively for SLRQA-NF-1, SLRQA-NF-2, and SLRQA-NF-3. The parameter w in SLRQA-NF-3 is set as $w_{i,k} = 10/(\sigma_i(\dot{\mathbf{X}}_{k-1}) + 10^{-4})$.

It is shown in Table 3 that the PSNR and SSIM values of the SLRQA-NF with quaternion representation are higher than SLRQA-NF with RGB representation for all different missing rate χ . Furthermore, the PSNR and SSIM values of different χ and different images are given in Figure 3 which shows that SLRQA-NF-1 with quaternion representation method outperforms SLRQA-NF-1 with RGB representation by a large margin. Moreover, the improvements in PSNR and SSIM increase with the rate of corruption.

It is concluded that the quaternion-based model achieves better denoising and inpainting performance. Hence, it is preferable to use the quaternion model in color image processing.

6.3 Color image denoising

NSS is a significant technique in color image denoising problems. The comparison without NSS directly reflects the superiority of the compared models, and the comparison with NSS better reflects the robustness of the models in practice. To fully compare the SLRQA with other state-of-the-art color image denoising methods, we tested their performance without and with the usage of non-local self-similarity (NSS) respectively in Section 6.3.1 and Section 6.3.2.

Table 3: PSNR/SSIM values of SLRQA-NF using the RGB and quaternion representations. “QR” denotes that the quaternion representation is used.

Model		Image									
		Image1	Image2	Image3	Image4	Image5	Image6	Image7	Image8	Image9	Image10
SLRQA-NF-1 ($\chi=0.3$)	QR	35.58/0.96	31.37/0.97	34.56/0.98	42.48/0.99	39.38/0.98	32.73/0.99	32.45/0.97	35.08/1.00	34.93/0.99	34.41/0.99
	RGB	34.66/0.93	30.83/0.96	33.66/0.97	40.19/0.98	38.63/0.99	30.10/0.90	30.85/0.92	33.91/0.98	34.11/0.99	33.61/0.99
SLRQA-NF-1 ($\chi=0.5$)	QR	32.03/0.94	28.04/0.94	30.40/0.96	37.56/0.98	34.82/0.98	25.75/0.98	27.88/0.92	31.06/0.97	31.58/0.98	31.28/0.98
	RGB	31.19/0.90	27.59/0.93	29.77/0.93	36.42/0.98	34.28/0.97	25.10/0.77	27.35/0.86	30.33/0.96	30.91/0.98	30.63/0.98
SLRQA-NF-1 ($\chi=0.7$)	QR	28.29/0.88	25.20/0.89	26.35/0.93	33.16/0.99	31.00/0.96	23.78/0.96	26.63/0.81	27.12/0.94	28.90/0.97	28.26/0.97
	RGB	25.49/0.71	22.53/0.79	23.23/0.75	29.27/0.89	28.42/0.86	20.59/0.59	24.48/0.77	24.72/0.86	25.85/0.77	25.53/0.93
SLRQA-NF-1 ($\chi=0.8$)	QR	25.88/0.84	23.14/0.86	24.91/0.90	30.74/0.95	28.63/0.93	21.61/0.93	25.29/0.74	25.30/0.92	25.54/0.96	26.67/0.96
	RGB	22.41/0.54	20.63/0.69	21.12/0.67	26.51/0.81	24.92/0.78	18.14/0.46	22.82/0.71	22.38/0.79	23.97/0.61	22.54/0.91
SLRQA-NF-2 ($\chi=0.3$)	QR	35.33/0.96	30.97/0.97	33.56/0.98	40.86/0.99	38.09/0.99	31.26/0.97	32.12/0.97	34.13/0.99	34.49/0.99	34.18/0.99
	RGB	34.18/0.95	30.83/0.97	33.15/0.98	39.19/0.99	37.81/0.99	26.62/0.99	26.85/0.95	33.54/0.98	33.97/0.99	33.84/0.99
SLRQA-NF-2 ($\chi=0.5$)	QR	31.25/0.94	27.53/0.94	29.65/0.96	36.27/0.99	33.75/0.98	26.62/0.91	28.91/0.94	30.15/0.97	31.08/0.98	30.83/0.98
	RGB	30.65/0.92	27.49/0.94	29.46/0.95	35.60/0.97	33.63/0.97	24.62/0.96	26.91/0.90	29.92/0.96	30.78/0.98	30.63/0.98
SLRQA-NF-2 ($\chi=0.7$)	QR	27.30/0.88	24.05/0.89	25.87/0.93	31.87/0.99	29.95/0.96	22.70/0.80	26.19/0.89	26.41/0.94	27.56/0.97	27.46/0.97
	RGB	25.90/0.86	23.19/0.87	25.63/0.90	31.27/0.96	27.39/0.94	20.26/0.77	24.52/0.85	25.17/0.93	25.53/0.96	25.25/0.96
SLRQA-NF-2 ($\chi=0.8$)	QR	24.54/0.79	22.24/0.84	23.61/0.89	28.74/0.94	27.09/0.91	20.11/0.71	24.52/0.86	23.89/0.90	25.56/0.95	25.33/0.95
	RGB	21.90/0.76	21.84/0.83	21.13/0.86	26.35/0.93	24.92/0.91	17.85/0.81	22.35/0.85	21.23/0.89	23.07/0.94	22.75/0.95
SLRQA-NF-3 ($\chi=0.3$)	QR	35.91/0.96	31.41/0.97	34.46/0.98	41.86/0.99	39.00/0.99	32.80/0.97	32.52/0.97	34.61/1.00	35.77/0.99	34.63/0.99
	RGB	34.66/0.93	30.83/0.96	33.66/0.97	40.19/0.99	38.63/0.99	28.79/0.95	30.33/0.95	33.91/0.98	34.11/0.99	33.61/0.99
SLRQA-NF-3 ($\chi=0.5$)	QR	32.02/0.93	28.21/0.94	30.52/0.96	37.69/0.99	34.80/0.98	27.97/0.92	29.33/0.94	30.92/0.97	32.14/0.98	31.60/0.98
	RGB	31.23/0.90	27.59/0.93	29.77/0.93	36.42/0.98	34.28/0.97	25.46/0.90	27.37/0.91	30.33/0.96	30.91/0.98	30.63/0.98
SLRQA-NF-3 ($\chi=0.7$)	QR	28.40/0.88	25.05/0.89	26.87/0.93	33.37/0.97	30.95/0.96	24.00/0.83	26.77/0.89	27.41/0.94	28.56/0.97	28.46/0.97
	RGB	25.59/0.72	22.53/0.80	23.23/0.76	29.27/0.90	28.42/0.89	22.10/0.80	24.86/0.85	24.72/0.87	25.85/0.78	25.53/0.94
SLRQA-NF-3 ($\chi=0.8$)	QR	26.08/0.84	23.36/0.86	25.11/0.91	30.86/0.95	28.70/0.93	21.83/0.76	25.43/0.86	25.58/0.92	26.74/0.96	26.75/0.96
	RGB	22.60/0.56	20.84/0.70	21.24/0.67	26.72/0.81	25.12/0.79	21.83/0.74	25.43/0.82	22.60/0.80	23.97/0.61	22.89/0.91

6.3.1 Color image denoising without NSS

The compared methods include SRRC[39], WNNM[14], LRQA[10], and DWT[5]³. SRRC exploits the weighted Schatten p -norm as the regularizer for the rank residual to obtain a new rank minimization model. WNNM uses the weighted nuclear norm as an alternative function to the rank function. LRQA is a quaternion-based model that makes use of the low-rankness property by a nonconvex surrogate function. Compared with SLRQA, none of SRRC, WNNM, and LRQA exploits the sparsity feature of the image. DWT [5] is a vanilla analysis-based approach (5) where low-rankness prior is not used and is implemented on our own. It is noted that SRRC, WNNM, and DWT are RGB-based methods, and LRQA and SLRQA are quaternion-based models. LRQA-1 and LRQA-2 denote the LRQA models using Schatten- γ and Laplace function, respectively. For the compared methods, we use the default parameters stated in the corresponding papers.

³The implementations that we use are available from:

SRRC: <https://github.com/zt9877/SRRC.git>

WNNM: <http://www4.comp.polyu.edu.hk/~cslzhang/papers.htm>

LRQA: <https://www.fst.um.edu.mo/personal/wp-content/uploads/2021/05/LRQA.zip>

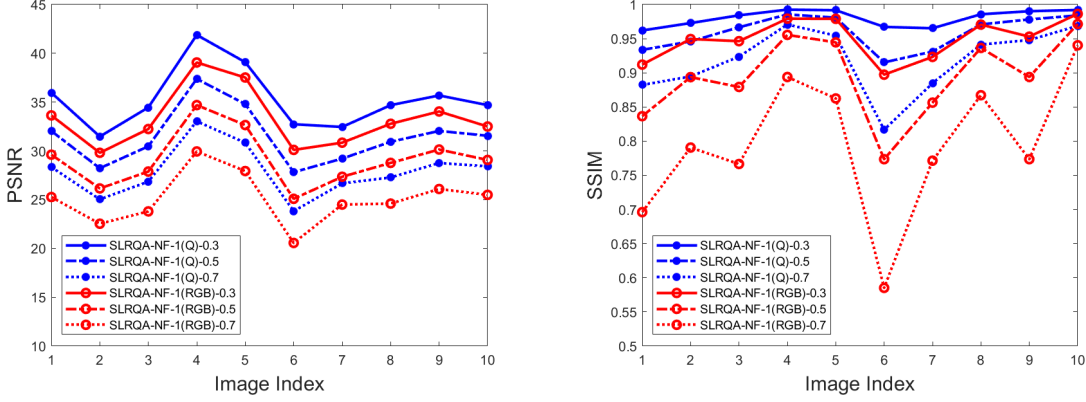


Figure 3: PSNR and SSIM comparisons of quaternion and RGB based SLRQA-NF-1. In the legend, the suffix (Q) means that quaternion representation is used, and (RGB) means that RGB representation is used. The numbers 0.3, 0.5, and 0.7 denote the missing rate of the images respectively.

The PSNR and SSIM results of the compared methods are shown in Table 4. It can be seen that SLRQA has better results than the other methods in terms of PSNR and SSIM in most cases. Furthermore, The PSNR value of SRRC, WNNM, and DWT are much lower than that of SLRQA when τ is large. Note that since NSS is not utilized in these methods, the results in Table 4 underscore the effectiveness and robustness of the SLRQA model and further validate the advanced nature and adaptability of its intrinsic architecture. We also give the visual comparison between all competing methods and SLRQA as shown in Figure 4. It can be seen in the highlighted red rectangles that when compared with other denoising methods, SLRQA can preserve more details of images. In particular, in terms of hair details, the images denoised by the DWT and LRQA-1 methods are still noisy. The images recovered by LRQA and SRRC methods contain blurry parts and hence the detail features of the images are lost. In contrast, the images recovered by SLRQA models have better results both numerically and visually.

To further analyze the details of PL-ADMM, we plot the empirical convergence of PL-ADMM for Problem (55) on ten tested images with $\tau = 30$. The results are shown in Figure 5. It can be observed that the error curve has a downward trend, illustrating the empirical convergence of Algorithm 1. We can observe that $\|\Delta\dot{\mathbf{X}}_{k+1}\|_F + \|\Delta\dot{\mathbf{W}}_{k+1}\|_F + \|\Delta\dot{\mathbf{A}}_{k+1}\|_F \rightarrow 0$. Hence, it follows from (42) that $\|\tilde{\mathbf{D}}_{k+1}\| \rightarrow 0$. According to the update of $\dot{\mathbf{A}}_{k+1}$ and Lemma 4.7, it follows that $(\dot{\mathbf{X}}, \dot{\mathbf{W}}, \dot{\mathbf{A}})$ converges to a stationary point of \mathcal{L}_β and hence a KKT point of the original problem in (55).

Table 4: PSNR/SSIM results on color image denoising problem of different methods without NSS.

Algorithm		SRRC[39]	WNNM[14]	DWT[5]	LRQA-1[10]	LRQA-2[10]	SLRQA-1	SLRQA-2	SLRQA-3
Image									
$\tau = 10$	Image1	29.23/0.70	28.06/0.73	27.67/0.61	28.48/0.61	29.21/0.65	31.55/0.76	31.45/0.78	32.86/0.81
	Image2	28.56/0.73	28.01/0.70	27.98/0.71	28.44/0.72	28.42/0.72	30.36/0.80	30.19/0.80	31.20/0.82
	Image3	28.03/0.60	27.81/0.61	28.21/0.61	28.49/0.64	28.56/0.65	31.33/0.77	31.79/0.78	32.03/0.84
	Image4	28.12/0.60	27.90/0.65	28.29/0.66	28.53/0.64	28.55/0.68	30.09/0.74	31.45/0.75	30.36/0.75
	Image5	28.82/0.66	28.72/0.64	28.67/0.64	28.85/0.65	28.71/0.67	32.13/0.85	31.18/0.80	32.50/0.87
	Image6	28.32/0.60	27.89/0.56	28.02/0.61	28.72/0.65	28.66/0.65	30.75/0.76	30.92/0.80	30.77/0.76
	Image7	28.45/0.62	27.32/0.58	28.02/0.59	28.65/0.60	29.04/0.94	30.95/0.73	30.82/0.75	31.10/0.80
	Image8	28.01/0.60	28.11/0.59	28.46/0.58	28.56/0.63	28.24/0.63	31.23/0.76	30.75/0.74	31.92/0.76
	Image9	28.02/0.74	27.98/0.73	27.62/0.71	28.82/0.76	29.10/0.76	30.14/0.70	29.66/0.78	30.80/0.79
	Image10	30.52/0.74	29.72/0.72	29.62/0.70	30.90/0.76	31.10/0.79	31.14/0.78	31.26/0.80	31.32/0.81
$\tau = 30$	Image1	20.32/0.30	20.41/0.25	20.36/0.28	20.49/0.27	20.80/0.30	25.47/0.66	24.30/0.61	26.40/0.67
	Image2	20.01/0.32	20.73/0.32	20.09/0.33	20.44/0.37	20.40/0.37	23.90/0.61	22.77/0.64	24.02/0.64
	Image3	00.12/0.21	20.24/0.22	20.55/0.25	20.50/0.27	21.10/0.31	26.15/0.65	25.21/0.64	26.22/0.68
	Image4	20.22/0.29	20.10/0.26	20.01/0.29	20.68/0.29	20.20/0.31	23.81/0.59	22.74/0.57	24.21/0.64
	Image5	21.02/0.32	20.58/0.33	20.65/0.37	21.23/0.30	21.30/0.33	26.60/0.68	25.32/0.58	26.34/0.68
	Image6	20.87/0.33	21.01/0.37	20.37/0.37	20.76/0.36	20.61/0.35	23.95/0.66	21.72/0.64	22.50/0.63
	Image7	20.33/0.29	20.71/0.29	20.94/0.22	20.93/0.26	20.21/0.21	25.12/0.63	24.39/0.68	26.42/0.68
	Image8	20.56/0.22	20.42/0.24	21.08/0.28	20.77/0.29	20.90/0.29	25.14/0.64	24.06/0.62	26.12/0.67
	Image9	24.82/0.58	24.22/0.58	23.62/0.55	24.90/0.58	25.10/0.61	25.30/0.64	25.45/0.68	25.80/0.68
	Image10	24.32/0.64	23.82/0.62	23.62/0.61	24.34/0.66	24.90/0.68	24.97/0.66	25.02/0.70	25.68/0.70
$\tau = 50$	Image1	17.92/0.17	17.01/0.14	18.01/0.18	17.66/0.17	17.30/0.18	23.33/0.50	23.50/0.51	23.90/0.51
	Image2	16.02/0.21	17.03/0.20	17.94/0.25	17.53/0.25	17.10/0.26	22.04/0.48	22.77/0.52	22.06/0.45
	Image3	17.75/0.15	17.40/0.21	17.24/0.19	17.56/0.17	17.90/0.18	24.21/0.51	24.91/0.58	24.99/0.60
	Image4	17.08/0.14	16.60/0.16	16.87/0.17	17.82/0.19	17.20/0.14	22.23/0.46	22.34/0.47	23.51/0.49
	Image5	18.04/0.17	18.08/0.17	18.31/0.18	18.39/0.19	18.30/0.17	21.84/0.52	21.62/0.67	22.72/0.65
	Image6	17.53/0.25	18.01/0.26	17.11/0.22	17.75/0.26	18.61/0.29	21.24/0.50	21.02/0.51	22.00/0.53
	Image7	17.60/0.17	18.21/0.18	17.11/0.13	18.08/0.17	18.71/0.17	23.57/0.48	23.09/0.45	23.92/0.53
	Image8	17.02/0.14	17.42/0.18	17.62/0.19	17.90/0.18	18.10/0.29	23.14/0.48	23.26/0.52	24.32/0.56
	Image9	22.02/0.51	21.92/0.49	21.62/0.46	22.34/0.52	22.67/0.55	22.78/0.56	23.02/0.62	23.04/0.63
	Image10	21.82/0.50	21.42/0.48	21.32/0.45	22.32/0.51	22.10/0.51	22.74/0.54	22.60/0.52	23.10/0.58

6.3.2 Color image denoising with NSS

For color image denoising problems with NSS, in addition to the methods compared in Section 6.3.1, we also compare SLRQA with CBM3D [11]⁴. Instead of constructing a denoising model, CBM3D employs block matching and sparse 3D collaborative filtering techniques to denoise the image, a process that cannot be achieved without using NSS. Hence we do not conduct a comparison with the CBM3D algorithm in the experiments of Section 6.3.1.

The NSS prior is based on the fact that for a given local patch in a natural image, one can find many similar patches across the whole image. This technique has been widely used for image processing problems, such as image denoising, image deblurring, and image repairing. Here, the NSS process in [10] is used. Specifically, a noisy image $\hat{\mathbf{Y}}$ is divided into n overlapping patches of size $\sqrt{d} \times \sqrt{d}$. Each patch is transformed into a vector $\hat{\mathbf{y}}^i \in \mathbb{H}^d, i = 1, 2, \dots, n$. Then for each patch, s nearest neighbor patches are selected from a searching window with $L \times L$ pixels to form a set K_i .

⁴The implementation is available from <http://www.cs.tut.fi/~foi/GCF-BM3D>.

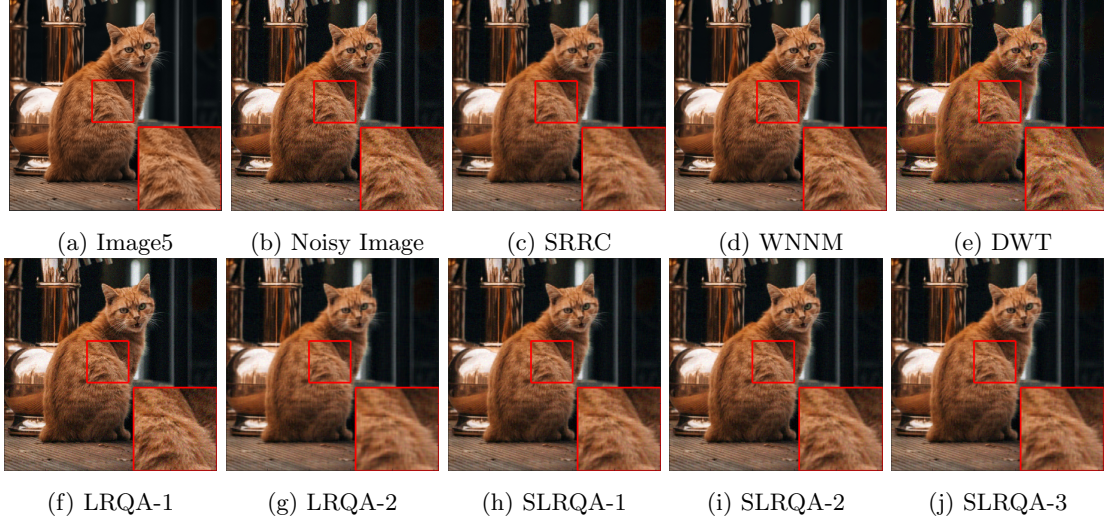


Figure 4: Color image denoising results of different methods on “Image5” with $\tau = 10$.

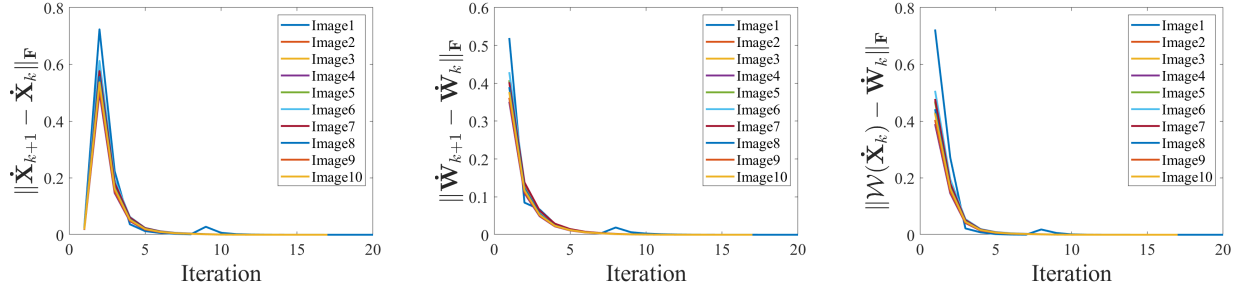


Figure 5: The error convergence of SLRQA-1 for image denoising problems.

All patches in K_i are stacked into a matrix $\dot{\mathbf{Y}}^i \in \mathbb{H}^{d \times s}$. We denoise $\dot{\mathbf{Y}}^i$ and aggregate all denoised patches together to form the clean color image $\dot{\mathbf{X}}$. Since all patches in each data matrix have similar structures, the constructed data matrix $\dot{\mathbf{Y}}^i$ is low rank. We also adopt the iterative regularization scheme in [10] and the iterative relaxation parameter is fixed to 0.1. For the parameter of NSS, we set patch size to 10×10 , 12×12 , and 14×14 for $\tau = 10$, 30, and 50, respectively. The number of selected non-local similar patches n is set as 70, 80, and 90, respectively. The searching window L is fixed at 30.

The parameter γ is set as 0.3, 0.8, and 0.3 respectively for SLRQA-1, SLRQA-2, and SLRQA-3. The parameter w in SLRQA-3 is set as $w_{i,k} = 10 / (\sigma_i(\dot{\mathbf{X}}_{k-1}) + 10^{-4})$. The multiple values of (λ, τ) are used, i.e., $(\lambda, \tau) = (0.001, 10)$, $(0.01, 30)$, and $(0.01, 50)$. Intuitively, NSS enhances the low-rank property of the image. Hence, the parameter λ is chosen to be smaller when compared to that without using NSS.

The PSNR and SSIM values of each image between the competing methods under different noise levels are reported in Table 5. Most proposed SLRQA methods achieve higher PSNR and

SSIM values than other methods. Moreover, SLRQA-3 achieves the best results in most cases. The visual comparisons of Image5 with $\tau = 30$ are shown in Figure 6 as a typical example. It is shown in Figure 6 that the images recovered by CBM3D and WNNM methods are still noisy. In addition, the images recovered by DWT, LRQA-1, and LRQA-2 are overly smooth, resulting in the loss of the features of the original images. In contrast, the image recovered by SLRQA-3 can not only remove the noise but also keep the features of the original images.

From the above numerical experiments, we can conclude that the SLRQA has better denoising performance compared to other methods with or without using NSS in the sense of PSNR and SSIM.

Table 5: PSNR/SSIM results on color image denoising problem of different methods with NSS.

Algorithm		CBM3D[11]	SRRRC[39]	WNNM[14]	DWT[5]	LRQA-1[10]	LRQA-2[10]	SLRQA-1	SLRQA-2	SLRQA-3
Image										
$\tau = 10$	Image1	35.71/0.92	35.67/0.92	34.85/0.91	34.62/0.91	35.19/0.92	35.34/0.92	35.69/0.92	35.57/0.92	35.86/0.93
	Image2	32.22/0.86	32.02/0.85	31.44/0.86	30.89/0.85	31.94/0.87	31.88/0.87	32.20/0.87	32.19/0.87	32.40/0.87
	Image3	34.67/0.88	34.72/0.88	34.37/0.88	34.22/0.88	34.63/0.88	34.72/0.88	34.75/0.88	34.79/0.88	35.03/0.88
	Image4	34.36/0.91	34.12/0.91	33.95/0.91	33.89/0.91	34.01/0.91	34.05/0.91	34.43/0.91	34.45/0.91	34.36/0.91
	Image5	37.08/0.95	36.82/0.94	35.94/0.95	35.87/0.94	36.48/0.95	36.71/0.95	37.10/0.95	37.18/0.95	37.50/0.95
	Image6	37.02/0.97	36.32/0.96	36.04/0.96	36.02/0.96	36.65/0.97	36.66/0.97	37.39/0.97	37.22/0.97	37.27/0.97
	Image7	34.25/0.91	34.01/0.89	33.80/0.90	33.92/0.90	34.25/0.90	34.24/0.90	34.74/0.91	34.82/0.91	35.00/0.91
	Image8	35.94/0.94	34.82/0.93	34.71/0.93	34.66/0.93	35.14/0.94	35.24/0.94	35.93/0.94	35.75/0.94	35.92/0.94
	Image9	33.25/0.81	32.81/0.79	32.60/0.79	32.32/0.75	33.75/0.80	34.14/0.88	34.24/0.90	34.92/0.89	35.01/0.90
	Image10	32.94/0.78	33.52/0.80	32.33/0.83	32.85/0.82	32.84/0.89	32.24/0.80	33.96/0.84	35.45/0.82	34.08/0.84
$\tau = 30$	Image1	30.82/0.85	30.76/0.84	30.41/0.85	30.36/0.85	30.66/0.86	31.00/0.86	31.30/0.87	31.30/0.87	31.40/0.88
	Image2	27.76/0.74	27.01/0.73	26.73/0.73	26.99/0.74	27.30/0.73	27.40/0.73	27.67/0.74	27.77/0.74	28.00/0.74
	Image3	31.02/0.81	30.82/0.80	30.74/0.80	30.55/0.80	30.93/0.81	31.10/0.81	31.15/0.81	31.21/0.81	31.22/0.81
	Image4	29.45/0.80	29.22/0.79	29.10/0.81	29.00/0.80	29.37/0.81	29.20/0.81	29.57/0.81	29.74/0.81	29.81/0.81
	Image5	32.21/0.85	31.02/0.85	31.08/0.85	30.65/0.84	31.34/0.85	31.30/0.85	31.50/0.86	31.32/0.85	31.34/0.85
	Image6	31.55/0.93	30.87/0.92	31.01/0.92	30.37/0.93	31.56/0.94	31.61/0.94	31.68/0.94	31.72/0.94	31.50/0.94
	Image7	29.23/0.80	28.81/0.79	28.71/0.79	28.94/0.79	29.09/0.80	29.21/0.80	29.32/0.80	29.39/0.80	29.42/0.80
	Image8	29.92/0.82	29.56/0.82	29.42/0.81	28.68/0.82	29.82/0.82	29.90/0.82	29.80/0.82	30.06/0.82	30.12/0.83
	Image9	29.25/0.80	29.01/0.79	28.80/0.74	28.12/0.69	29.05/0.80	29.24/0.80	29.74/0.81	29.82/0.81	30.02/0.82
	Image10	30.94/0.94	30.82/0.93	30.71/0.93	30.66/0.93	31.14/0.94	31.34/0.94	31.93/0.94	31.75/0.94	31.92/0.94
$\tau = 50$	Image1	28.32/0.82	27.92/0.81	28.01/0.81	28.15/0.82	28.31/0.82	28.30/0.82	28.60/0.82	28.50/0.82	28.60/0.82
	Image2	25.23/0.67	25.02/0.66	25.03/0.66	24.94/0.65	25.22/0.67	25.10/0.67	25.47/0.67	25.77/0.67	25.60/0.67
	Image3	28.82/0.28	28.75/0.77	28.74/0.76	28.24/0.75	28.85/0.77	28.90/0.77	28.95/0.78	28.91/0.78	28.99/0.78
	Image4	27.12/0.74	27.08/0.74	26.60/0.74	26.87/0.74	27.06/0.74	27.20/0.74	27.27/0.75	27.34/0.75	27.51/0.75
	Image5	28.56/0.76	28.34/0.76	28.08/0.76	28.01/0.76	28.41/0.77	28.30/0.77	28.50/0.77	28.62/0.78	28.72/0.78
	Image6	28.77/0.90	28.53/0.90	28.01/0.89	28.11/0.90	28.52/0.92	28.61/0.92	28.98/0.93	29.02/0.93	29.00/0.93
	Image7	26.53/0.75	26.43/0.75	26.21/0.74	26.11/0.74	26.74/0.75	26.71/0.74	26.82/0.75	26.89/0.75	26.92/0.75
	Image8	28.12/0.72	27.90/0.71	27.42/0.71	27.62/0.72	28.02/0.72	28.10/0.73	28.10/0.73	28.26/0.73	28.32/0.73
	Image9	26.65/0.66	26.71/0.66	26.80/0.68	26.02/0.63	27.05/0.69	27.24/0.70	27.34/0.70	27.62/0.71	28.70/0.74
	Image10	27.34/0.70	27.02/0.68	26.81/0.64	26.67/0.62	27.34/0.65	27.64/0.70	27.73/0.69	27.75/0.70	28.02/0.72

6.4 Color Image Inpainting

For color image inpainting problems, the compared methods include Bilinear Factorization (BF) methods such as LMAfit [31], MCNMF [33], and Rank Minimization (RM) methods such as LADM [21], LRQA [10], and WNNM [13]⁵. We note that the BF methods require a rank es-

⁵The implementations that we use are available from:

LMAfit: <https://github.com/optsuite/LMAfit>

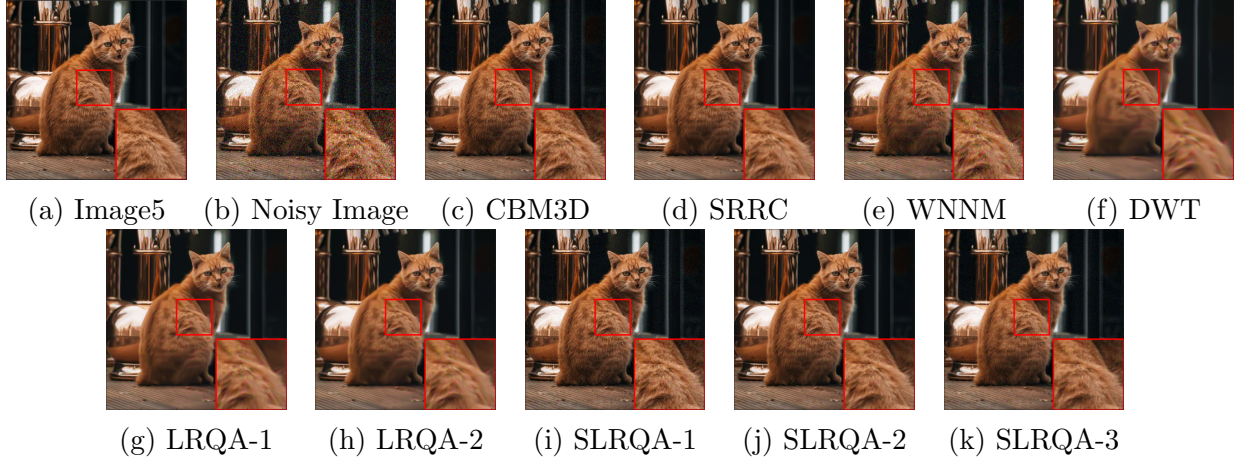


Figure 6: Color image denoising result of tested methods on “Image5” with $\tau = 30$.

timate as a prior. For fairness, the LADM is extended to quaternion representation, which is referred to as QLADM and performs better than the LADM method. To fully demonstrate the performance of LMaFit and MCNMF, we choose the best PSNR and SSIM from the initial rank range [50, 80, 100, 120, 150].

The results of all tested algorithms are shown in Table 6. It is shown therein that SLRQA-NF-3 always enjoys the best performance compared with other methods in terms of PSNR and SSIM. The visual comparisons between SLRQA-NF and all competing inpainting methods on the Image2 with $\chi = 0.7$ are shown in Figure 7 as a typical example. Although the LMaFit and MCNMF methods complete the image, the details of the recovered image are lost, and the recovered images are blurry. The images recovered by LRQA-1 and LRQA-2 methods have a relatively good effect, but the images are still slightly noisy or blurry. In addition, the images recovered by WNNM are noisy. In contrast, SLRQA-NF methods all demonstrate considerable inpainting results and have the highest PSNR and SSIM values.

7 Conclusion

In this paper, we propose a novel SLRQA model for the color image process problems. Different from most existing models which only consider one or two properties from low-rankness, sparsity, and quaternion representation, SLRQA utilizes these properties all. Furthermore, SLRQA does not need an initial rank estimate. A PL-ADMM algorithm is proposed to solve the SLRQA model. Furthermore, we prove that any limit point of PL-ADMM for SLRQA is a stationary point under mild assumptions. In addition, the global convergence analysis of the sequence generated by PL-ADMM under the KL-inequality assumption is presented. When the observation is noise-free, a SLRQA-NF model of the limiting case of SLRQA model is proposed. Subsequently, a nonconvex PL-

MCNMF: <https://xu-yangyang.github.io/codes/MCNF.zip>

LRQA: <https://www.fst.um.edu.mo/personal/wp-content/uploads/2021/05/LRQA.zip>

WNNM: https://www4.comp.polyu.edu.hk/cslzhang/code/WNNM_MC_code.zip

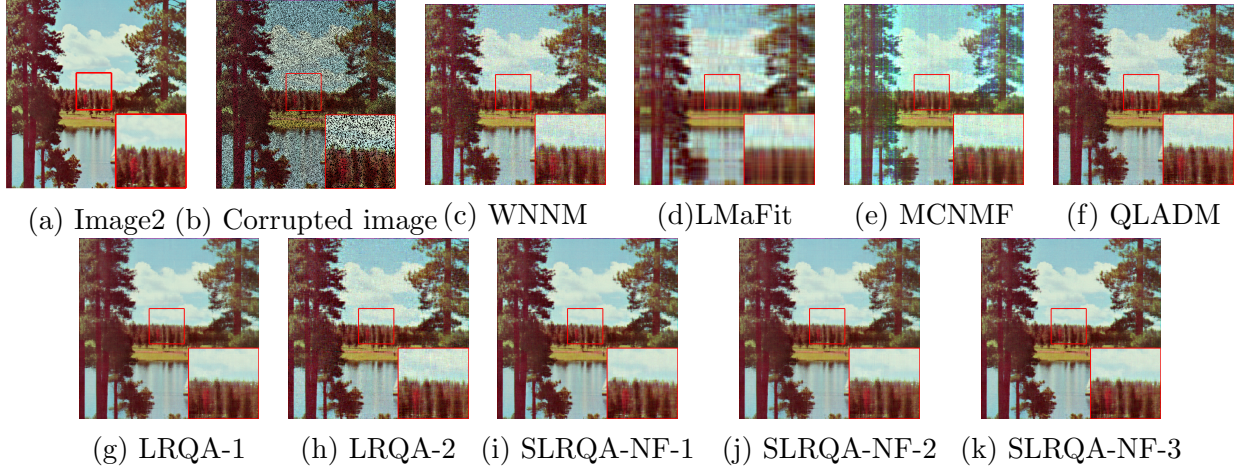


Figure 7: Color image inpainting result of tested methods on “Image2” with $\chi = 0.7$.

ADMM-NF algorithm is also proposed to solve the SLRQA-NF model. Extensive experiments for color image denoising and inpainting problems have demonstrated the robustness and effectiveness of SLRQA and SLRQA-NF.

References

- [1] *Quaternion Toolbox for Matlab*®. [Online], 2005.
- [2] A. BECK, *First-order methods in optimization*, SIAM, 2017.
- [3] J. BOLTE, S. SABACH, AND M. TEBoulLE, *Proximal alternating linearized minimization for nonconvex and nonsmooth problems*, *Mathematical Programming*, 146 (2014), pp. 459–494.
- [4] J.-F. CAI, E. J. CANDÈS, AND Z. SHEN, *A singular value thresholding algorithm for matrix completion*, *SIAM Journal on optimization*, 20 (2010), pp. 1956–1982.
- [5] J.-F. CAI, B. DONG, AND Z. SHEN, *Image restoration: a wavelet frame based model for piecewise smooth functions and beyond*, *Applied and Computational Harmonic Analysis*, 41 (2016), pp. 94–138.
- [6] E. J. CANDÈS AND B. RECHT, *Exact matrix completion via convex optimization*, *Foundations of Computational mathematics*, 9 (2009), pp. 717–772.
- [7] B. CHEN, Q. LIU, X. SUN, X. LI, AND H. SHU, *Removing gaussian noise for colour images by quaternion representation and optimisation of weights in non-local means filter*, *IET Image Processing*, 8 (2014), pp. 591–600.
- [8] L. CHEN, D. SUN, AND K.-C. TOH, *A note on the convergence of admm for linearly constrained convex optimization problems*, *Computational Optimization and Applications*, 66 (2017), pp. 327–343.

Table 6: PSNR/SSIM results on image inpainting problem of different methods.

Algorithm Image	LMaFit[31]	WNNM [13]	MCNMF [33]	QLADM[21]	LRQA-1 [10]	LRQA-2 [10]	SLRQA-NF-1	SLRQA-NF-2	SLRQA-NF-3	
$\chi = 0.5$	Image1	24.69/0.74	25.25/0.60	29.35/0.83	31.16/0.95	30.87/0.89	30.25/0.87	32.32/0.94	31.26/0.94	32.47/0.94
	Image2	22.14/0.80	23.55/0.81	24.22/0.86	30.89/0.85	26.63/0.91	26.20/0.90	28.04/0.94	27.54/0.94	28.16/0.94
	Image3	23.43/0.80	25.23/0.75	27.05/0.88	29.65/0.97	28.37/0.90	27.94/0.89	30.40/0.96	29.65/0.97	30.60/0.97
	Image4	29.09/0.91	31.16/0.85	34.73/0.96	36.39/0.99	35.99/0.97	35.51/0.97	37.69/0.99	36.27/0.98	37.90/0.99
	Image5	26.79/0.85	30.09/0.87	30.02/0.92	33.73/0.98	33.27/0.96	32.72/0.95	34.82/0.98	33.75/0.98	34.98/0.98
	Image6	19.64/0.61	22.01/0.61	22.04/0.87	26.56/0.92	25.27/0.79	25.72/0.80	28.25/0.93	26.62/0.91	27.97/0.92
	Image7	25.00/0.81	24.96/0.75	25.14/0.82	28.84/0.94	27.59/0.87	27.86/0.88	27.82/0.93	28.92/0.94	29.33/0.94
	Image8	24.18/0.87	25.17/0.86	27.21/0.92	30.03/0.97	29.62/0.95	29.06/0.94	31.06/0.97	30.16/0.97	31.22/0.97
	Image9	24.93/0.94	26.02/0.94	27.04/0.95	30.99/0.98	30.12/0.98	29.56/0.97	31.58/0.98	31.09/0.98	31.71/0.98
	Image10	24.36/0.93	26.18/0.94	23.73/0.92	30.69/0.98	29.86/0.98	29.20/0.97	31.28/0.98	30.84/0.98	31.43/0.98
$\chi = 0.7$	Image1	22.32/0.66	23.05/0.52	24.40/0.67	27.29/0.89	25.97/0.74	25.47/0.72	28.40/0.88	27.30/0.88	28.62/0.89
	Image2	20.19/0.73	20.13/0.67	21.52/0.77	24.19/0.89	22.51/0.79	22.44/0.79	25.05/0.90	24.30/0.89	25.21/0.90
	Image3	21.20/0.72	21.50/0.63	22.78/0.75	26.09/0.93	23.69/0.77	23.67/0.77	26.87/0.93	26.00/0.92	27.10/0.94
	Image4	25.87/0.85	28.34/0.80	28.50/0.89	31.89/0.97	31.07/0.93	30.44/0.92	33.37/0.97	31.80/0.97	33.63/0.98
	Image5	24.25/0.78	25.75/0.77	26.19/0.83	29.58/0.95	28.53/0.88	27.85/0.86	30.95/0.96	29.68/0.95	31.14/0.96
	Image6	17.49/0.52	18.13/0.44	19.66/0.67	22.78/0.82	20.28/0.57	19.86/0.55	23.78/0.81	22.70/0.80	24.00/0.83
	Image7	22.59/0.74	22.40/0.67	21.17/0.82	26.24/0.90	24.62/0.78	24.58/0.78	26.63/0.88	26.19/0.89	26.57/0.88
	Image8	21.79/0.81	22.34/0.79	23.17/0.84	26.34/0.94	24.87/0.87	24.54/0.87	27.41/0.94	26.42/0.94	27.60/0.95
	Image9	22.66/0.91	23.33/0.90	24.77/0.93	27.83/0.97	26.13/0.94	25.69/0.94	28.56/0.97	27.81/0.97	28.74/0.97
	Image10	21.55/0.89	23.22/0.90	24.18/0.92	27.54/0.96	25.95/0.95	25.34/0.94	28.46/0.97	27.58/0.96	28.64/0.97
$\chi = 0.8$	Image1	21.13/0.59	20.77/0.43	19.95/0.44	25.05/0.85	22.87/0.61	22.76/0.60	26.08/0.84	24.54/0.79	26.30/0.85
	Image2	19.32/0.68	17.72/0.54	17.87/0.58	22.34/0.84	19.44/0.65	20.27/0.69	23.36/0.86	22.25/0.84	23.53/0.86
	Image3	20.26/0.65	18.71/0.53	18.93/0.59	23.98/0.90	20.52/0.65	21.35/0.69	24.91/0.90	23.61/0.88	25.13/0.91
	Image4	24.62/0.79	25.48/0.72	23.53/0.75	29.09/0.95	27.75/0.87	27.20/0.85	30.74/0.96	28.73/0.94	31.04/0.96
	Image5	23.37/0.74	22.52/0.65	21.25/0.66	27.10/0.93	25.53/0.80	25.05/0.78	28.70/0.93	27.09/0.92	28.97/0.94
	Image6	16.86/0.46	15.41/0.30	15.94/0.34	20.82/0.74	17.93/0.45	14.65/0.31	21.61/0.74	20.10/0.70	21.82/0.76
	Image7	21.53/0.69	20.67/0.60	19.35/0.57	24.79/0.87	22.81/0.71	22.64/0.71	25.59/0.85	24.52/0.86	25.43/0.86
	Image8	20.53/0.77	19.88/0.71	19.22/0.71	24.26/0.91	21.69/0.79	21.93/0.80	25.30/0.92	23.90/0.90	25.50/0.92
	Image9	21.93/0.90	20.78/0.84	21.23/0.85	25.89/0.95	23.43/0.91	23.24/0.91	26.74/0.96	25.56/0.95	26.98/0.96
	Image10	20.47/0.87	20.48/0.84	20.34/0.85	25.52/0.95	23.10/0.90	22.85/0.90	26.67/0.96	25.32/0.95	26.90/0.96

- [9] Y. CHEN, Y. GUO, Y. WANG, D. WANG, C. PENG, AND G. HE, *Denoising of hyperspectral images using nonconvex low rank matrix approximation*, IEEE Transactions on Geoscience and Remote Sensing, 55 (2017), pp. 5366–5380.
- [10] Y. CHEN, X. XIAO, AND Y. ZHOU, *Low-rank quaternion approximation for color image processing*, IEEE Transactions on Image Processing, 29 (2019), pp. 1426–1439.
- [11] K. DABOV, A. FOI, V. KATKOVNIK, AND K. EGIAZAEIAN, *Color image denoising via sparse 3D collaborative filtering with grouping constraint in luminance-chrominance space*, IEEE International Conference on Image Processing, (2007), pp. 313–316.
- [12] W. FENG AND B. HU, *Quaternion discrete cosine transform and its application in color template matching*, in 2008 Congress on Image and Signal Processing, 2008, pp. 252–256.
- [13] S. GU, Q. XIE, D. MENG, W. ZUO, X. FENG, AND L. ZHANG, *Weighted nuclear norm minimization and its applications to low level vision*, International journal of computer vision, 121 (2017), pp. 183–208.
- [14] S. GU, L. ZHANG, W. ZUO, AND X. FENG, *Weighted nuclear norm minimization with application to image denoising*, in Proceedings of the IEEE conference on computer vision and pattern recognition, 2014, pp. 2862–2869.

- [15] Q. GUO, S. GAO, X. ZHANG, Y. YIN, AND C. ZHANG, *Patch-based image inpainting via two-stage low rank approximation*, IEEE transactions on visualization and computer graphics, 24 (2017), pp. 2023–2036.
- [16] W. R. HAMILTON, *Elements of quaternions*, London: Longmans, Green, & Company, 1866.
- [17] J. HAN, L. YANG, K. I. KOU, J. MIAO, AND L. LIU, *Low rank quaternion matrix completion based on quaternion qr decomposition and sparse regularizer*, arXiv preprint arXiv:2211.12793, (2022).
- [18] M. HONG, Z.-Q. LUO, AND M. RAZAVIYAYN, *Convergence analysis of alternating direction method of multipliers for a family of nonconvex problems*, SIAM Journal on Optimization, 26 (2016), pp. 337–364.
- [19] Z. KANG, C. PENG, J. CHENG, AND Q. CHENG, *Logdet rank minimization with application to subspace clustering*, Computational intelligence and neuroscience, 2015 (2015).
- [20] G. LANCKRIET AND B. K. SRIPERUMBUDUR, *On the convergence of the concave-convex procedure*, Advances in neural information processing systems, 22 (2009).
- [21] X. LIANG, X. REN, Z. ZHANG, AND Y. MA, *Repairing sparse low-rank texture*, in European Conference on Computer Vision, Springer, 2012, pp. 482–495.
- [22] Q. LIU, X. SHEN, AND Y. GU, *Linearized admm for nonconvex nonsmooth optimization with convergence analysis*, IEEE Access, 7 (2019), pp. 76131–76144.
- [23] C. LU, J. TANG, S. YAN, AND Z. LIN, *Generalized nonconvex nonsmooth low-rank minimization*, in Proceedings of the IEEE conference on computer vision and pattern recognition, 2014, pp. 4130–4137.
- [24] F. NIE, H. HUANG, AND C. DING, *Low-rank matrix recovery via efficient Schatten p -norm minimization*, in Proceedings of the AAAI Conference on Artificial Intelligence, vol. 26, 2012, pp. 655–661.
- [25] B. RECHT, M. FAZEL, AND P. A. PARRILO, *Guaranteed minimum-rank solutions of linear matrix equations via nuclear norm minimization*, SIAM review, 52 (2010), pp. 471–501.
- [26] W. REN, X. CAO, J. PAN, X. GUO, W. ZUO, AND M.-H. YANG, *Image deblurring via enhanced low-rank prior*, IEEE Transactions on Image Processing, 25 (2016), pp. 3426–3437.
- [27] W. RUDIN ET AL., *Principles of mathematical analysis*, vol. 3, McGraw-hill New York, 1964.
- [28] F. SHANG, Y. LIU, AND J. CHENG, *Scalable algorithms for tractable Schatten quasi-norm minimization*, in Proceedings of the AAAI Conference on Artificial Intelligence, vol. 30, 2016.
- [29] Y. WANG, W. YIN, AND J. ZENG, *Global convergence of admm in nonconvex nonsmooth optimization*, Journal of Scientific Computing, 78 (2019), pp. 29–63.

- [30] Z. WANG, A. C. BOVIK, H. R. SHEIKH, AND E. P. SIMONCELLI, *Image quality assessment: from error visibility to structural similarity*, IEEE transactions on image processing, 13 (2004), pp. 600–612.
- [31] Z. WEN, W. YIN, AND Y. ZHANG, *Solving a low-rank factorization model for matrix completion by a nonlinear successive over-relaxation algorithm*, Mathematical Programming Computation, 4 (2012), pp. 333–361.
- [32] Y. XIE, S. GU, Y. LIU, W. ZUO, W. ZHANG, AND L. ZHANG, *Weighted Schatten p -norm minimization for image denoising and background subtraction*, IEEE transactions on image processing, 25 (2016), pp. 4842–4857.
- [33] Y. XU, W. YIN, Z. WEN, AND Y. ZHANG, *An alternating direction algorithm for matrix completion with nonnegative factors*, Frontiers of Mathematics in China, 7 (2012), pp. 365–384.
- [34] L. YANG, K. I. KOU, J. MIAO, Y. LIU, AND M. P. M. HOI, *Quaternion tensor completion with sparseness for color video recovery*, arXiv preprint arXiv:2212.08361, (2022).
- [35] L. YANG, Y. LIU, AND K. I. KOU, *Quaternion optimized model with sparse regularization for color image recovery*, arXiv preprint arXiv:2204.08629, (2022).
- [36] M. YASHTINI, *Convergence and rate analysis of a proximal linearized admm for nonconvex nonsmooth optimization*, Journal of Global Optimization, 84 (2022), pp. 913–939.
- [37] F. ZHANG, *Quaternions and matrices of quaternions*, Linear algebra and its applications, 251 (1997), pp. 21–57.
- [38] H. ZHANG, J. GAO, J. QIAN, J. YANG, C. XU, AND B. ZHANG, *Linear regression problem relaxations solved by nonconvex ADMM with convergence analysis*, IEEE Transactions on Circuits and Systems for Video Technology, (2023).
- [39] T. ZHANG, D. WU, AND X. MO, *The rank residual constraint model with weighted Schatten p -norm minimization for image denoising*, Circuits, Systems, and Signal Processing, 42 (2023), pp. 4740–4758.
- [40] C. ZOU, K. I. KOU, AND Y. WANG, *Quaternion collaborative and sparse representation with application to color face recognition*, IEEE Transactions on image processing, 25 (2016), pp. 3287–3302.